On the formulation and implementation of mixed mode I and mode II extrinsic cohesive zone models with contact and friction

Nicholas Anton Collins-Craft, Franck Bourrier, Vincent Acary

On the formulation and implementation of mixed mode I and mode II extrinsic cohesive zone models with contact and friction

N.A. Collins-Craft[a], F. Bourrier[a,b], and V. Acary[a]

[a]Univ. Grenoble Alpes, Inria, CNRS, Grenoble INP, Institute of Engineering, LJK, 38000, Grenoble, France
[b]Univ. Grenoble Alpes, INRAE, IGE, CNRS, IRD, Grenoble INP, Grenoble 38000, France.

08/02/2024

Contents

Notation For vectors and tensors, we use the following notation:

$$\|\boldsymbol{x}\|^2 = \|x\|^2 = \underbrace{x_i x^i}_{\text{indicial notation}} = \underbrace{\boldsymbol{x}\cdot\boldsymbol{x}}_{\text{tensor notation}} = \underbrace{x^\top x}_{\text{vector notation}} . \tag{1}$$

Abstract

An extrinsic cohesive zone model for mixed mode I and mode II fracture that encompasses contact and Coulomb friction is developed in the framework of non-smooth mechanics. The model is extended to include the effects of dynamics with impact and sliding, and is discretised in time so that it can be written as a linear complementarity problem (LCP). The LCP is proved to have a solution, subject to a condition on the size of the time-step. Finally, we study the behaviour of the LCP system numerically, by observing the response of a simple test geometry to rapid loading, and observe the numerical method reproduces analytically predicted and experimentally observed behaviours, without requiring impracticably small time-steps.

1 Introduction

Fracture mechanics is of wide interest in both theoretical and applied mechanics, as it plays an important role in phenomena ranging from geological scales such as earthquake rupture (Okubo et al., 2019) and avalanches initiation (Bergfeld et al., 2021), to microscopic scales such as the behaviour of grains of sandstone (Jiang et al., 2021) under mechanical loading or metal alloys (Auth et al., 2022) in high temperature environments.

The classical description of linear elastic fracture mechanics (LEFM) was given by Griffith (1921), and while this model remains fundamental to how fracture is understood today, it suffers from significant problems. Most prominently, the stress field diverges at the crack tip, rendering the model non-physical in an area that is referred to as the "fracture process zone". Cohesive zone models (CZMs) were introduced by Dugdale (1960) and Barenblatt (1962), which served to regularise LEFM models by ensuring finite tractions across the incipient crack surface. The CZMs are described in terms of a traction–separation law, and the total area under the graph of this law is equivalent to the critical fracture energy G_c of LEFM. It is convenient to describe the evolution of the interface in terms of the intensity of the cohesion, which we will denote $\beta \in [0, 1]$. In the following, we will take $\beta = 1$ to indicate a perfectly intact surface, while $\beta = 0$ represents a completely broken interface.

Cohesive zones are extremely difficult to observe experimentally, due to their generally small size (that can be on the order of nanometres (Azab et al., 2020)) and the extremely rapid motion that is characteristic of fracture processes under all but the most idealised conditions. Careful experimentation has allowed some direct observations to be made (Célarié et al., 2003; "The direct observation of the core region of a propagating fracture crack in glass" 1996) of classical fractures, while the discovery that frictional ruptures behave in ways that are analogous to cracks allows another potential source of insight into the phenomenology of cohesive zones (Berman et al., 2020; Gvirtzman and Fineberg, 2021). Given the difficulty that experimentalists have had in obtaining clear observations of the fracture process zone, and hence in calibrating CZMs, typically calibration must be performed using sophisticated back-analysis of substantial amounts of data observed at the structural level (Réthoré and Estevez, 2013; Vargas et al., 2020), and the particular values of the material parameters such as G_c, the critical traction σ_c (at which softening commences) and the critical length δ_c (the point at which the graph of the traction–separation law is zero) can vary substantially, depending on the details of the chosen model.

Cohesive zone models all ultimately derive from one of two families, intrinsic or extrinsic cohesive zone models. Intrinsic models feature an initial elasticity, with the critical traction being obtained when the separation reaches the hardening length δ_h (Falk et al., 2001). These elements are typically inserted into the mesh prior to simulation (whence their name, as they are intrinsic to the mesh), which makes code parallelisation relatively straightforward (Nguyen, 2014). However, the cohesive elements act like nonlinear springs due to their initial elastic branch, inducing a softening of the apparent stiffness of the structure. This phenomenon is referred to as artificial compliance, and it becomes more severe with increasing numbers of cohesive elements (that is to say, the more we refine the mesh, the worse our results) (Falk et al., 2001). This difficulty can be somewhat alleviated by increasing the initial elasticity of the cohesive law, but this in turn imposes unwanted costs on our simulation. For quasi-static analyses (that typically use implicit integration), the stiffness results in very unstable numerical integrations, while in dynamic analyses (that typically use explicit integration), the stiffness imposes such severe restrictions on the stable time-step size that the method becomes essentially unusable (Nguyen, 2014). In both cases, having an elasticity associated with the interface also allows for non-physical results such as interface interpenetration, and hence negative displacement jumps, in the case where the two surfaces are pushed back into contact (Acary and Monerie, 2006). Finally, it is not actually possible to measure the stiffness across an interface before that interface exists, and as such whatever stiffness is determined is necessarily an arbitrary numerical property rather than a real physical parameter, as is hinted at by the ease with which modellers are willing to modify it to avoid artificial compliance.

Extrinsic models are characterised by an initial rigidity, and thus start to decohere only once the critical traction across the surface is exceeded (Kubair and Geubelle, 2003; Seagraves and Radovitzky, 2009). Due to their rigidity, this family of models do not effect the elasticity of the bulk, but they are typically inserted into the simulation on-the-fly (whence their name, as they are extrinsic to the mesh) (Zhou and Molinari, 2004). Given the absence of artificial compliance, extrinsic models are typically used for dynamic analyses, but great care must be taken to ensure the time-continuity of the system. Failure to do so typically results in spurious oscillations of the system or an inability to converge in time (Papoulia et al., 2003; Sam et al., 2005), but sufficiently sophisticated formulations are able to guarantee correct behaviour (Cazes et al., 2013). While extrinsic models do not demonstrate the pathological mesh-dependency that is characteristic of intrinsic models, the large number of elements and remeshing required to fully resolve the system for arbitrary crack paths is generally impractical, and so simulations are often not fully converged. The use of more sophisticated finite element techniques such as extended finite element (Moës and Belytschko, 2002) or discontinuous Galerkin (Versino et al., 2015) may lead to truly mesh-independent results, but come with their own implementation difficulties.

Regardless of how highly-refined the mesh is, cohesive zone models are still subject to difficulties related to ill-posedness (Foulk, 2010). In particular, in quasi-static simulations, solution jumps can appear in "soft" systems where the system stores more energy elastically than the cohesive zone is able to release by fully decohering (Acary and Monerie, 2006). In order to try and maintain well-posedness, researchers have either turned to sophisticated finite element schemes (Samimi et al., 2011) or

viscous regularisation (Chaboche et al., 2001), however in our previous work we were able to show that for pure mode I fracture and contact problems, working in dynamics (with a small enough time-step) is sufficient to maintain a well-posed problem.

While (carefully implemented) extrinsic models demonstrate desirable behaviour under monotonic loading, in more realistic loading cases such as those generated by multiple impacts or complex stress waves, cohesive elements may experience partial decohesion before being subject to unloading and reloading cycles. Almost all existing extrinsic cohesive zone models possess an elastic unload–reload branch (e.g. see Bybordiani and Dias-da-Costa (2021), Camacho and Ortiz (1996), Parrinello (2020), Parrinello and Borino (2020), and Sam et al. (2005)), and such models can be described as being "shifted intrinsic models", as they have the same underlying mathematical structure as intrinsic models (Kubair and Geubelle, 2003). These shifted intrinsic models can demonstrate all the same pathologies as classical intrinsic models, as the elasticity of the unload–reload branch induces the same artificial compliance, and allows the same non-physical behaviour such as interface interpenetration, and can have an arbitrarily large value for small amounts of decohesion. As such, there is a strong motivation to formulate extrinsic cohesive zone models that completely eliminate this unload–reload elasticity, and guarantee physically correct behaviour regardless of the loading history.

The correct mathematical framework in which to develop such extrinsic cohesive zone models is convex analysis, and in particular we follow the works of Jean-Jacques Moreau, who both developed and applied this mathematical framework to create non-smooth mechanics (Moreau, 1970, 1974, 1986). This formulation requires a careful specification of the energy and pseudo-potential of dissipation using indicator functions of convex sets, which are non-differentiable functions. Using this framework allows the development of thermodynamically admissible evolution laws for the system that can include unilateral constraints on the internal variables and their rates (Halphen and Nguyen, 1975; Houlsby, 2019; Marigo, 1981). This formulation has been extended to cohesive zone modelling by Michel Frémond (Frémond, 1988, 2002, 2012a,b), which has in turn been extended in various ways for intrinsic cohesive zone models (Acary and Monerie, 2006; Chaboche et al., 2001; Monerie and Acary, 2001; Nkoumbou Kaptchouang et al., 2021; Perales et al., 2010; Raous et al., 1999), but which has only been minimally exploited for the development of extrinsic cohesive zone models (Jean et al., 2001; Talon and Curnier, 2003).

In our previous work (Collins-Craft et al., 2022), we used the non-smooth mechanics framework to specify a mode I (opening mode) cohesive zone model that also included contact. Using this formulation, the model could be straightforwardly constrained to only admit physical solutions (*i.e.* the cohesion variable $\beta \in [0, 1]$ is strictly enforced, interface interpenetration is strictly forbidden), and in addition succeeded in eliminating the unload–reload elasticity from the formulation. The problem was then reformulated in terms of dynamics, and the discrete-in-space-and-time problem was able to be written as a linear complementarity problem. This problem formulation is particularly favourable, as it enabled a proof of the well-posedness of the problem, and is able to be numerically resolved in a very efficient manner, with comparatively large time-steps. The aim of this paper is to extend the mode I model to mixed modes I and II (opening and sliding modes) fracturing, and include contact and Coulomb friction in the formulation.

Novelty of the contribution and outline of the article. The novelty of our work is that we formulate an extrinsic cohesive zone model that:

1. is based on non-smooth thermo-mechanics principles, takes into account inertia and the inequality constraints on state variables and their rates such as unilateral contact and irreversibility and has a straightforward unload–reload behaviour that avoids any of the problems of shifted intrinsic model structures, and
2. accounts for both pure mode I and pure mode II fracture as well as mixed mode fracture without any mathematical singularities when the displacement jumps are zero, and
3. includes the contact and friction problem within the same mathematical framework as the cohesive zone problem,

and a numerical algorithm that benefits from the following properties:

1. an implicit time-stepping scheme that is consistent with the non-smooth contact dynamics approach that uses the Moreau–Jean scheme, that is (weakly) dissipative in discrete time, and which provides a stable numerical scheme at reasonably large time-steps, and
2. a linear complementarity problem formulation for the space-and-time-discretised problem with a proof of the existence of the solution that solves all of the constraints in an implicit manner, that in practice avoids solution jumps that occur in quasi-statics for models that are not regularised by viscosity or higher-order deformations, and
3. a formulation as a monolithic complementarity problem that allows the exploitation of efficient and robust algorithms developed by the mathematical programming community for this class of problems.

Finally, we demonstrate the practical interest of our approach by applying the model to a pertinent example system and observe that the results match the expected physical behaviour.

2 Formulation of extrinsic cohesive zone models with contact and friction

First, we define the state variables of our model, and the corresponding powers associated with them. Then, using the principle of virtual power, we express the equilibrium equations and boundary conditions for our system. We then specify a particular constitutive model, study the continuous-time energy balance, and demonstrate its analytical solution for a single contact point.

2.1 State variables, powers and principle of virtual power

We start by considering a body $\Omega \in \mathbb{R}^d, d \in [\![1,3]\!]$. The current position is defined by the vector $\boldsymbol{x}$ and the initial position by $\boldsymbol{X}$. We then define a vector of the displacement $\boldsymbol{u}(\boldsymbol{x})$, from which we obtain the velocity $\boldsymbol{v}(\boldsymbol{x}) = \dot{\boldsymbol{u}}(\boldsymbol{x})$. We consider that the body is initially undamaged, and hence at a point $\boldsymbol{x} \in \Omega, \boldsymbol{x} \in \mathbb{R}^d$, the displacement $\boldsymbol{u}(\boldsymbol{x})$ and the velocity $\boldsymbol{v}(\boldsymbol{x})$ are continuously differentiable functions of $\boldsymbol{x}$. When an interface is created by the process of fracture, two material points $\boldsymbol{x}_l$ and $\boldsymbol{x}_r$ are defined by splitting the bodies assuming that they correspond to the material point $\boldsymbol{X}$ initially. For ease of notation, we denote $\boldsymbol{x}_l$ by $\boldsymbol{x}$. The displacement jump that characterises the crack is defined by the difference in the position of the material point that was at $\boldsymbol{X}$ initially, with respect to $\boldsymbol{x}$ and $\boldsymbol{x}_r$, that is $[\![\boldsymbol{u}(\boldsymbol{x}, \boldsymbol{x}_r)]\!] = \boldsymbol{u}(\boldsymbol{x}_r) - \boldsymbol{u}(\boldsymbol{x})$. We define an orthonormal local frame on the interface defined by $(\boldsymbol{x}, \boldsymbol{n}, \boldsymbol{t})$ where $\boldsymbol{n} \in \mathbb{R}^d$ is the normal unit vector from $\boldsymbol{x}$ towards $\boldsymbol{x}_r$ and the vector $\boldsymbol{t} = [\boldsymbol{t}_{\text{II}}, \boldsymbol{t}_{\text{III}}] \in \mathbb{R}^{d\times(d-1)}$ gives the tangential directions along the fracture surface. In this work we consider the normal displacement (jump), defined by $u_{\text{N}}(\boldsymbol{x}, \boldsymbol{x}_r) = [\![\boldsymbol{u}(\boldsymbol{x}, \boldsymbol{x}_r)]\!] \cdot \boldsymbol{n} \in \mathbb{R}$, and the tangential displacement (jump) in the along-crack direction, defined by $u_{\text{T}}(\boldsymbol{x}, \boldsymbol{x}_r) = [\![\boldsymbol{u}(\boldsymbol{x}, \boldsymbol{x}_r)]\!] \cdot \boldsymbol{t}_{\text{II}} \in \mathbb{R}$. The relative normal velocity (jump in space) is given by $v_{\text{N}} = \dot{u}_{\text{N}}$, while the tangential velocity (jump in space) is given by $v_{\text{T}} = \dot{u}_{\text{T}}$. When the body is undamaged and the interface does not yet exist, we assume that u_{N}, v_{N}, u_{T} and v_{T} vanish regardless of the choice of the local frame since $\boldsymbol{u}$ and $\boldsymbol{v}$ are continuous.

To describe the state of the cohesion we introduce the cohesion variable $\beta(\boldsymbol{x}) \in [0,1]$, using the notation introduced by Frémond for describing the intensity of cohesion. For a point $\boldsymbol{x}$ on the interface, the power of the cohesion for a surface Γ is defined by

$$\mathcal{P}_{\mathsf{coh}} = \int_\Gamma \dot{\beta} A \,\mathrm{d}x, \tag{2}$$

where we have introduced A which is the thermodynamic dual force (driving force) associated with β. Now, over the same surface, the power of contact is given by

$$\mathcal{P}_{\mathsf{con}} = \int_\Gamma (v_{\text{N}} r_{\text{N}} + v_{\text{T}} r_{\text{T}}) \,\mathrm{d}x, \tag{3}$$

where r_{N} is the normal reaction force related to the stress $\boldsymbol{\sigma}(x)$ at the interface by $r_{\text{N}} = -\boldsymbol{\sigma} \cdot \boldsymbol{n} \cdot \boldsymbol{n}$, and r_{T} is the corresponding tangential reaction force $r_{\text{T}} = -\boldsymbol{\sigma} \cdot \boldsymbol{n} \cdot \boldsymbol{t}_{\text{II}}$.

For the material in Ω, the power of the external, internal and inertial forces are respectively given by

$$\mathcal{P}_{\mathsf{ext}} = \int_\Omega \boldsymbol{v} \cdot \boldsymbol{f} \,\mathrm{d}x - \int_{\Gamma_{\mathcal{N}}} \boldsymbol{v} \cdot \boldsymbol{\tau} \,\mathrm{d}x - \int_\Gamma \dot{\beta} \Theta \,\mathrm{d}x, \tag{4}$$

$$\mathcal{P}_{\mathsf{int}} = -\int_\Omega \boldsymbol{\sigma} : \dot{\boldsymbol{\varepsilon}} \,\mathrm{d}x + \int_\Gamma v_{\text{N}} r_{\text{N}} \,\mathrm{d}x + \int_\Gamma v_{\text{T}} r_{\text{T}} \,\mathrm{d}x + \int_\Gamma \dot{\beta} A \,\mathrm{d}x, \tag{5}$$

$$\mathcal{P}_{\mathsf{acc}} = \int_\Omega \rho \boldsymbol{v} \cdot \dot{\boldsymbol{v}} \,\mathrm{d}x, \tag{6}$$

where $\boldsymbol{f}$ is the body force in Ω, $\boldsymbol{\tau}$ is the surface traction on $\Gamma_{\mathcal{N}}$ (*i.e.* the region of the surface where the Neumann boundary condition is applied), Θ is an external force that does work on the cohesion (such forces can occur due to thermal or chemical effects) that we take to be identically zero in this work, $\boldsymbol{\varepsilon}$ is the strain in Ω, ρ is the density and $\dot{\boldsymbol{v}}$ is the acceleration.

The principle of virtual power states that for any virtual velocities $\bar{\boldsymbol{v}}$, $\dot{\bar{\boldsymbol{\varepsilon}}}$ and $\dot{\bar{\beta}}$, we have

$$\begin{aligned} \bar{\mathcal{P}}_{\mathsf{acc}} &= \bar{\mathcal{P}}_{\mathsf{ext}} + \bar{\mathcal{P}}_{\mathsf{int}}, \\ \int_\Omega \rho \bar{\boldsymbol{v}} \cdot \dot{\boldsymbol{v}} \,\mathrm{d}x &= \int_\Omega \bar{\boldsymbol{v}} \cdot \boldsymbol{f} \,\mathrm{d}x - \int_{\Gamma_{\mathcal{N}}} \bar{\boldsymbol{v}} \cdot \boldsymbol{\tau} \,\mathrm{d}x - \int_\Gamma \dot{\bar{\beta}} \Theta \,\mathrm{d}x - \int_\Omega \boldsymbol{\sigma} : \dot{\bar{\boldsymbol{\varepsilon}}} \,\mathrm{d}x + \int_\Gamma (\bar{v}_{\text{N}} r_{\text{N}} + \bar{v}_{\text{T}} r_{\text{T}}) \,\mathrm{d}x + \int_\Gamma \dot{\bar{\beta}} A \,\mathrm{d}x. \end{aligned} \tag{7}$$

For further details, a rigorous mathematical treatment of this principle may be found in Frémond (1988). Given sufficient smoothness assumptions on the fields, the equations describing the equilibrium and boundary conditions of the system are

given by localisation as:

$$\begin{cases} \boldsymbol{\nabla}\cdot\boldsymbol{\sigma}+\boldsymbol{f}=\rho\dot{\boldsymbol{v}} & \text{in } \Omega,\\ A=\Theta=0 & \text{on } \Gamma,\\ \boldsymbol{\tau}=\boldsymbol{\sigma}\cdot\boldsymbol{n} & \text{on } \Gamma_{\mathcal{N}},\\ r_{\text{N}}=-\boldsymbol{\sigma}\cdot\boldsymbol{n}\cdot\boldsymbol{n} & \text{on } \Gamma,\\ r_{\text{T}}=-\boldsymbol{\sigma}\cdot\boldsymbol{n}\cdot\boldsymbol{t}_{\text{II}} & \text{on } \Gamma. \end{cases} \tag{8}$$

2.2 A non-smooth thermo-mechanics potential

In defining our model, we begin by defining a ratio between the critical shear traction to the critical opening traction. Then, we write the free energy potential for the bulk and surface, from which we derive the state laws. By specifying a dissipation pseudo-potential, we obtain the laws describing the irreversible behaviour, and thus we are able to describe the complete model as a complementarity problem. Finally, we then describe the energy balance of the system, from which we obtain an expression for the fracture energy.

Critical traction ratio. We start by firstly introducing the ratio of the critical shear traction to the critical opening traction $\gamma=\dfrac{\sigma_{c,\text{II}}}{\sigma_{c,\text{I}}}$. From hereon, we denote $\sigma_{c,\text{I}}$ by σ_c for the sake of notational simplicity.

Free energy and reversible state laws. We consider the free energy of the system, from which we obtain the laws describing the reversible behaviour of the system. The total free energy Ψ of the system is the sum of the free energy in the bulk with the free energy of the surface:

$$\Psi=\int_{\Omega}\Psi_e(\boldsymbol{\varepsilon})\,\mathrm{d}x+\int_{\Gamma}\Psi_s(u_{\text{N}},u_{\text{T}},\beta)\,\mathrm{d}x, \tag{9}$$

where Ψ_e and Ψ_s are the volume and surface free energies, respectively. As we consider an elasto-brittle system in this work, we will assume that all strain is elastic. Firstly, the stresses may be obtained by assuming a classical linear elastic potential for the bulk:

$$\Psi_e(\boldsymbol{\varepsilon})=\frac{1}{2}\boldsymbol{\varepsilon}:\boldsymbol{E}:\boldsymbol{\varepsilon}, \tag{10}$$

$$\boldsymbol{\sigma}(\boldsymbol{\varepsilon})=\frac{\partial\Psi_e(\boldsymbol{\varepsilon})}{\partial\boldsymbol{\varepsilon}}=\boldsymbol{E}:\boldsymbol{\varepsilon}, \tag{11}$$

where $\boldsymbol{E}$ is a fourth order stiffness tensor. The stress-like variables for the surface are similarly derived from the surface potential by

$$\begin{cases} -r_{\text{N}}^{\text{r}}\in\partial_{u_{\text{N}}}\Psi_s(u_{\text{N}},u_{\text{T}},\beta),\\ -r_{\text{T}}^{\text{r}}\in\partial_{u_{\text{T}}}\Psi_s(u_{\text{N}},u_{\text{T}},\beta),\\ -A^{\text{r}}\in\partial_{\beta}\Psi_s(u_{\text{N}},u_{\text{T}},\beta), \end{cases} \tag{12}$$

where r_{N}^{r} is the reversible part of the normal reaction force, r_{T}^{r} is the reversible part of the tangential reaction force, and ∂u_{N}, $\partial_{u_{\text{T}}}$ and ∂_β indicate the subdifferentials with respect to u_{N}, u_{T} and β of a convex (in each individual variable) but non-smooth potential. The first assumption in our model is that the normal displacement is constrained to be positive, *i.e.* $u_{\text{N}}\geqslant 0$, which is enforced as a unilateral constraint, while the cohesion variable is constrained to be $0\leqslant\beta\leqslant 1$. Under these constraints, a rather generic form of the surface free energy may be specified by

$$\Psi_s(u_{\text{N}},u_{\text{T}},\beta)=\psi(u_{\text{N}},u_{\text{T}},\beta)+\mathcal{I}_{\mathbb{R}^+}(u_{\text{N}})+\mathcal{I}_{[0,1]}(\beta), \tag{13}$$

where $\mathcal{I}_C$ is the indicator function of a convex set C. In order to obtain an extrinsic CZM, the model must have no tangent stiffness when $u_{\text{N}}\geqslant 0$ or $|u_{\text{T}}|\geqslant 0$. This constrains the possible forms of (13) to those functions that fulfil the conditions $\dfrac{\partial^2\psi}{\partial {u_{\text{N}}}^2}=0$ and $\left.\dfrac{\partial^2\psi}{\partial {u_{\text{T}}}^2}\right|_{u_{\text{T}}\neq 0}=0$. One such free energy is given by

$$\Psi_s(u_{\text{N}},u_{\text{T}},\beta)=\beta\sigma_c u_{\text{N}}+\beta\sigma_c\gamma|u_{\text{T}}|+wf(\beta)+\mathcal{I}_{\mathbb{R}^+}(u_{\text{N}})+\mathcal{I}_{[0,1]}(\beta), \tag{14}$$

where $w>0$ is the surface free energy which is released by decohesion and $f(\beta)$ is a function that parametrises the evolution of β as decohesion progresses.

Remark 1. *We separate the contribution of the normal opening mode from that of the tangential sliding mode. This is to recover the model specified in Collins-Craft et al. (2022) in the absence of tangential displacements, but also to avoid pathological behaviours such as vanishing cohesive tractions at $u_N=0$ or $u_T=0$, which may arise when u_N and u_T are combined to given an "effective" displacement of the form $\delta=\sqrt{{u_N}^2+\gamma^2{u_T}}$.*

The state laws in their specific form are then obtained by applying (12) to (14):

$$\begin{cases} -(r_{\text{N}}^{\text{r}} + \beta\sigma_c) \in \partial\mathcal{I}_{\mathbb{R}^+}(u_{\text{N}}), \\ -r_{\text{T}}^{\text{r}} \in \beta\sigma_c\gamma\partial|u_{\text{T}}|, \\ -(A^{\text{r}} + \sigma_c u_{\text{N}} + \sigma_c\gamma|u_{\text{T}}| + wf'(\beta)) \in \partial\mathcal{I}_{[0,1]}(\beta). \end{cases} \tag{15}$$

The surface free energy Ψ_s is not a convex function of its arguments $(u_{\text{N}}, u_{\text{T}}, \beta)$. However, Ψ_s is convex with respect to u_{N} and u_{T}. So long as we respect the condition $f''(\beta) \geqslant 0$, Ψ_s will remain convex with respect to β. The continuous part of the free energy in (14) is composed of three terms. The first two terms $\beta\sigma_c u_{\text{N}}$ and $\beta\sigma_c\gamma|u_{\text{T}}|$ account for the potential energy of the normal and tangential cohesive forces $\beta\sigma_c$ and $\beta\sigma_c\gamma$ in the displacement field given by u_{N} and u_{T}. The third term $wf(\beta)$ accounts for the surface free energy released by decohesion at a given β. We also place certain constraints on the form of the function f. When the interface is intact and $\beta = 1$, we require that $f(1) = 0$, as there cannot be any free energy on a surface that does not yet exist. When the interface is fully broken and $\beta = 0$, the cohesive free energy w must have been completely released, and hence $f(0) = 1$. Finally, the release of the cohesive free energy with β must be monotonic, and hence $f'(\beta) \leqslant 0$. Given these conditions, and provided the minimum of f is attained at $\beta = 1$, f will then be a convex function. In this work, we propose a triangle cohesive law that fulfils these requirements, although other shapes that satisfy these requirements are also possible.

Dissipation pseudo-potential and irreversible processes. In order to respect the second law of thermodynamics, we define a dissipation function describing the irreversible part of the decohesion process under isothermal conditions:

$$\mathcal{D} = -\mathcal{P}_{\text{int}} - \int_\Omega \dot{\Psi}_e(\varepsilon)\,\mathrm{d}x - \int_\Gamma \dot{\Psi}_s(u_{\text{N}}, u_{\text{T}}, \beta). \tag{16}$$

This function must be non-negative for all admissible values of the state variables. In order to be able to compute the time derivatives of a non-smooth and non-convex pseudo-potential, we must make certain assumptions. The functions $u_{\text{N}}(t)$, $u_{\text{T}}(t)$ and $\beta(t)$ are assumed to be absolutely continuous, and hence they have a derivative almost everywhere but not necessarily at any given point. As absolutely continuous functions have bounded variations, the left and right derivatives exist for all of these functions. Assuming $\dot{\Psi}_s$ is convex in u_{N}, u_{T} and in β separately, and $\dot{\Psi}_s(u_{\text{N}}, u_{\text{T}}, \beta)$ is also an absolutely continuous function for $u_{\text{N}} \geqslant 0, |u_{\text{T}}| \geqslant 0, \beta \in [0, 1]$, a result in Frémond (2002, Appendix A.1.9) provides us with the following inequality:

$$\dot{\Psi}_s(u_{\text{N}}, u_{\text{T}}, \beta) \leqslant -v_{\text{N}} r_{\text{N}}^{\text{r}} - v_{\text{T}} r_{\text{T}}^{\text{r}} - \dot{\beta} A^{\text{r}}, \tag{17}$$

for any r_{N}^{r}, r_{T}^{r} and $\dot{\beta}$ that satisfies the inclusions in (15). Now, substituting this inequality into the definition of the dissipation rate given by (16)

$$\mathcal{D} \geqslant \int_\Omega \boldsymbol{\sigma} : \dot{\boldsymbol{\varepsilon}}\,\mathrm{d}x - \int_\Gamma \left(v_{\text{N}} r_{\text{N}} + v_{\text{T}} r_{\text{T}} + \dot{\beta} A\right)\mathrm{d}x - \int_\Omega \frac{\partial\Psi_e(\boldsymbol{\varepsilon})}{\partial\boldsymbol{\varepsilon}}\dot{\boldsymbol{\varepsilon}}\,\mathrm{d}x + \int_\Gamma \left(v_{\text{N}} r_{\text{N}}^{\text{r}} + v_{\text{T}} r_{\text{T}}^{\text{r}} + \dot{\beta} A^{\text{r}}\right)\mathrm{d}x. \tag{18}$$

In (18), the terms integrated over the bulk Ω cancel out. Considering only the surface Γ, we obtain

$$\mathcal{D} \geqslant \int_\Gamma \left(-v_{\text{N}} r_{\text{N}} - v_{\text{T}} r_{\text{T}} - \dot{\beta} A + v_{\text{N}} r_{\text{N}}^{\text{r}} + v_{\text{T}} r_{\text{T}}^{\text{r}} + \dot{\beta} A^{\text{r}}\right)\mathrm{d}x. \tag{19}$$

Since the laws of thermodynamics strictly require that $\mathcal{D} \geqslant 0$, we will assume that

$$-v_{\text{N}} r_{\text{N}} - v_{\text{T}} r_{\text{T}} - \dot{\beta} A + v_{\text{N}} r_{\text{N}}^{\text{r}} + v_{\text{T}} r_{\text{T}}^{\text{r}} + \dot{\beta} A^{\text{r}} \geqslant 0, \text{ or equivalently, } -v_{\text{N}} r_{\text{N}}^{\text{ir}} + v_{\text{T}} r_{\text{T}}^{\text{ir}} - \dot{\beta} A^{\text{ir}} \geqslant 0, \tag{20}$$

where we have exploited the standard decompositions $r_{\text{N}} = r_{\text{N}}^{\text{r}} + r_{\text{N}}^{\text{ir}}$, $r_{\text{T}} = r_{\text{T}}^{\text{r}} + r_{\text{T}}^{\text{ir}}$ and $A = A^{\text{r}} + A^{\text{ir}}$ for the irreversible parts of the stress-like variables. We may guarantee that this inequality will be respected by specifying a proper closed convex pseudo-potential of dissipation $\Phi(v_{\text{N}}, v_{\text{T}}, \dot{\beta})$, from which the irreversible stress-like variables may be derived:

$$\begin{cases} -r_{\text{N}}^{\text{ir}} \in \partial_{v_{\text{N}}}\Phi(v_{\text{N}}, v_t, \dot{\beta}), \\ -r_{\text{T}}^{\text{ir}} \in \partial_{v_{\text{T}}}\Phi(v_{\text{N}}, v_t, \dot{\beta}), \\ -A^{\text{ir}} \in \partial_{\dot{\beta}}\Phi(v_{\text{N}}, v_t, \dot{\beta}). \end{cases} \tag{21}$$

For reasons of simplicity, we will assume that the dissipation process of fracture depends exclusively on the rate of β, and that it does so in a linear way, resulting in a rate-independent dissipative behaviour. However, we also wish to include the effects of frictional contact in our model. To do so, we specify the pseudo-potential of dissipation as

$$\Phi(v_{\text{N}}, v_{\text{T}}, \dot{\beta}) = \mathcal{I}_{\mathbb{R}^-}(\dot{\beta}) + \mu(r_{\text{N}} + \beta\sigma_c)|v_{\text{T}}|, \tag{22}$$

where the last term is the standard pseudo-potential associated with the Coulomb friction, modified to take into account the cohesive force, and μ is the dynamic coefficient of friction. We assume that the static and dynamic coefficients of friction are

identical. This model of dissipation imposes that the evolution of β must decrease with time, *i.e.* $\dot{\beta} \leqslant 0$. The dissipative laws are thus

$$\begin{cases} -r_{\mathrm{N}}^{\mathsf{ir}} = 0, \\ -r_{\mathrm{T}}^{\mathsf{ir}} \in \mu(r_{\mathrm{N}} + \beta\sigma_c)\partial|v_{\mathrm{T}}|, \\ -A^{\mathsf{ir}} \in \partial\mathcal{I}_{\mathbb{R}^-}(\dot{\beta}). \end{cases} \tag{23}$$

We may also write the last line of (23) as

$$\dot{\beta} \in \partial\mathcal{I}_{\mathbb{R}^+}(-A^{\mathsf{ir}}), \tag{24}$$

which allows us to easily interpret that A^{ir} is the force that drives the evolution of $\dot{\beta}$. In (8), $A = 0$, so as a consequence $A^{\mathsf{r}} = -A^{\mathsf{ir}}$, and hence we may conclude

$$\dot{\beta} \in \partial\mathcal{I}_{\mathbb{R}^+}(A^{\mathsf{r}}). \tag{25}$$

Remark 2. *The dissipation pseudo-potential in* (22) *can be straightforwardly generalised to generate models that are rate-dependent for the decohesion process, the frictional sliding, or both, by making the dissipation nonlinear in the relevant dissipative variable (see Acary and Monerie (2006) for further details).*

Complete extrinsic cohesive zone model. We start by noting that since $r_{\mathrm{N}}^{\mathsf{ir}} = 0$, we must have $r_{\mathrm{N}} = r_{\mathrm{N}}^{\mathsf{r}}$. Thus, the complete model of the interface is given by

$$\begin{cases} \dot{\beta} \in \partial\mathcal{I}_{\mathbb{R}^+}(A^{\mathsf{r}}), \\ -(r_{\mathrm{N}} + \beta\sigma_c) \in \partial\mathcal{I}_{\mathbb{R}^+}(u_{\mathrm{N}}), \\ -r_{\mathrm{T}}^{\mathsf{r}} \in \beta\sigma_c\gamma\partial|u_{\mathrm{T}}|, \\ -r_{\mathrm{T}}^{\mathsf{ir}} \in \mu(r_{\mathrm{N}} + \beta\sigma_c)\partial|v_{\mathrm{T}}|, \\ -(A^{\mathsf{r}} + \sigma_c u_{\mathrm{N}} + \sigma_c\gamma|u_{\mathrm{T}}| + wf'(\beta)) \in \partial\mathcal{I}_{[0,1]}(\beta). \end{cases} \tag{26}$$

Remark 3 (Nonconvexity of Ψ_S)**.** *Even if we consider that $f(\beta)$ is convex, Ψ_S is not a priori a convex function. Let us consider for a while that $\beta = (0, 1)$ and $u_N \geqslant 0$. The surface free energy reduces to*

$$\Psi_S(u_N, u_T, \beta) = \psi(u_N, u_T, \beta) = \beta\sigma_c u_N + \beta\sigma_c\gamma|u_T| + wf(\beta). \tag{27}$$

Let us consider that we have an evolution with $\dot{\beta} < 0$, then $-A^{\mathsf{ir}} = A^{\mathsf{r}} = 0$ and from (26)*, we get*

$$\sigma_c u_N + \sigma_c\gamma|u_T| = -wf'(\beta). \tag{28}$$

In this case, the surface free energy reduces to

$$\Psi_S(u_N, u_T, \beta) = w(f(\beta) - \beta f'(\beta)) := g(\beta) \tag{29}$$

Computing the second derivative of the function $g(\beta)$ yields

$$g''(\beta) = -w(f''(\beta) + \beta f'''(\beta)) \tag{30}$$

Assuming that f is strictly convex ($f''(\beta) < 0$) and at least C^3, we can remark that $g''(\beta) < 0$ for small value of β. A priori, we can conclude that Ψ_S can be non convex.

Energy Balance With the chosen constitutive laws, the power of internal forces can be written as

$$\begin{aligned} \mathcal{P}_{\mathsf{int}} &= -\int_\Omega \boldsymbol{\varepsilon} : \boldsymbol{E} : \dot{\boldsymbol{\varepsilon}}\,\mathrm{d}x + \int_\Gamma r_{\mathrm{N}} v_{\mathrm{N}}\,\mathrm{d}x + \int_\Gamma r_{\mathrm{T}} v_{\mathrm{T}}\,\mathrm{d}x + \int_\Gamma A\dot{\beta}\,\mathrm{d}x, \\ &= -\frac{\mathrm{d}}{\mathrm{d}t}\left(\int_\Omega \boldsymbol{\varepsilon} : \boldsymbol{E} : \boldsymbol{\varepsilon}\,\mathrm{d}x\right) + \int_\Gamma \left(r_{\mathrm{N}} v_{\mathrm{N}} + r_{\mathrm{T}} v_{\mathrm{T}} + A\dot{\beta}\right)\mathrm{d}x, \\ &= -\dot{\mathcal{U}} + \mathcal{P}_{s,\mathsf{int}}, \end{aligned} \tag{31}$$

where $\mathcal{U}$ is the potential elastic strain energy, and $\mathcal{P}_{s,\mathsf{int}}$ the power of surface internal forces defined by $\mathcal{P}_{s,\mathsf{int}} = \displaystyle\int_\Gamma \left(r_{\mathrm{N}} v_{\mathrm{N}} + r_{\mathrm{T}} v_{\mathrm{T}} + A\dot{\beta}\right)\mathrm{d}x$.
Now, let us expand and simplify the terms inside the integral, using the constitutive laws described above:

$$\begin{aligned} r_{\mathrm{N}} v_{\mathrm{N}} + r_{\mathrm{T}} v_{\mathrm{T}} + A\dot{\beta} &= v_{\mathrm{N}}\left(r_{\mathrm{N}}^{\mathsf{ir}} + r_{\mathrm{N}}^{\mathsf{r}}\right) + v_{\mathrm{T}}\left(r_{\mathrm{T}}^{\mathsf{ir}} + r_{\mathrm{T}}^{\mathsf{r}}\right) + \dot{\beta}\left(A^{\mathsf{ir}} + A^{\mathsf{r}}\right), \\ &= v_{\mathrm{N}}\left(r_{\mathrm{N}}^{\mathsf{ir}} + \nu - \beta\sigma_c\right) + v_{\mathrm{T}}\left(r_{\mathrm{T}}^{\mathsf{ir}} + r_{\mathrm{T}}^{\mathsf{r}}\right) + \dot{\beta}\left[A^{\mathsf{ir}} + \xi - \sigma_c u_{\mathrm{N}} - \sigma_c\gamma|u_{\mathrm{T}}| - wf'(\beta)\right], \\ &= v_{\mathrm{N}} r_{\mathrm{N}}^{\mathsf{ir}} + v_{\mathrm{N}}(\nu - \beta\sigma_c) + v_{\mathrm{T}} r_{\mathrm{T}}^{\mathsf{ir}} + v_{\mathrm{T}} r_{\mathrm{T}}^{\mathsf{r}} + \dot{\beta}A^{\mathsf{ir}} + \dot{\beta}\left[\xi - \sigma_c u_{\mathrm{N}} - \sigma_c\gamma|u_{\mathrm{T}}| - wf'(\beta)\right], \\ &= -v_{\mathrm{N}}\beta\sigma_c + v_{\mathrm{T}} r_{\mathrm{T}}^{\mathsf{ir}} + v_{\mathrm{T}} r_{\mathrm{T}}^{\mathsf{r}} + \dot{\beta}\left[-\sigma_c u_{\mathrm{N}} - \sigma_c\gamma|u_{\mathrm{T}}| - wf'(\beta)\right], \end{aligned} \tag{32}$$

where in order to pass from the second-last to last line we have exploited that $r_{\mathrm{N}}^{\mathsf{ir}} = 0$, and as $-\nu \in \mathrm{N}_{\mathbb{R}^+}(u_{\mathrm{N}})$, $-\xi \in \mathrm{N}_{[0,1]}(\beta)$ and $\dot{\beta} \in \mathrm{N}_{\mathbb{R}^+}(-A^{\mathsf{ir}})$, the products $v_{\mathrm{N}}\nu$, $\dot{\beta}\xi$ and $\dot{\beta}A^{\mathsf{ir}}$ are equal to zero almost everywhere. Then, in order to clarify the structure, we introduce the frictional power as

$$\mathcal{F} = v_{\mathrm{T}} r_{\mathrm{T}}^{\mathsf{ir}} = -\mu(r_{\mathrm{N}} + \beta\sigma_c)|v_{\mathrm{T}}|, \tag{33}$$

since $-r_{\mathrm{T}}^{\mathsf{ir}} \in \mu\,(r_{\mathrm{N}} + \beta\sigma_c)\,\mathrm{sgn}(v_{\mathrm{T}})$.Thus (32) becomes

$$\begin{aligned} r_{\mathrm{N}}v_{\mathrm{N}} + r_{\mathrm{T}}v_{\mathrm{T}} + A\dot{\beta} &= \mathcal{F} - v_{\mathrm{N}}\beta\sigma_c + v_{\mathrm{T}}r_{\mathrm{T}}^{\mathsf{r}} + \dot{\beta}\left[-\sigma_c u_{\mathrm{N}} - \sigma_c\gamma|u_{\mathrm{T}}| - wf'(\beta)\right], \\ &= \mathcal{F} + v_{\mathrm{T}}r_{\mathrm{T}}^{\mathsf{r}} - v_{\mathrm{N}}\frac{\partial\psi}{\partial u_{\mathrm{N}}} - \dot{\beta}\frac{\partial\psi}{\partial\beta} \end{aligned} \tag{34}$$

Since almost everywhere we assume that the following relation holds

$$\dot{\psi} = v_{\mathrm{T}}r_{\mathrm{T}}^{\mathsf{r}} + v_{\mathrm{N}}\frac{\partial\psi}{\partial u_{\mathrm{N}}} + \dot{\beta}\frac{\partial\psi}{\partial\beta} \text{ with } -r_{\mathrm{T}}^{\mathsf{r}} \in \partial_{u_{\mathrm{T}}}\psi(u_{\mathrm{N}}, u_{\mathrm{T}}, \beta) \tag{35}$$

for a feasible trajectory, we obtain

$$r_{\mathrm{N}}v_{\mathrm{N}} + r_{\mathrm{T}}v_{\mathrm{T}} + A\dot{\beta} = \mathcal{F} - \dot{\psi} \text{ almost everywhere.} \tag{36}$$

Another expression of the surface internal power can also be derived if we consider $A = 0$ and again $v_{\mathrm{N}}\nu = 0$ and $\dot{\beta}\xi = 0$:

$$r_{\mathrm{N}}v_{\mathrm{N}} + r_{\mathrm{T}}v_{\mathrm{T}} + A\dot{\beta} = \mathcal{F} + \beta\sigma_c v_{\mathrm{N}} + v_{\mathrm{T}}r_{\mathrm{T}}^{\mathsf{r}}, \tag{37}$$

Hence, we are able to conclude that the the power of the surface internal forces is almost everywhere equal to the frictional power and the change of the continuous part of the free energy of the surface, and hence may write

$$\mathcal{P}_{s,\mathsf{int}} = -\int_\Gamma \left(-\mathcal{F} + \dot{\psi}\right) \mathrm{d}x = \int_\Gamma \left[\mathcal{F} + \beta\sigma_c v_{\mathrm{N}} + v_{\mathrm{T}}r_{\mathrm{T}}^{\mathsf{r}}\right] \mathrm{d}x. \tag{38}$$

Then, we can apply the principle of virtual power for the velocities of the system to write the balance equation for the kinetic energy $\mathcal{K}$, almost everywhere given by $\dot{\mathcal{K}} = \mathcal{P}_{\mathsf{ext}} + \mathcal{P}_{\mathsf{int}}$. Then, substituting in (31) and (38) we arrive at the expression

$$\dot{\mathcal{K}} + \dot{\mathcal{U}} + \int_\Gamma \left(-\mathcal{F} + \dot{\psi}\right) \mathrm{d}x = \mathcal{P}_{\mathsf{ext}}. \tag{39}$$

We apply the first law of thermodynamics and assume isothermal conditions, which results in the energy balance $\dot{\mathcal{K}} + \dot{\mathcal{E}} = \mathcal{P}_{\mathsf{ext}}$, where $\mathcal{E}$ is the internal energy. It is then straightforward to substitute the kinetic energy balance and (31) to arrive at

$$\dot{\mathcal{E}} = -\mathcal{P}_{\mathsf{int}} = \int_\Gamma \left(-\mathcal{F} + \dot{\psi}\right) \mathrm{d}x + \dot{\mathcal{U}}. \tag{40}$$

As the frictional power is only activated at $u_{\mathrm{N}} = 0$ and with $v_{\mathrm{T}} \neq 0$, and as $\Psi_s = \psi$ for all admissible u_{N}, u_{T} and β, we conclude that the fracture energy must be given by

$$\mathcal{G} = \int\int_\Gamma \beta\sigma_c v_{\mathrm{N}} + v_{\mathrm{T}}r_{\mathrm{T}}^{\mathsf{r}}\,\mathrm{d}x\,\mathrm{d}t = -\int\int_\Gamma \dot{\psi}\,\mathrm{d}x\,\mathrm{d}t = -\int\int_\Gamma \dot{\Psi}_s\,\mathrm{d}x\,\mathrm{d}t. \tag{41}$$

Thus, the work done by the friction power in the case of $u_{\mathrm{N}} = 0$ and $v_{\mathrm{T}} \neq 0$ is given by

$$\mathcal{W}_{\mathcal{F}} = -\int\int_\Gamma \mathcal{F}\,\mathrm{d}x\,\mathrm{d}t. \tag{42}$$

We can then write the incremental energy balance of the system as

$$\Delta\mathcal{K} + \Delta\mathcal{U} + \Delta\mathcal{G} + \Delta\mathcal{W}_{\mathcal{F}} = \int_{t_1}^{t_2} \mathcal{P}_{\mathsf{ext}}\,\mathrm{d}t, \text{ and } \Delta\mathcal{E} = \Delta\mathcal{U} + \Delta\mathcal{G}. \tag{43}$$

Remark 4. (41) *allows us to conclude that to pass from an intact interface with $u_{\mathrm{N}} = 0, u_{\mathrm{T}} = 0$ and $\beta = 1$ to a broken interface with $\beta = 0$ on Γ, we must have $\Delta\mathcal{G} = \displaystyle\int_\Gamma w\,\mathrm{d}x$.*

2.3 A linear evolution of the cohesion: triangle law

In order to obtain a specific cohesive zone model from our general framework, we specify the exact form of the surface potential. This potential must fulfil certain conditions, namely that when the surface doesn't exist, *i.e.* $u_{\mathrm{N}} = 0$, $u_{\mathrm{T}} = 0$ and $\beta = 1$, $\Psi_s = 0$, and that when the surface is fully decohered, *i.e.* $\beta = 0$, $\Psi_s = w$. We assume that this decohesion is complete when the displacement jump has surpassed a critical length $\delta_c > 0$, which can be different in each direction. Choosing

$$\begin{cases} w = \frac{1}{2}\sigma_c\delta_{c,\mathrm{N}} = \frac{1}{2}\sigma_c\gamma\delta_{c,\mathrm{T}} = G_c, \\ f(\beta) = (\beta-1)^2, \end{cases} \tag{44}$$

fulfils the required conditions for the energy while ensuring that the potential remains convex in β.

Remark 5. *Our formulation for* (44) *is essentially determined by our conceptual framework, where we consider fracture in elasto-brittle systems to be a process of transforming bulk strain energy to surface energy and kinetic energy. As such, the energy of a surface cannot be determined by the type of fracture that formed it (i.e. mode I, II or III), and thus there can be only a single value of G_c for the material. This does not prevent different values of the critical traction in each direction, but the critical opening distance must in turn adjust to maintain a constant G_c. Such a formulation is common with other authors that adopt a similar energetic picture to us e.g Talon and Curnier (2003) or Lorentz (2008). It is certainly possible to have different values of G_c depending on the fracture mode, such as in the seminal paper of Camanho et al. (2003) or more recent works in the same framework (Venzal et al., 2020). Differing values of G_c depending on the mode implies that significant plasticity is being captured by the cohesive zone model.*

While $\beta \in [0,1]$ and $\dot\beta < 0$, $A^{\mathsf{r}} = 0$ and $\xi = 0$, meaning that after substituting the form (44) into the expression for A^{r}, we obtain $\beta = 1 - \dfrac{u_{\mathrm{N}} + \gamma|u_{\mathrm{T}}|}{\delta_{c,\mathrm{N}}}$. Substituting the displacement-cohesion law into the free energy (14), we get:

$$\Psi_s(u_{\mathrm{N}}, u_{\mathrm{T}}) = \sigma_c\left(u_{\mathrm{N}} + \gamma|u_{\mathrm{T}}|\right) - \frac{\sigma_c}{\delta_{c,\mathrm{N}}}\left(u_{\mathrm{N}} + \gamma|u_{\mathrm{T}}|\right)^2 + \mathcal{I}_{\mathbb{R}^+}(u_{\mathrm{N}}) + \mathcal{I}_{[0,1]}\left(1 - \frac{u_{\mathrm{N}} + \gamma|u_{\mathrm{T}}|}{\delta_{c,\mathrm{N}}}\right). \tag{45}$$

The linear evolution of β, obtained as a consequence of (44), is depicted in Figure 1:

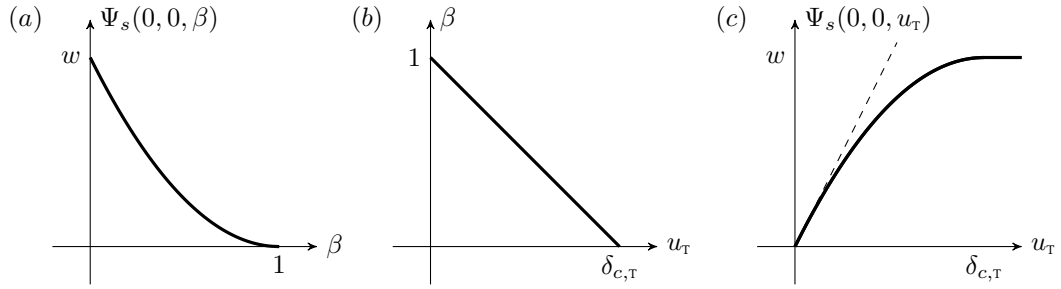

Figure 1: (a) The shape of the surface potential Ψ_s with respect to β. (b) The consequent linear evolution of β with u_{T}, assuming $u_{\mathrm{N}} = 0$. (c) The shape of the surface potential Ψ_s with respect to u_{T}, assuming $u_{\mathrm{N}} = 0$, where the initial slope is equivalent to the value of $\sigma_c\gamma$, and the final value is w.

The model is now specified for a triangle law by inserting (44) in (**??**):

$$\begin{cases} \dot\beta = -\lambda, \quad \sigma_c\delta_{c,\mathrm{N}}(\beta-1) + A^{\mathsf{r}} + \sigma_c u_{\mathrm{N}} + \sigma_c\gamma|u_{\mathrm{T}}| = \xi, \quad r_{\mathrm{N}} + \beta\sigma_c = \nu, \quad 0 \leqslant \nu \perp u_{\mathrm{N}} \geqslant 0, \\ 0 \leqslant \xi \perp \beta \geqslant 0, \quad 0 \leqslant \lambda \perp A^{\mathsf{r}} \geqslant 0, \quad -u_{\mathrm{T}} \in \mathrm{N}_{[-\beta\sigma_c\gamma,\beta\sigma_c\gamma]}(r^{\mathsf{r}}_{\mathrm{T}}), \quad -v_{\mathrm{T}} \in \mathrm{N}_{[-\mu\nu,\mu\nu]}(r^{\mathsf{ir}}_{\mathrm{T}}). \end{cases} \tag{46}$$

Analytical expressions for an experiment with a given driven tangential displacement The model in (46) is sufficiently explicit for us to study analytically. Let us assume that $\beta(0) = \beta_0 \leqslant 1$, and that v_{T} is a function of time t given by the following piecewise linear function:

$$v_{\mathrm{T}}(t) = \begin{cases} \frac{1}{2} & \text{for } 0 \leqslant t < 1, \\ -\frac{1}{2} & \text{for } 1 \leqslant t < 2, \\ \frac{1}{2} & \text{for } 2 \leqslant t, \end{cases} \tag{47}$$

which produces the tangential displacements

$$u_{\mathrm{T}}(t) = \begin{cases} \frac{1}{2}t & \text{for } 0 \leqslant t < 1, \\ 1 - \frac{1}{2}t & \text{for } 1 \leqslant t < 2, \\ -1 + \frac{1}{2}t & \text{for } 2 \leqslant t, \end{cases} \tag{48}$$

assuming $u_{\mathrm{T}}(0) = 0$, and where the displacement u_{T} is measured in mm, and the time t in ms. The time integration of the model described in (46) leads to the following piecewise linear response, where we use $\sigma_c = 0.5$ MPa, $\delta_{c,\mathrm{N}} = 1$ mm, $\gamma = 1$ and a friction coefficient $\mu = 0.5$. We assume that the evolution is continuous, and that $u_{\mathrm{N}} = 0$ *i.e.* that the system is always in contact.

- *First loading phase* $0 \leqslant t < 1$
  Since $v_{\mathrm{T}}(t) > 0$ for $t \in [0, 1)$, the dissipative frictional force is $r_{\mathrm{T}}^{\mathsf{ir}}(t) = -\mu\nu(t)$. Similarly, since $u_{\mathrm{T}}(t) \geqslant 0$, the tangential cohesive force is $r_{\mathrm{T}}^{\mathsf{r}}(t) = -\beta(t)\sigma_c\gamma$. Let us assume that $\beta(t) > 0$ for $t \in [0, 1)$. We deduce that $\xi(t) = 0$. Let us note that $A^{\mathsf{r}}(0) = -\sigma_c\delta_{c,\mathrm{N}}(\beta_0 - 1) - \sigma_c\gamma|u_{\mathrm{T}}(0)| = 0$. Let us assume that $\lambda(t) = 0, t \in [0, \varepsilon], \varepsilon > 0$ or equivalently $\dot\beta(t) = 0, t \in [0, \varepsilon], \varepsilon > 0$. In that case, we get $\dot A^{\mathsf{r}}(t) = -\sigma_c\gamma v_{\mathrm{T}}(t) < 0$ and then $A^{\mathsf{r}}(\varepsilon) < 0$, for $\varepsilon > 0$ which is impossible as A^{r} is constrained to be non-negative. Let us try with $\dot\beta(t) < 0$, then $A^{\mathsf{r}}(t) = 0$ and $\beta(t) = 1 - \dfrac{\gamma|u_{\mathrm{T}}(t)|}{\delta_{c,\mathrm{N}}}$ and $\dot\beta(t) = -\dfrac{\gamma v_{\mathrm{T}}(t)}{\delta_{c,\mathrm{N}}} < 0$. Since $\beta(1) = 1 - \dfrac{\gamma}{2\delta_{c,\mathrm{N}}} > 0$, this is the only consistent solution for $t \in [0, 1)$.

- *Unloading phase* $1 \leqslant t < 2$
  Since $v_{\mathrm{T}}(t) < 0$ for $t \in [1, 2)$, the dissipative frictional force is $r_{\mathrm{T}}^{\mathsf{ir}}(t) = \mu\nu(t)$. Similarly, since $u_{\mathrm{T}}(t) \geqslant 0$, the tangential cohesive force is $r_{\mathrm{T}}^{\mathsf{r}}(t) = -\beta(t)\sigma_c\gamma$. Let us assume that $\beta(t) > 0$ for $t \in [1, 2)$ and $\xi(t) = 0$. Let us assume that $\lambda(t) = 0, t \in [1, 2)$ or equivalently $\dot\beta(t) = 0$. In that case, we get $\dot A^{\mathsf{r}}(t) = -\sigma_c\gamma v_{\mathrm{T}}(t) > 0$. Hence $A^{\mathsf{r}}(t) = -\sigma_c\delta_{c,\mathrm{N}}(\beta(1) - 1) - \sigma_c\gamma|u_{\mathrm{T}}(t)| > 0$. This solution satisfies the complementarity condition up to $t = 2$.

- *Second loading phase* $2 \leqslant t$
  Since $v_{\mathrm{T}}(t) > 0$ for $t \geqslant 2$, the dissipative frictional force is $r_{\mathrm{T}}^{\mathsf{ir}}(t) = -\mu\nu(t)$. Similarly, since $u_{\mathrm{T}}(t) \geqslant 0$, the tangential cohesive force is $r_{\mathrm{T}}^{\mathsf{r}}(t) = -\beta(t)\sigma_c\gamma$. Let us assume that $\beta(t) > 0$ for $t \in [t_1, t_2)$ and $\xi(t) = 0$. Let us assume that $\lambda(t) = 0, t \in [2, 2 + \varepsilon], \varepsilon > 0$ or equivalently $\dot\beta(t) = 0$. In that case, we get $\dot A^{\mathsf{r}}(t) = -\sigma_c\gamma v_{\mathrm{T}}(t) < 0$ and then $A^{\mathsf{r}}(t) = -\sigma_c\delta_{c,\mathrm{N}}(\beta(1) - 1) - \sigma_c\gamma|u_{\mathrm{T}}(t)|$ which is positive for $t < 3$. For $t \geqslant 3$, the only possible solution of the complementarity leads to $\dot\beta(t) = -\dfrac{\gamma v_{\mathrm{T}}(t)}{\delta_{c,\mathrm{N}}} < 0$ and $A^{\mathsf{r}}(t) = 0$. The cohesion variable β is then $\beta(t) = 1 - \dfrac{\gamma|u_{\mathrm{T}}(t)|}{\delta_{c,\mathrm{N}}}$ which is positive for $t < 4$. For $t \geqslant 4$, the solution is $\beta(t) = 0$, $A^{\mathsf{r}}(t) = 0$ and $\xi(t) = \sigma_c\gamma u_{\mathrm{T}}(t) - \sigma_c\delta_{c,\mathrm{N}}$.

As we are interested in the tangential response, we will simulate the system as if some normal pressure is being applied by setting $r_{\mathrm{N}} = 1$ MPa, in order to consistently obtain a frictional force. The solution of this experiment is depicted in Figure 2.

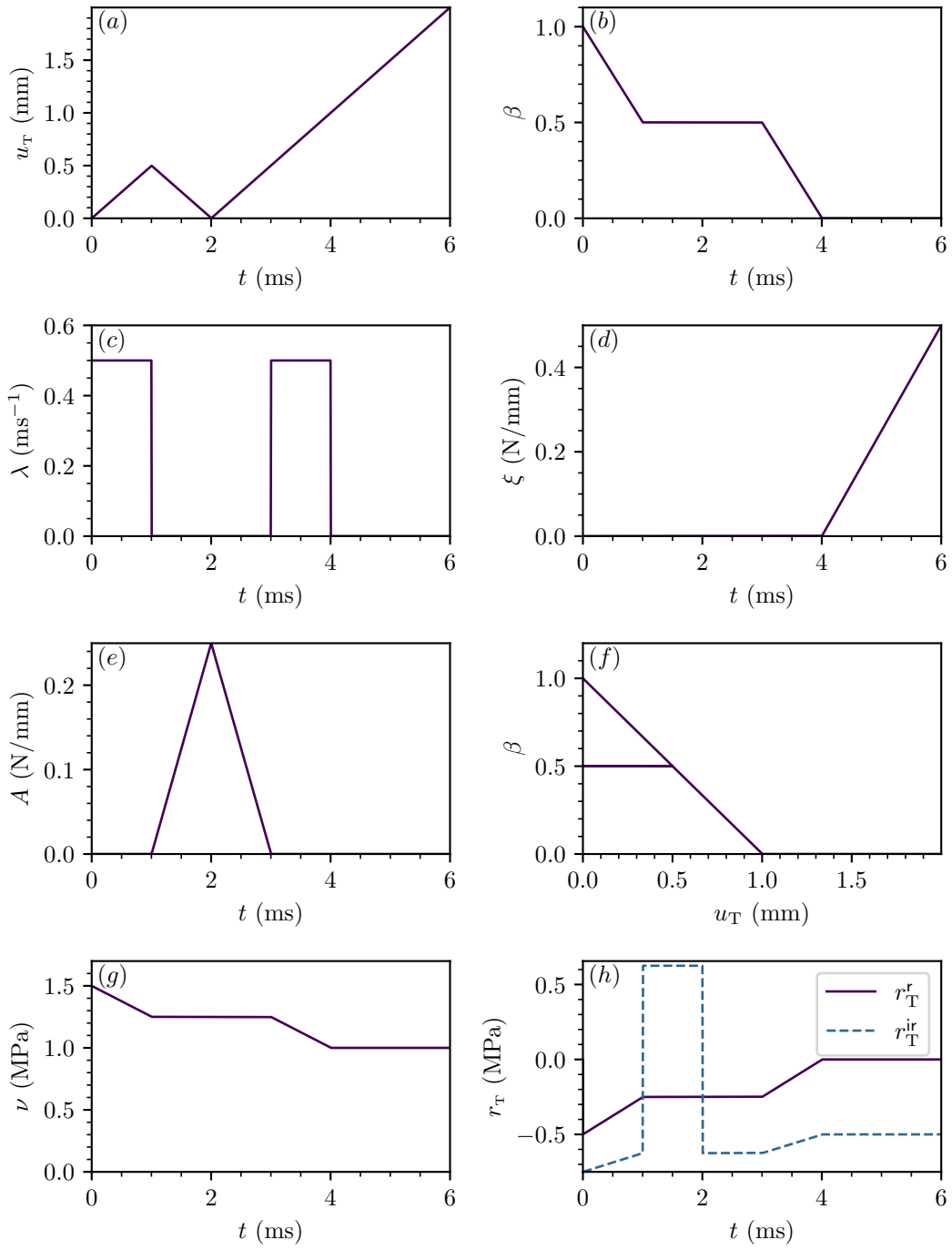

Figure 2: Illustration of the extrinsic cohesize law with a linear evolution of cohesion. (a) The displacement u_{T} as a function of time t. (b) The cohesion β as a function of time t. (c) The slack variable λ as a function of time t. (d) The slack variable ξ as a function of time t. (e) The thermodynamic driving force A^{r} as a function of time. (f) The cohesion β as a function of displacement u_{T}. (g) The slack variable ν as a function of time t. (h) The reversible tangential force $r_{\mathrm{T}}^{\mathrm{r}}$ and the irreversible tangential force $r_{\mathrm{T}}^{\mathrm{ir}}$ as a function of time t.

Remark 6. *This model separates clearly cohesion and friction, while treating them within the same framework.*

Remark 7. *When the interface has fully decohered, we retrieve a standard unilateral contact model with Coulomb friction.*

3 Non-smooth elasto-dynamics of finite-dimensional systems

Now, we will extend our model to consider bodies with finite numbers of degrees of freedom, which may possess masses and stiffnesses, and to which external forces may be applied. These degrees of freedom may form part of a cohesive zone, but equally may not. We also consider the dynamic interaction of multiple bodies via the formulation of impact laws for the system.

3.1 Finite-dimensional systems via space-discretisation

We start by considering a finite-dimensional model of a linear elastic mechanical system, of the sort which may arise after a space-discretisation using the finite element method (FEM). Let us note by $u \in \mathbb{R}^n$ the displacements of the system and $v = \dot{u}$ the velocity. Starting from the principle of virtual power (7), the equilibrium equation can be written as

$$M\dot{v} + Ku = F, \quad \dot{u} = v, \tag{49}$$

where $M \in \mathbb{R}^{n\times n}$ is the mass matrix, assumed to be symmetric positive definite, $K \in \mathbb{R}^{n\times n}$ is the symmetric positive semi-definite structural stiffness matrix and $F \in \mathbb{R}^n$ is the external applied force.

Let us now add that the cohesive zone is applied on a finite set of cohesive contact points that are indexed by $\alpha \in [\![1, m]\!]$. We will work in a system of small perturbations, and hence the local normal displacements at contact $u_{\mathrm{N}} = \mathrm{col}(\mathrm{u}_{\mathrm{N}}^{\alpha}, \alpha \in [\![1, \mathrm{m}]\!])$ are related to the displacements u by a linear relation written as

$$u_{\mathrm{N}} = H_{\mathrm{N}}u + b_{\mathrm{N}}, \tag{50}$$

where $H_{\mathrm{N}} \in \mathbb{R}^{m\times n}$ is a selection matrix for the normal degrees of freedom and $b_{\mathrm{N}} \in \mathbb{R}^m$ is a linear adjustment to express misalignment between nodes. In a similar fashion, the local tangential displacements at contact $u_{\mathrm{T}} = \mathrm{col}(\mathrm{u}_{\mathrm{T}}^{\alpha}, \alpha \in [\![1, \mathrm{m}]\!])$ are related to the global displacements u by

$$u_{\mathrm{T}} = H_{\mathrm{T}}u + b_{\mathrm{T}}, \tag{51}$$

where $H_{\mathrm{T}} \in \mathbb{R}^{m\times n}$ is a selection matrix for the tangential degrees of freedom and $b_{\mathrm{T}} \in \mathbb{R}^m$ is another linear adjustment expressing misalignment between nodes. Collecting all variables at contact in the same way ($x = \mathrm{col}(x^{\alpha}, \alpha \in [\![1, m]\!])$), the equilibrium equations of the system are given by

$$\begin{cases} M\dot{v} + Ku = F + H_{\mathrm{N}}^{\top} S r_{\mathrm{N}} + H_{\mathrm{T}}^{\top} S r_{\mathrm{T}}, \\ \dot{u} = v, \quad u_{\mathrm{N}} = H_{\mathrm{N}}u + b_{\mathrm{N}}, \quad u_{\mathrm{T}} = H_{\mathrm{T}}u + b_{\mathrm{T}}, \end{cases} \tag{52}$$

coupled with (46) to describe the cohesive zone behaviour. $S \in \mathbb{R}^{m\times m}$ is a diagonal matrix that contains the tributary area of each cohesive zone node after space-discretisation of the interface. For the sake of simplicity, we assume that the parameters of the cohesive zone model do not depend on α, but this can be straightforwardly extended.

3.2 Non-smooth dynamics and impacts

In the presence of unilateral contacts, solutions of finite-dimensional dynamical systems with a regular mass matrix (with finite masses associated with all degrees of freedom) exhibit jumps in velocities. In this context, the non-smooth dynamics must be carefully treated to obtain a consistent time-discretisation (Moreau, 1999). To this end, the equations of motion of a discrete (finite-dimensional) mechanical system, and the relation with contact variables are written in terms of differential measures by

$$\begin{cases} M\,\mathrm{d}v + Ku\,\mathrm{d}t = F\,\mathrm{d}t + H_{\mathrm{N}}^{\top}\,\mathrm{d}i_{\mathrm{N}} + H_{\mathrm{T}}^{\top}\,\mathrm{d}i_{\mathrm{T}}, \\ \dot{u} = v, \end{cases} \tag{53}$$

where $\mathrm{d}v$ is the differential measure associated with the velocity v, assumed to be a bounded value function, $\mathrm{d}i_{\mathrm{N}}$ is the measure of the normal reaction at the contact, and $\mathrm{d}i_{\mathrm{T}}$ is the measure of the tangential reactions at the contact. For the cohesive zone model, several further assumptions are made:

- We assume that the reaction due to cohesion force $r_{\mathrm{N}}^{\mathsf{c}}$ is bounded. In other words, the corresponding impulse does not contain atoms (Dirac measures);
- We assume that β and A^{r} are absolutely continuous functions of time. Since the evolution of the cohesion variable (and hence the driving force) is governed by the displacements u_{N} and u_{T}, that are both assumed to be absolutely continuous in time, we assume the same regularity for β and A^{r}.

The normal reaction at the contact can then be decomposed into the "contact impulse" $\mathrm{d}p_{\mathrm{N}}$ (that is integrated over the area of the contact $\bar{S}$), and the contribution of the cohesive forces by

$$\mathrm{d}i_{\mathrm{N}} = \mathrm{d}p_{\mathrm{N}} - S\sigma_c\beta\,\mathrm{d}t. \tag{54}$$

When the interface is completely broken, we want to retrieve a contact law with impact and friction. We will make use of Moreau's impact law

$$0 \leqslant \mathrm{d}p_{\mathrm{N}} \perp v_{\mathrm{N}}^{t^+} + e v_{\mathrm{N}}^{t^-} \geqslant 0 \text{ if } u_{\mathrm{N}} \leqslant 0, \text{ else } \mathrm{d}p_{\mathrm{N}} = 0, \tag{55}$$

where e is the Newton coefficient of restitution and t^- and t^+ indicate the times immediately before and after impact. In terms of normal cone inclusion, this is equivalent to

$$-\,\mathrm{d}p_{\mathrm{N}} \in \mathrm{N}_{\mathrm{T}_{\mathbb{R}^+}(u_{\mathrm{N}})}\left(v_{\mathrm{N}}^{t^+} + e v_{\mathrm{N}}^{t^-}\right), \text{ or equivalently, } -\left(\mathrm{d}i_{\mathrm{N}} + S\sigma_c\beta\,\mathrm{d}t\right) \in \mathrm{N}_{\mathrm{T}_{\mathbb{R}^+}(u_{\mathrm{N}})}\left(v_{\mathrm{N}}^{t^+} + e v_{\mathrm{N}}^{t^-}\right). \tag{56}$$

In a similar fashion, we decompose the tangential impulse into the "frictional impulse" $\mathrm{d}p_{\mathrm{T}}$, integrated over the area of the contact, and the contribution of the tangential cohesive forces by

$$\mathrm{d}i_{\mathrm{T}} = S r_{\mathrm{T}}^{\mathsf{ir}}\,\mathrm{d}t + \mathrm{d}p_{\mathrm{T}}. \tag{57}$$

Changing from the continuous normal force to the contact impulse means that we must also express the friction law accounting for the change to measures. In order to write the expression in this way (in terms of impulses and velocities, rather than forces and velocities), we have implicitly made the assumption that the signs of the force and the velocity do not change over the measure $\mathrm{d}t$. We switch between the signum function and the normal cone, allowing us to now write

$$-v_{\mathrm{T}} \in \mathrm{N}_{[-\mu(\mathrm{d}p_{\mathrm{N}} + S\beta\sigma_c\,\mathrm{d}t),\mu(\mathrm{d}p_{\mathrm{N}} + S\beta\sigma_c\,\mathrm{d}t)]}\left(\mathrm{d}p_{\mathrm{T}}\right). \tag{58}$$

Now, considering the displacements, we have

$$-r_{\mathrm{T}}^{\mathsf{r}} \in \beta\sigma_c\,\mathrm{sgn}(u_{\mathrm{T}}). \tag{59}$$

We can now write the expression after decomposition and switching between the signum and normal cone as:

$$-u_{\mathrm{T}} \in \mathrm{N}_{[-\beta\sigma_c\gamma,\beta\sigma_c\gamma]}\left(r_{\mathrm{T}}^{\mathsf{r}}\right). \tag{60}$$

Thus, we can write the full set of equations for the system as

$$\begin{cases} M\,\mathrm{d}v + Ku\,\mathrm{d}t = F\,\mathrm{d}t + H_{\mathrm{N}}^{\top}\left(\mathrm{d}p_{\mathrm{N}} - S\sigma_c\beta\,\mathrm{d}t\right) + H_{\mathrm{T}}^{\top}\left(S r_{\mathrm{T}}^{\mathsf{r}}\,\mathrm{d}t + \mathrm{d}p_{\mathrm{T}}\right), \\ \dot{u} = v, \quad u_{\mathrm{N}} = H_{\mathrm{N}}u + b_{\mathrm{N}}, \quad v_{\mathrm{N}} = H_{\mathrm{N}}v, \quad u_{\mathrm{T}} = H_{\mathrm{T}}u + b_{\mathrm{T}}, \quad v_{\mathrm{T}} = H_{\mathrm{T}}v, \end{cases} \tag{61}$$

coupled to the cohesive zone model. In complementarity terms, we write the model as

$$\begin{cases} M\,\mathrm{d}v + Ku\,\mathrm{d}t = F\,\mathrm{d}t + H_{\mathrm{N}}^{\top}\left(\mathrm{d}p_{\mathrm{N}} - S\sigma_c\beta\,\mathrm{d}t\right) + H_{\mathrm{T}}^{\top}\left(S r_{\mathrm{T}}^{\mathsf{r}}\,\mathrm{d}t + \mathrm{d}p_{\mathrm{T}}\right), \\ \dot{u} = v, \quad u_{\mathrm{N}} = H_{\mathrm{N}}u + b_{\mathrm{N}}, \quad v_{\mathrm{N}} = H_{\mathrm{N}}v, \quad u_{\mathrm{T}} = H_{\mathrm{T}}u + b_{\mathrm{T}}, \quad v_{\mathrm{T}} = H_{\mathrm{T}}v, \\ \dot{\beta} = -\lambda, \quad A^{\mathsf{r}} + \sigma_c u_{\mathrm{N}} + \sigma_c\gamma|u_{\mathrm{T}}| + w f'(\beta) = \xi, \quad 0 \leqslant \xi \perp \beta \geqslant 0, \quad 0 \leqslant \lambda \perp A^{\mathsf{r}} \geqslant 0, \\ -u_{\mathrm{T}} \in \mathrm{N}_{[-\beta\sigma_c\gamma,\beta\sigma_c\gamma]}\left(r_{\mathrm{T}}^{\mathsf{r}}\right) \quad 0 \leqslant \mathrm{d}p_{\mathrm{N}} \perp v_{\mathrm{N}}^{+} + e v_{\mathrm{N}}^{-} \geqslant 0 \text{ if } u_{\mathrm{N}} \leqslant 0, \text{ else } \mathrm{d}p_{\mathrm{N}} = 0, \\ -\,\mathrm{d}p_{\mathrm{T}} \in \mu(\mathrm{d}p_{\mathrm{N}} + S\beta\sigma_c\,\mathrm{d}t)\,\mathrm{sgn}(v_{\mathrm{T}}) \text{ if } u_{\mathrm{N}} \leqslant 0, \text{ else } \mathrm{d}p_{\mathrm{T}} = 0. \end{cases} \tag{62}$$

4 Numerical time integration

Here we present the time-discretisation of the system that allows us to write a fully-discretised system suitable for numerical integration. In particular, we demonstrate that we are able to write the discrete system as a linear complementarity problem, and that the solution of this problem exists. We then finally demonstrate that the discrete energy balance is in general dissipative and symplectic in the absence of contact and friction.

4.1 Principles of the time integration scheme

We choose a time-integration scheme that is based on the Moreau–Jean scheme (Acary and Brogliato, 2008; Jean, 1999; Jean and Moreau, 1992; Moreau, 1999), which is widely used in contact dynamics. For the impulsive terms which appear in (62), the measure of the time interval $(k, k+1]$ is kept as a primary unknown:

$$p_{\mathrm{N},k,k+1} \approx \mathrm{d}p_{\mathrm{N}}((k,k+1]) = \int_{(k,k+1]} \mathrm{d}p_{\mathrm{N}} \text{ and } i_{\mathrm{N},k,k+1} \approx \mathrm{d}i_{\mathrm{N}}((k,k+1]) = \int_{(k,k+1]} \mathrm{d}i_{\mathrm{N}}, \tag{63}$$

in the normal direction, and

$$p_{\mathrm{T},k,k+1} \approx \mathrm{d}p_{\mathrm{T}}((k,k+1]) = \int_{(k,k+1]} \mathrm{d}p_{\mathrm{T}} \text{ and } i_{\mathrm{T},k,k+1} \approx \mathrm{d}i_{\mathrm{T}}((k,k+1]) = \int_{(k,k+1]} \mathrm{d}i_{\mathrm{T}}, \tag{64}$$

in the tangential direction. We approximate all of the continuous or bounded value terms using a θ-method given by

$$\int_{t_k}^{t_{k+1}} x(t)\,\mathrm{d}t \approx h x_{k+\theta}, \tag{65}$$

where we use the notation $x_{k+\theta} = \theta x_k + (1-\theta)x_{k+1}$ with $\theta \in [0,1]$ and h is the size of the time-step. For the cohesive normal reaction force that we assume is bounded, we have

$$\int_{(k,k+1]} \mathrm{d}i_{\mathrm{N}} = \int_{(k,k+1]} \mathrm{d}p_{\mathrm{N}} - S\sigma_c \int_{t_k}^{t_{k+1}} \beta \, \mathrm{d}t, \tag{66}$$

that is approximated by

$$i_{\mathrm{N},k,k+1} = p_{\mathrm{N},k,k+1} - h\sigma_c S\beta_{k+\theta}, \tag{67}$$

while for the tangential reaction force, also assumed to be bounded, we have

$$\int_{(k,k+1]} \mathrm{d}i_{\mathrm{T}} = \int_{(k,k+1]} \mathrm{d}p_{\mathrm{T}} + S \int_{t_k}^{t_{k+1}} r_{\mathrm{T}}^{\mathsf{r}} \, \mathrm{d}t, \tag{68}$$

that is approximated by

$$i_{\mathrm{T},k,k+1} = p_{\mathrm{T},k,k+1} + hSr_{\mathrm{T},k+\theta}^{\mathsf{r}}. \tag{69}$$

The contact percussion in (62) is discretised as follows:

$$0 \leqslant p_{\mathrm{N},k,k+1} \perp v_{\mathrm{N},k+1} + ev_{\mathrm{N},k} \geqslant 0 \text{ if } \tilde{u}_{\mathrm{N},k} \leqslant 0, \text{ else } p_{\mathrm{N},k,k+1} = 0, \tag{70}$$

where a conditional statement determining whether contact occurs is defined by an approximation of the displacement usually defined as:

$$\tilde{u}_{n,k} = u_{\mathrm{N},k} + \frac{h}{2} v_{\mathrm{N},k}. \tag{71}$$

Similarly, the tangential percussion is discretised by

$$-p_{\mathrm{T},k,k+1} \in \mu \left(p_{\mathrm{N},k,k+1} + h\sigma_c S\beta_{k+\theta} \right) \operatorname{sgn}(v_{\mathrm{T},k+1}) \text{ if } \tilde{u}_{\mathrm{N},k} \leqslant 0, \text{ else } p_{\mathrm{T},k,k+1} = 0, \tag{72}$$

where once again (71) determines if the condition is active. In the following, we consider the index set $I_k = \{\alpha, \tilde{u}_{\mathrm{N},k}^{\alpha} \leqslant 0\}$ and the following compact notation $p_{\mathrm{N},k,k+1} = \operatorname{col}(p_{\mathrm{N},k,k+1}^{\alpha}, \alpha \in I_k)$, $v_{\mathrm{N},k+1} = \operatorname{col}(v_{\mathrm{N},k+1}^{\alpha}, \alpha \in I_k)$, $\bar{H}_{\mathrm{N}} = \operatorname{row}(H_{\mathrm{N},I_\alpha \bullet}, \alpha \in I_k) = H_{\mathrm{N},I_\alpha \bullet}$, $\bar{H}_{\mathrm{T}} = \operatorname{row}(H_{\mathrm{T},I_\alpha \bullet}, \alpha \in I_k) = H_{\mathrm{T},I_\alpha \bullet}$.

Remark 8. *While it would appear that the index sets outlined above would exclude contact points on surfaces not formed by fracture from consideration in our model, in fact such points can easily be included in the matrices H_N and H_T by considering them as cohesive zones where the value of β has been set to zero.*

We also discretise the tangential cohesive force by

$$-r_{\mathrm{T},k+1} \in \sigma_c \gamma \beta_{k+1} \operatorname{sgn}(u_{\mathrm{T},k+1}). \tag{73}$$

Thus, we can write a discrete system in terms of normal cones and sign functions for a single contact that encompasses contact and cohesion:

$$\begin{aligned}
-p_{\mathrm{N},k,k+1} &\in \mathrm{N}_{\mathbb{R}^+}(v_{\mathrm{N},k+1} + ev_{\mathrm{N},k}) \text{ if } \tilde{u}_{\mathrm{N},k} \leqslant 0, \\
-p_{\mathrm{T},k,k+1} &\in \mu(p_{\mathrm{N},k,k+1} + h\sigma_c S\beta_{k+\theta}) \operatorname{sgn}(v_{\mathrm{T},k+1}) \text{ if } \tilde{u}_{\mathrm{N},k} \leqslant 0, \\
-r_{\mathrm{T},k+1} &\in \sigma_c \gamma \beta_{k+1} \operatorname{sgn}(u_{\mathrm{T},k+1}), \\
-\beta_{k+1} &\in \mathrm{N}_{\mathbb{R}^+}(\xi_{k+1}).
\end{aligned} \tag{74}$$

Now, we seek a formulation that will allow us to write our problem as a linear complementarity problem (LCP). While there are multiple possibilities for transforming the inclusions featuring the tangential terms into forms that can lead to an LCP, for reasons of ease of demonstrating existence of the solution and computational efficiency, we follow the approach described in Stewart and Trinkle (1996), and decompose $p_{\mathrm{T},k,k+1}$ into two components:

$$p_{\mathrm{T},k,k+1} = p_{\mathrm{T},k,k+1}^{+} - p_{\mathrm{T},k,k+1}^{-}. \tag{75}$$

Both the components in the positive and negative directions are always non-negative. It is important to emphasise that the sign indicates the direction of the percussion, which is opposite to the velocity *i.e.* if the velocity is in the positive direction, the percussion will be negative ($p_{\mathrm{T},k,k+1}^{+} = 0$ and $p_{\mathrm{T},k,k+1}^{-} > 0$), and *vice versa.* We further introduce the following compact notation:

$$\hat{p}_{\mathrm{T},k,k+1} = \begin{bmatrix} p_{\mathrm{T},k,k+1}^{+} \\ p_{\mathrm{T},k,k+1}^{-} \end{bmatrix}, \tag{76}$$

that is accompanied by the matrix $D = [1, -1]^\top$ for a single contact point, allowing us to write $p_{\mathrm{T},k,k+1} = D\hat{p}_{\mathrm{T},k,k+1}$. In a similar fashion, we can apply a similar process for the tangential cohesive forces, decomposing $r^{\mathsf{r}}_{\mathrm{T},k+1}$ into two parts:

$$r^{\mathsf{r}}_{\mathrm{T},k+1} = r^{\mathsf{r}+}_{\mathrm{T},k+1} - r^{\mathsf{r}-}_{\mathrm{T},k+1}, \tag{77}$$

where once again both components are always non-negative, and the sign indicates the direction of the force, opposite to the tangential displacement which is resisted by it. Introducing the compact notation

$$\hat{r}^{\mathsf{r}}_{\mathrm{T},k+1} = \begin{bmatrix} Sr^{\mathsf{r}+}_{\mathrm{T},k+1} \\ Sr^{\mathsf{r}-}_{t,k+1} \end{bmatrix}, \tag{78}$$

we can write $Sr_{\mathrm{T},k+1} = D\hat{r}^{\mathsf{r}}_{\mathrm{T},k+1}$, where D is as previously defined. Then, we introduce two new slack variables $\zeta_{k+1} \in \mathbb{R}^+$ and $\chi_{k+1} \in \mathbb{R}^+$ and a matrix $\mathbb{1} = [1, 1]^\top$ for a single contact. In combination with Lemma 2, these new variables and matrices allow us to write a complementarity problem at a single point as follows:

$$\begin{cases} p_{\mathrm{T},k,k+1} = D\hat{p}_{\mathrm{T},k,k+1}, \\ 0 \leqslant p_{\mathrm{N},k,k+1} \perp v_{\mathrm{N},k+1} + ev_{\mathrm{N},k} \geqslant 0, \\ 0 \leqslant \hat{p}_{\mathrm{T},k,k+1} \perp \mathbb{1}\zeta_{k+1} + D^\top v_{\mathrm{T},k+1} \geqslant 0, \\ 0 \leqslant \zeta_{k+1} \perp \mu\left(p_{\mathrm{N},k,k+1} + h\sigma_c S\beta_{k+\theta}\right) - \mathbb{1}^\top \hat{p}_{\mathrm{T},k,k+1} \geqslant 0, \\ Sr^{\mathsf{r}}_{\mathrm{T},k+1} = D\hat{r}^{\mathsf{r}}_{\mathrm{T},k+1}, \\ 0 \leqslant \hat{r}^{\mathsf{r}}_{\mathrm{T},k+1} \perp \mathbb{1}\chi_{k+1} + D^\top u_{\mathrm{T},k+1} \geqslant 0, \\ 0 \leqslant \chi_{k+1} \perp \sigma_c\gamma S\beta_{k+1} - \mathbb{1}^\top \hat{r}^{\mathsf{r}}_{\mathrm{T},k+1} \geqslant 0, \\ \beta_{k+1} \perp \xi_{k+1}. \end{cases} \tag{79}$$

When sliding occurs, ζ_{k+1} takes the physical meaning of the magnitude of the sliding velocity $v_{\mathrm{T},k+1}$. However, when there is no sliding and no frictional percussions, ζ_{k+1} can take any positive value and does not have any particular physical meaning. Similarly, when tangential displacement has occurred, χ_{k+1} has a physical meaning, namely the magnitude of the displacement, while in the absence of both displacement and force it can take any positive value and does not carry a clear physical meaning.

Now, for the case of multiple cohesive-contact points, we can understand each of the physical and slack variables as column vectors in $\mathbb{R}^n$ ($\hat{p}_{\mathrm{T},k,k+1}$ and $\hat{r}^{\mathsf{r}}_{\mathrm{T},k+1}$ are in $\mathbb{R}^{2n}$), and generalise $D \in \mathbb{R}^{n\times 2n}$ such that

$$D = \begin{bmatrix} 1 & -1 & 0 & 0 & \dots & 0 & 0 \\ 0 & 0 & 1 & -1 & \dots & 0 & 0 \\ \vdots & \vdots & \vdots & \vdots & \ddots & \vdots & \vdots \\ 0 & 0 & 0 & 0 & \dots & 1 & -1 \end{bmatrix}, \tag{80}$$

and generalise $\mathbb{1} \in \mathbb{R}^{2n\times n}$ such that

$$\mathbb{1} = \begin{bmatrix} 1 & 0 & \dots & 0 \\ 1 & 0 & \dots & 0 \\ 0 & 1 & \dots & 0 \\ 0 & 1 & \dots & 0 \\ \vdots & \vdots & \ddots & \vdots \\ 0 & 0 & \dots & 1 \\ 0 & 0 & \dots & 1 \end{bmatrix}, \tag{81}$$

which allows us to straightforwardly extend the notation to multiple contact points.

Following the principles above, the time-stepping scheme for the full elasto-dynamic cohesive-frictional-contact problem is

written as follows:

$$\begin{cases} M(v_{k+1}-v_k)+hKu_{k+\theta}=hF_{k+\theta}-h\sigma_c H_{\text{N}}^\top S\beta_{k+\theta}+\bar{H}_{\text{N}}^\top p_{\text{N},k,k+1}+\bar{H}_{\text{T}}^\top D\hat{p}_{\text{T},k,k+1}+hH_{\text{T}}^\top D\hat{r}^{\text{r}}_{\text{T},k+\theta}, \\ Sr^{\text{r}}_{\text{T},k+1}=D\hat{r}^{\text{r}}_{\text{T},k+1}, \\ p_{\text{T},k,k+1}=D\hat{p}_{\text{T},k,k+1}, \\ u_{k+1}=u_k+hv_{k+\theta}, \\ u_{\text{N},k+1}=H_{\text{N}}u_{k+1}+b_{\text{N},k+1}, \quad u_{\text{T},k+1}=H_{\text{T}}u_{k+1}+b_{\text{T},k+1}, \\ v_{\text{N},k+1}=\bar{H}_{\text{N}}v_{k+1}, \quad v_{\text{T},k+1}=\bar{H}_{\text{T}}v_{k+1}, \\ \beta_{k+1}=\beta_k-h\lambda_{k+1}, \\ \sigma_c\delta_{c,\text{N}}(\beta_{k+1}-1)+\sigma_c u_{\text{N},k+1}+\sigma_c\gamma|u_{\text{T},k+1}|+A^{\text{r}}{}_{k+1}=\xi_{k+1}, \\ 0\leqslant SA^{\text{r}}{}_{k+1}\perp\lambda_{k+1}\geqslant 0, \\ 0\leqslant S\beta_{k+1}\perp\xi_{k+1}\geqslant 0, \\ 0\leqslant p_{\text{N},k,k+1}\perp v_{\text{N},k+1}+ev_{\text{N},k}\geqslant 0, \\ 0\leqslant \hat{p}_{\text{T},k,k+1}\perp \mathbb{1}\zeta_{k+1}+D^\top v_{\text{T},k+1}\geqslant 0, \\ 0\leqslant \zeta_{k+1}\perp \mu\left(p_{\text{N},k,k+1}+h\sigma_c S\beta_{k+\theta}\right)-\mathbb{1}^\top\hat{p}_{\text{T},k,k+1}\geqslant 0, \\ 0\leqslant \hat{r}^{\text{r}}_{\text{T},k+1}\perp \mathbb{1}\chi_{k+1}+D^\top u_{\text{T},k+1}\geqslant 0, \\ 0\leqslant \chi_{k+1}\perp S\beta_{k+1}\sigma_c\gamma-\mathbb{1}^\top\hat{r}^{\text{r}}_{\text{T},k+1}\geqslant 0. \end{cases} \tag{82}$$

4.2 The discrete linear complementarity problem

Now, in order to obtain a workable formulation to express as an LCP, we first consider the entries in the complementarity variable vectors w and z that are given by (82):

$$w=\begin{bmatrix} h\lambda_{k+1} \\ \xi_{k+1} \\ v_{\text{N},k+1}+ev_{\text{N},k} \\ \mathbb{1}\zeta_{k+1}+D^\top v_{\text{T},k+1} \\ \mu(p_{\text{N},k,k+1}+h\sigma_c S\beta_{k+\theta})-\mathbb{1}^\top\hat{p}_{\text{T},k,k+1} \\ \mathbb{1}\chi_{k+1}+D^\top u_{\text{T},k+1} \\ \sigma_c\gamma S\beta_{k+1}-\mathbb{1}^\top\hat{r}^{\text{r}}_{\text{T},k+1} \end{bmatrix}, \quad z=\begin{bmatrix} SA^{\text{r}}{}_{k+1} \\ S\beta_{k+1} \\ p_{\text{N},k,k+1} \\ \hat{p}_{\text{T},k,k+1} \\ \zeta_{k+1} \\ \hat{r}^{\text{r}}_{\text{T},k+1} \\ \chi_{k+1} \end{bmatrix}, \tag{83}$$

where all of the cohesive zone variables should be understood as vectors.

Remark 9. *As in Collins-Craft et al. (2022), we take $h\lambda_{k+1}$ as the complementarity variable (rather than λ_{k+1}) in order to avoid an ill-conditioned matrix as $h\to 0$.*

Having constructed the LCP in this way, the expression for w_1 is trivial:

$$\begin{aligned} h\lambda_{k+1}&=S^{-1}\left(S\beta_k-S\beta_{k+1}\right), \\ w_1&=-S^{-1}z_2+\beta_k. \end{aligned} \tag{84}$$

Likewise, the expression for w_7:

$$w_7=\sigma_c\gamma z_2-\mathbb{1}^\top z_6. \tag{85}$$

The expression for w_5 is only slightly more elaborate:

$$\begin{aligned} w_5=&\mu\left(p_{\text{N},k,k+1}+h\sigma_c S\beta_{k+\theta}\right)-\mathbb{1}^\top\hat{p}_{\text{T},k,k+1}, \\ =&\mu\left(p_{\text{N},k,k+1}+h(1-\theta)\sigma_c S\beta_k+h\theta\sigma_c S\beta_{k+1}\right)-\mathbb{1}^\top\hat{p}_{\text{T},k,k+1}, \\ =&h\theta\mu\sigma_c z_2+\mu z_3-\mathbb{1}^\top z_4+h(1-\theta)\mu\sigma_c S\beta_k. \end{aligned} \tag{86}$$

We start the development of the expressions for the more involved terms by expanding the first line of (82) with the appropriate θ-method substitutions. We arrive at

$$\begin{aligned} M(v_{k+1}-v_k)+hK\left(u_k+h\theta\left[(1-\theta)v_k+\theta v_{k+1}\right]\right)=&h\left[(1-\theta)F_k+\theta F_{k+1}\right]-h\sigma_c H_{\text{N}}^\top\left[(1-\theta)S\beta_k+\theta S\beta_{k+1}\right] \\ &+\bar{H}_{\text{N}}^\top p_{\text{N},k,k+1}+\bar{H}_{\text{T}}^\top D\hat{p}_{\text{T},k,k+1} \\ &+hH_{\text{T}}^\top D\left[(1-\theta)\hat{r}^{\text{r}}_{\text{T},k}+\theta\hat{r}^{\text{r}}_{\text{T},k+1}\right]. \end{aligned} \tag{87}$$

We denote the augmented mass matrix as $\hat{M} = M + h^2\theta^2 K$ and the free impulse (without the contribution of the cohesive zone model) $\hat{i}_{k,k+1} = Mv_k - hK\left(u_k + h\theta(1-\theta)v_k\right) + h\left[(1-\theta)F_k + \theta F_{k+1}\right]$. When necessary, we modify the augmented mass matrix $\hat{M}$ and the free impulse $\hat{i}$ to take into account Dirichlet boundary conditions. Thus, the velocities can be determined by

$$v_{k+1} = \hat{M}^{-1}\left(\hat{i}_{k,k+1} - h\sigma_c H_{\text{N}}^\top\left[(1-\theta)S\beta_k + \theta S\beta_{k+1}\right] + \bar{H}_{\text{N}}^\top p_{\text{N},k,k+1} + \bar{H}_{\text{T}}^\top D\hat{p}_{\text{T},k,k+1} + hH_{\text{T}}^\top D\left[(1-\theta)\hat{r}^{\text{r}}_{\text{T},k} + \theta\hat{r}^{\text{r}}_{\text{T},k+1}\right]\right). \tag{88}$$

Then, we can get the normal velocities:

$$\begin{aligned}
v_{\text{N},k+1} =& \bar{H}_{\text{N}}\hat{M}^{-1}\hat{i}_{k,k+1} - h\sigma_c\bar{H}_{\text{N}}\hat{M}^{-1}H_{\text{N}}^\top\left[(1-\theta)S\beta_k + \theta S\beta_{k+1}\right] + \bar{H}_{\text{N}}\hat{M}^{-1}\bar{H}_{\text{N}}^\top p_{\text{N},k,k+1}\\
&+ \bar{H}_{\text{N}}\hat{M}^{-1}\bar{H}_{\text{T}}^\top D\hat{p}_{\text{T},k,k+1} + h\bar{H}_{\text{N}}\hat{M}^{-1}H_{\text{T}}^\top D\left[(1-\theta)\hat{r}^{\text{r}}_{\text{T},k} + \theta\hat{r}^{\text{r}}_{\text{T},k+1}\right],\\
=& -h\theta\sigma_c V_{\text{NN}}S\beta_{k+1} + W_{\text{NN}}p_{\text{N},k,k+1} + W_{\text{NT}}D\hat{p}_{\text{T},k,k+1} + h\theta V_{\text{NT}}D\hat{r}^{\text{r}}_{\text{T},k+1}\\
&+ \bar{H}_{\text{N}}\hat{M}^{-1}\hat{i}_{k,k+1} - h(1-\theta)\sigma_c V_{\text{NN}}S\beta_k + h(1-\theta)V_{\text{NT}}D\hat{r}^{\text{r}}_{\text{T},k},\\
=& -h\theta\sigma_c V_{\text{NN}}z_2 + W_{\text{NN}}z_3 + W_{\text{NT}}Dz_4 + h\theta V_{\text{NT}}Dz_6\\
&+ \bar{H}_{\text{N}}\hat{M}^{-1}\hat{i}_{k,k+1} - h(1-\theta)\sigma_c V_{\text{NN}}S\beta_k + h(1-\theta)V_{\text{NT}}D\hat{r}^{\text{r}}_{\text{T},k},
\end{aligned} \tag{89}$$

and the tangential velocities:

$$\begin{aligned}
v_{\text{T},k+1} =& \bar{H}_{\text{T}}\hat{M}^{-1}\hat{i}_{k,k+1} - h\sigma_c\bar{H}_{\text{T}}\hat{M}^{-1}H_{\text{N}}^\top\left[(1-\theta)S\beta_k + \theta S\beta_{k+1}\right] + \bar{H}_{\text{T}}\hat{M}^{-1}\bar{H}_{\text{N}}^\top p_{\text{N},k,k+1}\\
&+ \bar{H}_{\text{T}}\hat{M}^{-1}\bar{H}_{\text{T}}^\top D\hat{p}_{\text{T},k,k+1} + h\bar{H}_{\text{T}}\hat{M}^{-1}H_{\text{T}}^\top D\left[(1-\theta)\hat{r}^{\text{r}}_{\text{T},k} + \theta\hat{r}^{\text{r}}_{\text{T},k+1}\right],\\
=& -h\theta\sigma_c V_{\text{TN}}S\beta_{k+1} + W_{\text{TN}}p_{\text{N},k,k+1} + W_{\text{TT}}D\hat{p}_{\text{T},k,k+1} + h\theta V_{\text{TT}}D\hat{r}^{\text{r}}_{\text{T},k+1}\\
&+ \bar{H}_{\text{T}}\hat{M}^{-1}\hat{i}_{k,k+1} - h(1-\theta)\sigma_c V_{\text{TN}}S\beta_k + h(1-\theta)V_{\text{TT}}D\hat{r}^{\text{r}}_{\text{T},k},\\
&- h\theta\sigma_c V_{\text{TN}}z_2 + W_{\text{TN}}z_3 + W_{\text{TT}}Dz_4 + h\theta V_{\text{TT}}Dz_6\\
&+ \bar{H}_{\text{T}}\hat{M}^{-1}\hat{i}_{k,k+1} - h(1-\theta)\sigma_c V_{\text{TN}}S\beta_k + h(1-\theta)V_{\text{TT}}D\hat{r}^{\text{r}}_{\text{T},k},
\end{aligned} \tag{90}$$

where $W_{\text{NN}} = \bar{H}_{\text{N}}\hat{M}^{-1}\bar{H}_{\text{N}}$ and $W_{\text{TT}} = \bar{H}_{\text{T}}\hat{M}^{-1}\bar{H}_{\text{T}}$ are the Delassus matrices for the degrees of freedom involved in the purely normal and purely tangential contact problems, while $W_{\text{NT}} = \bar{H}_{\text{N}}\hat{M}^{-1}\bar{H}_{\text{T}}$ and $W_{\text{TN}} = \bar{H}_{\text{T}}\hat{M}^{-1}\bar{H}_{\text{N}}$ are the Delassus matrices for the interaction terms between the normal and tangential parts of the contact problem. The matrices $V_{\text{NN}} = \bar{H}_{\text{N}}\hat{M}^{-1}H_{\text{N}}$, $V_{\text{TT}} = \bar{H}_{\text{T}}\hat{M}^{-1}H_{\text{T}}$, $V_{\text{NT}} = \bar{H}_{\text{N}}\hat{M}^{-1}H_{\text{T}}$ and $V_{\text{TN}} = \bar{H}_{\text{T}}\hat{M}^{-1}H_{\text{T}}$ capture the effect of the cohesive terms on the contact and friction degrees of freedom.

From (89) and (90) we can straightforwardly get first w_3:

$$\begin{aligned}
w_3 =& -h\theta\sigma_c V_{\text{NN}}z_2 + W_{\text{NN}}z_3 + W_{\text{NT}}Dz_4 + h\theta V_{\text{NT}}Dz_6\\
&+ \bar{H}_{\text{N}}\hat{M}^{-1}\hat{i}_{k,k+1} - h(1-\theta)\sigma_c V_{\text{NN}}S\beta_k + h(1-\theta)V_{\text{NT}}D\hat{r}^{\text{r}}_{\text{T},k} + ev_{\text{N},k},
\end{aligned} \tag{91}$$

and then w_4:

$$\begin{aligned}
w_4 =& -h\theta\sigma_c D^\top V_{\text{TN}}z_2 + D^\top W_{\text{TN}}z_3 + D^\top W_{\text{TT}}Dz_4 + \mathbb{1}z_5 + h\theta D^\top V_{\text{TT}}Dz_6\\
&+ D^\top\bar{H}_{\text{T}}\hat{M}^{-1}\hat{i}_{k,k+1} - h(1-\theta)\sigma_c D^\top V_{\text{TN}}S\beta_k + h(1-\theta)D^\top V_{\text{TT}}D\hat{r}^{\text{r}}_{\text{T},k}.
\end{aligned} \tag{92}$$

In the same way as for the velocity, we can expand the expressions for the normal and tangential displacements. Firstly in the normal direction:

$$\begin{aligned}
u_{\text{N},k+1} =& u_{\text{N},k} + h(1-\theta)H_{\text{N}}v_k + h\theta H_{\text{N}}v_{k+1} + b_{\text{N},k+1} - b_{\text{N},k},\\
=& -h^2\theta^2\sigma_c U_{\text{NN}}S\beta_{k+1} + h\theta X_{\text{NN}}p_{\text{N},k,k+1} + h\theta X_{\text{NT}}D\hat{p}_{\text{T},k,k+1} + h^2\theta^2 U_{\text{NT}}D\hat{r}^{\text{r}}_{\text{T},k+1}\\
&+ h\theta\bar{H}_{\text{N}}\hat{M}^{-1}\hat{i}_{k,k+1} - h^2\theta(1-\theta)\sigma_c U_{\text{NN}}S\beta_k + h^2\theta(1-\theta)U_{\text{NT}}D\hat{r}^{\text{r}}_{\text{T},k} + u_{\text{N},k} + h(1-\theta)H_{\text{N}}v_k + b_{\text{N},k+1} - b_{\text{N},k},\\
=& -h^2\theta^2\sigma_c U_{\text{NN}}z_2 + h\theta X_{\text{NN}}z_3 + h\theta X_{\text{NT}}Dz_4 + h^2\theta^2 U_{\text{NT}}Dz_6\\
&+ h\theta H_{\text{N}}\hat{M}^{-1}\hat{i}_{k,k+1} + u_{\text{N},k} + h(1-\theta)H_{\text{N}}v_k - h^2\theta(1-\theta)\sigma_c U_{\text{NN}}S\beta_k + h^2\theta(1-\theta)U_{\text{NT}}SD\hat{r}^{\text{r}}_{\text{T},k} + b_{\text{N},k+1} - b_{\text{N},k},
\end{aligned} \tag{93}$$

and then in the tangential direction:

$$\begin{aligned}
u_{\text{T},k+1} =& u_{\text{T},k} + h(1-\theta)H_{\text{T}}v_k + h\theta H_{\text{T}}v_{k+1} + b_{\text{T},k+1} - b_{\text{T},k},\\
=& -h^2\theta^2\sigma_c U_{\text{TN}}S\beta_{k+1} + h\theta X_{\text{TN}}p_{\text{N},k,k+1} + h\theta X_{\text{TT}}D\hat{p}_{\text{T},k,k+1} + h^2\theta^2 U_{\text{TT}}D\hat{r}^{\text{r}}_{\text{T},k+1}\\
&+ h\theta H_{\text{T}}\hat{M}^{-1}\hat{i}_{k,k+1} + u_{\text{T},k} + h(1-\theta)H_{\text{T}}v_k - h^2\theta(1-\theta)\sigma_c U_{\text{TN}}S\beta_k + h^2\theta(1-\theta)U_{\text{TT}}D\hat{r}^{\text{r}}_{\text{T},k} + b_{\text{T},k+1} - b_{\text{T},k},
\end{aligned} \tag{94}$$

where $U_{\text{NN}} = H_{\text{N}}\hat{M}^{-1}H_{\text{N}}^{\top}$ and $U_{\text{TT}} = H_{\text{T}}\hat{M}^{-1}H_{\text{T}}^{\top}$ are the complete Delassus matrices for the normal and tangential degrees of freedom, while $U_{\text{NT}} = H_{\text{N}}\hat{M}^{-1}H_{\text{T}}^{\top}$ and $U_{\text{TN}} = H_{\text{T}}\hat{M}^{-1}H_{\text{N}}^{\top}$ are the Delassus matrices for the interaction terms between the two. The matrices $X_{\text{NN}} = H_{\text{N}}\hat{M}^{-1}\bar{H}_{\text{N}}^{\top}$, $X_{\text{NT}} = H_{\text{N}}\hat{M}^{-1}\bar{H}_{\text{T}}^{\top}$,$X_{\text{TN}} = H_{\text{T}}\hat{M}^{-1}\bar{H}_{\text{N}}^{\top}$ and $X_{\text{TT}} = H_{\text{T}}\hat{M}^{-1}\bar{H}_{\text{T}}^{\top}$ capture the effect of the contact and frictional terms on the cohesive terms, and in this sense these matrices complement the V matrices. Once again the mixed subscripts capture the interaction effects between the opening and sliding modes.

From these expressions, we can easily obtain expressions for u_{N} and u_{T} in terms of the z entries:

$$u_{\text{N},k+1} = -h^2\theta^2\sigma_c U_{\text{NN}}z_2 + h\theta X_{\text{NN}}z_3 + h\theta X_{\text{NT}}Dz_4 + h^2\theta^2 U_{\text{NT}}Dz_6 + q_{u_{\text{N}}}, \tag{95}$$

$$u_{\text{T},k+1} = -h^2\theta^2\sigma_c U_{\text{TN}}z_2 + h\theta X_{\text{TN}}z_3 + h\theta X_{\text{TT}}Dz_4 + h^2\theta^2 U_{\text{TT}}Dz_6 + q_{u_{\text{T}}}, \tag{96}$$

where $q_{u_{\text{N}}} = h\theta H_{\text{N}}\hat{M}^{-1}\hat{i}_{k,k+1} + u_{\text{N},k} + h(1-\theta)H_{\text{N}}v_k - h^2\theta(1-\theta)\sigma_c U_{\text{NN}}S\beta_k + h^2\theta(1-\theta)U_{\text{NT}}D\hat{r}^{\text{r}}_{\text{T},k} + b_{\text{N},k+1} - b_{\text{N},k}$ and $q_{u_{\text{T}}} = h\theta H_{\text{T}}\hat{M}^{-1}\hat{i}_{k,k+1} + u_{\text{T},k} + h(1-\theta)H_{\text{T}}v_k - h^2\theta(1-\theta)\sigma_c U_{\text{TN}}S\beta_k + h^2\theta(1-\theta)U_{\text{TT}}D\hat{r}^{\text{r}}_{\text{T},k} + b_{\text{T},k+1} - b_{\text{T},k}$. The latter expression leads directly to one for w_6:

$$w_6 = -h^2\theta^2\sigma_c D^{\top}U_{\text{TN}}z_2 + h\theta D^{\top}X_{\text{TN}}z_3 + h\theta D^{\top}X_{\text{TT}}Dz_4 + h^2\theta^2 D^{\top}U_{\text{TT}}Dz_6 + \mathbb{1}z_7 + D^{\top}q_{u_{\text{T}}}. \tag{97}$$

Finally, we consider our expression for the slack variable $\xi_{k+1} = A^{\text{r}}{}_{k+1} + \sigma_c\delta_{c,\text{N}}(\beta_{k+1} - \mathbf{1}) + \sigma_c u_{\text{N},k+1} + \sigma_c\gamma|u_{\text{T},k+1}|$ where $\mathbf{1}$ represents a vector of ones, using the expressions of $u_{\text{N},k+1}$ and $u_{\text{T},k+1}$ for all cohesive points. Our expression for ξ_{k+1} features a dependence on an absolute value $|u_{\text{T},k+1}|$. This does not pose any problems for the trailing terms, but must be eliminated for the terms dependant on the entries of z in order to obtain an LCP. As shown in Lemma 2, we have $\beta_{k+1}\sigma_c\gamma|u_{\text{T},k+1}| = \beta_{k+1}\sigma_c\gamma\chi_{k+1}$. For $\beta_{k+1} > 0$, we have $|u_{\text{T},k+1}| = \chi_{k+1}$. For $\beta_{k+1} = 0$ when the interface is broken, we have $|u_{\text{T},k+1}| \geqslant \chi_{k+1}$. However, as noted below in §5, at this point we no longer solve this line as part of the LCP, and so we can calculate ξ_{k+1} as a function of the absolute value of $u_{\text{T},k+1}$ without any difficulty. Hence, in order to form our LCP we substitute χ_{k+1} in place of $|u_{\text{T},k+1}|$, and then substitute (95) into our expression for ξ_{k+1} to obtain

$$\begin{aligned}
\xi_{k+1} =& A^{\text{r}}{}_{k+1} + \sigma_c u_{\text{N},k+1} + \sigma_c\gamma|u_{\text{T},k+1}| + \sigma_c\delta_{c,\text{N}}\left(\beta_{k+1} - \mathbf{1}\right), \\
=& A^{\text{r}}{}_{k+1} + \sigma_c u_{\text{N},k+1} + \sigma_c\gamma\chi_{k+1} + \sigma_c\delta_{c,\text{N}}\left(\beta_{k+1} - \mathbf{1}\right), \\
=& S^{-1}z_1 + \sigma_c\left(\delta_{c,\text{N}}S^{-1} - h^2\theta^2\sigma_c U_{\text{NN}}\right)z_2 + h\theta\sigma_c X_{\text{NN}}z_3 + h\theta\sigma_c X_{\text{NT}}Dz_4 \qquad (98) \\
&+ h^2\theta^2\sigma_c U_{\text{NT}}Dz_6 + \sigma_c\gamma z_7 + \sigma_c\left(q_{u_{\text{N}}} - \delta_{c,\text{N}}\mathbf{1}\right), \qquad (99)
\end{aligned}$$

which gives us the expression for w_2 directly.

In the most general case of multiple cohesive zones with boundary conditions enforced, the $\mathrm{LCP}(L,q)$ is defined by

$$w = \begin{bmatrix} h\lambda_{k+1} \\ \xi_{k+1} \\ v_{\mathrm{N},k+1} + ev_{\mathrm{N},k} \\ \mathbb{1}\zeta_{k+1} + D^\top v_{\mathrm{T},k+1} \\ \mu(p_{\mathrm{N},k,k+1} + h\sigma_c S\beta_{k+\theta}) - \mathbb{1}^\top \hat{p}_{\mathrm{T},k,k+1} \\ \mathbb{1}\chi_{k+1} + D^\top u_{\mathrm{T},k+1} \\ \sigma_c\gamma S\beta_{k+1} - \mathbb{1}^\top \hat{r}^{\mathsf{r}}_{\mathrm{T},k+1} \end{bmatrix}, \quad z = \begin{bmatrix} SA^{\mathsf{r}}{}_{k+1} \\ S\beta_{k+1} \\ p_{\mathrm{N},k,k+1} \\ \hat{p}_{\mathrm{T},k,k+1} \\ \zeta_{k+1} \\ \hat{r}^{\mathsf{r}}_{\mathrm{T},k+1} \\ \chi_{k+1} \end{bmatrix},$$

$$L = \begin{bmatrix} \mathbf{0}^{n\times n} & -S^{-1} & \mathbf{0}^{n\times n} & \mathbf{0}^{n\times 2n} & \mathbf{0}^{n\times n} & \mathbf{0}^{n\times 2n} & \mathbf{0}^{n\times n} \\ S^{-1} & \sigma_c(\delta_{c,\mathrm{N}}S^{-1} - h^2\theta^2\sigma_c U_{\mathrm{NN}}) & h\theta\sigma_c X_{\mathrm{NN}} & h\theta\sigma_c X_{\mathrm{NT}}D & \mathbf{0}^{n\times n} & h^2\theta^2\sigma_c U_{\mathrm{NT}}D & \sigma_c\gamma I \\ \mathbf{0}^{n\times n} & -h\theta\sigma_c V_{\mathrm{NN}} & W_{\mathrm{NN}} & W_{\mathrm{NT}}D & \mathbf{0}^{n\times n} & h\theta V_{\mathrm{NT}}D & \mathbf{0}^{n\times n} \\ \mathbf{0}^{2n\times n} & -h\theta\sigma_c D^\top V_{\mathrm{TN}} & D^\top W_{\mathrm{TN}} & D^\top W_{\mathrm{TT}}D & \mathbb{1} & h\theta D^\top V_{\mathrm{TT}}D & \mathbf{0}^{2n\times n} \\ \mathbf{0}^{n\times n} & h\theta\mu\sigma_c I & \mu I & -\mathbb{1}^\top & \mathbf{0}^{n\times n} & \mathbf{0}^{n\times 2n} & \mathbf{0}^{n\times n} \\ \mathbf{0}^{2n\times n} & -h^2\theta^2\sigma_c D^\top U_{\mathrm{TN}} & h\theta D^\top X_{\mathrm{TN}} & h\theta D^\top X_{\mathrm{TT}}D & \mathbf{0}^{2n\times n} & h^2\theta^2 D^\top U_{\mathrm{TT}}D & \mathbb{1} \\ \mathbf{0}^{n\times n} & \sigma_c\gamma I & \mathbf{0}^{n\times n} & \mathbf{0}^{n\times 2n} & \mathbf{0}^{n\times n} & -\mathbb{1}^\top & \mathbf{0}^{n\times n} \end{bmatrix},$$

$$q = \begin{bmatrix} \beta_k \\ \sigma_c\left(q_{u_{\mathrm{N}}} - \delta_{c,\mathrm{N}}\mathbf{1}\right) \\ \bar{H}_{\mathrm{N}}\hat{M}^{-1}\hat{i}_{k,k+1} - h(1-\theta)\sigma_c V_{\mathrm{NN}}S\beta_k + h(1-\theta)V_{\mathrm{NT}}D\hat{r}^{\mathsf{r}}_{\mathrm{T},k} + ev_{\mathrm{N},k} \\ D^\top\bar{H}_{\mathrm{T}}\hat{M}^{-1}\hat{i}_{k,k+1} - h(1-\theta)\sigma_c D^\top V_{\mathrm{TN}}S\beta_k + h(1-\theta)D^\top V_{\mathrm{TT}}D\hat{r}^{\mathsf{r}}_{\mathrm{T},k} \\ h(1-\theta)\mu\sigma_c S\beta_k \\ D^\top q_{u_{\mathrm{T}}} \\ \mathbf{0}^n \end{bmatrix}. \tag{100}$$

where $\mathbf{0}^{a\times b}$ corresponds to a matrix of zeros with a rows and b columns.

4.3 Existence of the solution of the discrete LCP

We want to show that the system $\mathrm{LCP}(L,q)$ has at least one solution, although we are unable to mathematically guarantee its uniqueness. As a consequence, whether our system is well-posed is an open question, but we do not know of any existing tools or results that would allow this property to be demonstrated.

Assumption 1. *The time-step h is chosen small enough that $\sigma_c(\delta_{c,N}S^{-1} - h^2\theta^2\sigma_c U_{NN})$ is positive definite.*

Since $\sigma_c\delta_{c,\mathrm{N}}S^{-1}$ is a positive definite matrix, a time-step exists such that Assumption 1 holds.

Lemma 1. *Under Assumption 1, L is copositive on the positive orthant.*

Proof Let us recall that L is copositive on the positive orthant if $z^\top Lz \geqslant 0$ for all $z \geqslant 0$. Since $z^\top Lz = \dfrac{1}{2}z^\top(L+L^\top)z$, we first compute the symmetric part of L

$$\frac{1}{2}\left(L+L^\top\right) = \begin{bmatrix} \mathbf{0}^{n\times n} & \mathbf{0}^{n\times n} & \mathbf{0}^{n\times n} & \mathbf{0}^{n\times 2n} & \mathbf{0}^{n\times n} & \mathbf{0}^{n\times 2n} & \mathbf{0}^{n\times n} \\ \mathbf{0}^{n\times n} & \sigma_c(\delta_{c,\mathrm{N}}S^{-1} - h^2\theta^2\sigma_c U_{\mathrm{NN}}) & \mathbf{0}^{n\times n} & \mathbf{0}^{n\times 2n} & \frac{1}{2}h\theta\mu\sigma_c I & \mathbf{0}^{n\times 2n} & \sigma_c\gamma I \\ \mathbf{0}^{n\times n} & \mathbf{0}^{n\times n} & W_{\mathrm{NN}} & W_{\mathrm{NT}}D & \frac{1}{2}\mu I & h\theta V_{\mathrm{NT}}D & \mathbf{0}^{n\times n} \\ \mathbf{0}^{2n\times n} & \mathbf{0}^{2n\times n} & D^\top W_{\mathrm{TN}} & D^\top W_{\mathrm{TT}}D & \mathbf{0}^{2n\times n} & h\theta D^\top V_{\mathrm{TT}}D & \mathbf{0}^{2n\times n} \\ \mathbf{0}^{n\times n} & \frac{1}{2}h\theta\mu\sigma_c I & \frac{1}{2}\mu I & \mathbf{0}^{n\times 2n} & \mathbf{0}^{n\times n} & \mathbf{0}^{n\times 2n} & \mathbf{0}^{n\times n} \\ \mathbf{0}^{2n\times n} & \mathbf{0}^{2n\times n} & h\theta D^\top X_{\mathrm{TN}} & h\theta D^\top X_{\mathrm{TT}}D & \mathbf{0}^{2n\times n} & h^2\theta^2 D^\top U_{\mathrm{TT}}D & \mathbf{0}^{2n\times n} \\ \mathbf{0}^{n\times n} & \sigma_c\gamma I & \mathbf{0}^{n\times n} & \mathbf{0}^{n\times 2n} & \mathbf{0}^{n\times n} & \mathbf{0}^{n\times 2n} & \mathbf{0}^{n\times n} \end{bmatrix}. \tag{101}$$

By splitting the matrix, it is possible to obtain the following relation:

$$\begin{aligned}\frac{1}{2}z^\top\left(L+L^\top\right)z =& z_2^\top\left(\sigma_c(\delta_{c,\text{N}}S^{-1}-h^2\theta^2\sigma_c U_{\text{NN}})\right)z_2\\ &+\begin{bmatrix}z_3\\z_4\\z_6\end{bmatrix}^\top\begin{bmatrix}W_{\text{NN}} & W_{\text{NT}}D & h\theta V_{\text{NT}}D\\ D^\top W_{\text{TN}} & D^\top W_{\text{TT}}D & h\theta D^\top V_{\text{TT}}D\\ h\theta D^\top X_{\text{TN}} & h\theta D^\top X_{\text{TT}}D & h^2\theta^2 D^\top U_{\text{TT}}D\end{bmatrix}\begin{bmatrix}z_3\\z_4\\z_6\end{bmatrix}\\ &+h\theta\mu\sigma_c z_5^\top z_2+2\sigma_c\gamma z_7^\top z_2+\mu z_3^\top z_5.\end{aligned}\tag{102}$$

Under Assumption 1, the first term is nonnegative

$$z_2^\top\left(\sigma_c(\delta_{c,\text{N}}S^{-1}-h^2\theta^2\sigma_c U_{\text{NN}})\right)z_2\geqslant 0,\tag{103}$$

and

$$h\theta\mu\sigma_c z_5^\top z_2+2\sigma_c\gamma z_7^\top z_2+\mu z_3^\top z_5\geqslant 0 \text{ for all } z\geqslant 0.\tag{104}$$

For the remaining term in (102), let us rewrite the matrix as

$$\begin{bmatrix}W_{\text{NN}} & W_{\text{NT}}D & h\theta V_{\text{NT}}D\\ D^\top W_{\text{TN}} & D^\top W_{\text{TT}}D & h\theta D^\top V_{\text{TT}}D\\ h\theta D^\top X_{\text{TN}} & h\theta D^\top X_{\text{TT}}D & h^2\theta^2 D^\top U_{\text{TT}}D\end{bmatrix}=\begin{bmatrix}I & \mathbf{0}^{n\times 2n} & \mathbf{0}^{n\times 2n}\\ \mathbf{0}^{n\times n} & D & \mathbf{0}^{n\times 2n}\\ \mathbf{0}^{n\times n} & \mathbf{0}^{n\times 2n} & h\theta D\end{bmatrix}^\top\begin{bmatrix}\bar{H}_{\text{N}}\\ \bar{H}_{\text{T}}\\ H_{\text{T}}\end{bmatrix}\hat{M}^{-1}\begin{bmatrix}\bar{H}_{\text{N}}\\ \bar{H}_{\text{T}}\\ H_{\text{T}}\end{bmatrix}^\top\begin{bmatrix}I & \mathbf{0}^{n\times 2n} & \mathbf{0}^{n\times 2n}\\ \mathbf{0}^{n\times n} & D & \mathbf{0}^{n\times 2n}\\ \mathbf{0}^{n\times n} & \mathbf{0}^{n\times 2n} & h\theta D\end{bmatrix}.\tag{105}$$

Since $\hat{M}^{-1}$ is a positive definite matrix, and $ABA^\top$ is a positive semi-definite matrix if A is non-singular and B is rank-deficient (which is the case for $\hat{M}^{-1}$ and D respectively), the matrix on the left-hand side of (105) is a positive semi-definite matrix, and we can conclude that

$$\begin{bmatrix}z_3\\z_4\\z_6\end{bmatrix}^\top\begin{bmatrix}W_{\text{NN}} & W_{\text{NT}}D & h\theta V_{\text{NT}}D\\ D^\top W_{\text{TN}} & D^\top W_{\text{TT}}D & h\theta D^\top V_{\text{TT}}D\\ h\theta D^\top X_{\text{TN}} & h\theta D^\top X_{\text{TT}}D & h^2\theta^2 D^\top U_{\text{TT}}D\end{bmatrix}\begin{bmatrix}z_3\\z_4\\z_6\end{bmatrix}\geqslant 0.\tag{106}$$

Each component of the sum in (102) is nonnegative, and so L is copositive on the positive orthant. □

Proposition 1. *If Assumption 1 holds then the* $\text{LCP}(L,q)$ *has a solution for all* $\beta_k\geqslant 0$.

Proof Let us first compute the set of solutions of the homogeneous $\text{LCP}(L,0)$, also called the kernel of the LCP, given by

$$\mathcal{K}(L)=\{z\geqslant 0, Lz\geqslant 0, z^\top Lz=0\}.\tag{107}$$

Using (102) and (105), the relation $z^\top Lz=0$ with Assumption 1 is equivalent to

$$z_2=0,\bar{H}_{\text{N}}^\top z_3=0,\bar{H}_{\text{T}}^\top Dz_4=0,H_{\text{T}}^\top Dz_6=0,\tag{108}$$

for $h\theta>0$. The relations $z\geqslant 0, Lz\geqslant 0$ further implies

$$z_1=0,z_5\geqslant 0,z_7\geqslant 0.\tag{109}$$

The set of solutions of the homogeneous $\text{LCP}(L,0)$ is then given by

$$\mathcal{K}(L)=\{z\mid z_1=0,z_2=0,\bar{H}_{\text{N}}^\top z_3=0,\bar{H}_{\text{T}}^\top Dz_4=0,z_5\geqslant 0,H_{\text{T}}^\top Dz_6=0,z_7\geqslant 0\}.\tag{110}$$

For $z\in\mathcal{K}(L)$, we have

$$\begin{aligned}q^\top z=&\left[\bar{H}_{\text{N}}\left(\hat{M}^{-1}\hat{i}_{k,k+1}-h(1-\theta)\sigma_c\hat{M}^{-1}H_{\text{N}}S\beta_k+h(1-\theta)\hat{M}^{-1}H_{\text{T}}D\hat{r}^{\text{r}}_{\text{T},k}+ev_k\right)\right]^\top z_3\\ &+\left[D^\top\bar{H}_{\text{T}}\left(\hat{M}^{-1}\hat{i}_{k,k+1}-h(1-\theta)\sigma_c\hat{M}^{-1}H_{\text{N}}S\beta_k+h(1-\theta)\hat{M}^{-1}H_{\text{T}}D\hat{r}^{\text{r}}_{\text{T},k}\right)\right]^\top z_4\\ &+\left[h(1-\theta)\mu\sigma_c S\beta_k\right]^\top z_5+\Big[D^\top H_{\text{T}}\Big(h\theta\hat{M}^{-1}\hat{i}_{k,k+1}+h(1-\theta)v_k\\ &-h^2\theta(1-\theta)\sigma_c\hat{M}^{-1}H_{\text{N}}S\beta_k+h^2\theta(1-\theta)\hat{M}^{-1}H_{\text{T}}D\hat{r}^{\text{r}}_{\text{T},k}+v_k\Big)+D^\top(b_{\text{T},k+1}-b_{\text{T},k})\Big]^\top z_6.\end{aligned}\tag{111}$$

As the transpose of a matrix product $(AB)^\top = B^\top A^\top$, we can look at the first two terms of (111) and see that we will have a vector left-multiplying $\bar{H}_{\text{N}}^\top z_3$ and another vector left-multiplying $\bar{H}_{\text{T}}^\top Dz_4$. Similarly, looking at the first part of the last term, we will have a vector left-multiplying $H_{\text{T}}^\top Dz_6$. From (108) we know that $\bar{H}_{\text{N}}^\top z_3 = 0, \bar{H}_{\text{T}}^\top Dz_4 = 0, H_{\text{T}}^\top Dz_6$ which allows us to simplify (111) as

$$q^\top z = \left[h(1-\theta)\mu\sigma_c S\beta_k\right] z_5^\top + (b_{\text{T},k+1} - b_{\text{T},k})^\top Dz_6. \tag{112}$$

Since $b_{\text{T},k+1} - b_{\text{T},k} = H_{\text{T}}(q_{k+1} - q_k) = hH_{\text{T}}v_{k+\theta}$, the equations can be further simplified to

$$\begin{aligned} q^\top z &= \left[h(1-\theta)\mu\sigma_c S\beta_k\right] z_5^\top + (hH_{\text{T}}v_{k+\theta})^\top Dz_6, \\ &= \left[h(1-\theta)\mu\sigma_c S\beta_k\right] z_5^\top + hv_{k+\theta}^\top H_{\text{T}}^\top Dz_6, \\ &= \left[h(1-\theta)\mu\sigma_c S\beta_k\right] z_5^\top, \end{aligned} \tag{113}$$

because $H_{\text{T}}^\top Dz_6 = 0$ from (108). For $\beta_k \geqslant 0$, we can conclude

$$q^\top z \geqslant 0 \text{ for all } z \in \mathcal{K}(L). \tag{114}$$

Since L is a copositive matrix, the condition (114) implies that the $\text{LCP}(L, q)$ has a solution by virtue of Theorem 3.8.6 in Cottle et al. (2009). □

4.4 Discrete energy balance

In this section, we will show that the time-stepping scheme described in (82) satisfies the discrete energy balance, even in the case of impacts. We will start by considering the momentum balance given in (61), and multiplying by $\frac{1}{2}\left(v^+ + v^-\right)^\top$:

$$\begin{aligned} \frac{1}{2}\left(v^+ + v^-\right)^\top M\,\mathrm{d}v + \frac{1}{2}\left(v^+ + v^-\right)^\top Ku\,\mathrm{d}t =& \frac{1}{2}\left(v^+ + v^-\right)^\top F\,\mathrm{d}t + \frac{1}{2}\left(v^+ + v^-\right)^\top H_{\text{N}}^\top\left(\mathrm{d}p_{\text{N}} - S\sigma_c\beta\,\mathrm{d}t\right) \\ &+ \frac{1}{2}\left(v^+ + v^-\right)^\top H_{\text{T}}^\top\left(Sr_{\text{T}}^{\text{r}}\,\mathrm{d}t + \mathrm{d}p_{\text{T}}\right). \end{aligned} \tag{115}$$

As $v^+\,\mathrm{d}t = v^-\,\mathrm{d}t = v\,\mathrm{d}t$and M and K are symmetric matrices, we are able to rewrite (115) as

$$\begin{aligned} \mathrm{d}\left(\frac{1}{2}v^\top Mv\right) + \mathrm{d}\left(\frac{1}{2}u^\top Ku\right) =& v^\top F\,\mathrm{d}t + \left[\frac{1}{2}H_{\text{N}}\left(v^+ + v^-\right)\right]^\top \mathrm{d}p_{\text{N}} - v_{\text{N}}^\top S\sigma_c\beta\,\mathrm{d}t \\ &+ v_{\text{T}}Sr_{\text{T}}^{\text{r}}\,\mathrm{d}t + \left[\frac{1}{2}H_{\text{T}}\left(v^+ + v^-\right)\right]^\top \mathrm{d}p_{\text{T}}. \end{aligned} \tag{116}$$

As the space-discretised kinetic and strain energies are given by $\mathsf{K} = \frac{1}{2}v^\top Mv$ and $\mathsf{U} = \frac{1}{2}u^\top Ku$, we can write

$$\mathrm{d}\mathsf{K} + \mathrm{d}\mathsf{U} = v^\top F\,\mathrm{d}t + \frac{1}{2}\left(v_{\text{N}}^+ + v_{\text{N}}^-\right)^\top \mathrm{d}p_{\text{N}} - v_{\text{N}}^\top S\sigma_c\beta\,\mathrm{d}t + v_{\text{T}}^\top Sr_{\text{T}}^{\text{r}}\,\mathrm{d}t + \frac{1}{2}\left(v_{\text{T}}^+ + v_{\text{T}}^-\right)^\top \mathrm{d}p_{\text{T}}. \tag{117}$$

We now specify the space-discretised version of the continuous fracture energy given in (41):

$$\mathsf{G} = \int \sigma_c S\beta v_{\text{N}} + v_{\text{T}}r_{\text{T}}^{\text{r}}\,\mathrm{d}t, \tag{118}$$

which lets us write the energy balance of the space-discretised system:

$$\mathrm{d}\mathsf{K} + \mathrm{d}\mathsf{U} + \mathrm{d}\mathsf{G} = v^\top F\,\mathrm{d}t + \frac{1}{2}\left(v_{\text{N}}^+ + v_{\text{N}}^-\right)^\top \mathrm{d}p_{\text{N}} + \frac{1}{2}\left(v_{\text{T}}^+ + v_{\text{T}}^-\right)^\top \mathrm{d}p_{\text{T}}. \tag{119}$$

Let us define the total energy of the system as $\mathsf{T} = \mathsf{K} + \mathsf{U} + \mathsf{G}$, and integrate (119) over a time interval of $(t_1, t_2]$. We thus obtain the incremental energy balance:

$$\Delta\mathsf{T} = \mathsf{T}^+(t_2) - \mathsf{T}^-(t_1) = \Delta W_{\text{ext}} + \Delta W_{\text{impact}} + \Delta W_{\text{friction}}, \tag{120}$$

where the increment of work done by the external forces, impact and friction is given by

$$\Delta W_{\text{ext}} = \int_{t_1}^{t_2} v^\top F\,\mathrm{d}t, \tag{121}$$

$$\Delta W_{\text{impact}} = \int_{(t_1,t_2]} \frac{1}{2}\left(v_{\text{N}}^+ + v_{\text{N}}^-\right)^\top \mathrm{d}p_{\text{N}}, \tag{122}$$

$$\Delta W_{\text{friction}} = \int_{(t_1,t_2]} \frac{1}{2}\left(v_{\text{T}}^+ + v_{\text{T}}^-\right)^\top \mathrm{d}p_{\text{T}}. \tag{123}$$

The contact law specified in (55) has been shown to dissipate energy *i.e.* $\Delta W_{\text{impact}} \leqslant 0$ (Acary, 2016). We can examine the frictional laws specified in (62), noting that $-\,\mathrm{d}p_{\text{T}} \in \mu(\mathrm{d}p_{\text{N}} + S\beta\sigma_c\,\mathrm{d}t)\,\mathrm{sgn}(v_{\text{T}})$ when $v_{\text{T}} = 0$, in which case $\frac{1}{2}\left(v_{\text{T}}^{+} + v_{\text{T}}^{-}\right)^{\top}\mathrm{d}p_{\text{T}} = 0$, or $-\,\mathrm{d}p_{\text{T}} = \mu(\mathrm{d}p_{\text{N}} + S\beta\sigma_c\,\mathrm{d}t)\,\mathrm{sgn}(v_{\text{T}})$ when $v_{\text{T}} \neq 0$, in which case $\frac{1}{2}\left(v_{\text{T}}^{+} + v_{\text{T}}^{-}\right)^{\top}\mathrm{d}p_{\text{T}} \leqslant 0$. Hence, we can conclude that $\Delta W_{\text{friction}} \leqslant 0$. We can in turn conclude that

$$\Delta \mathsf{T} - \Delta W_{\text{ext}} = \Delta W_{\text{impact}} + \Delta W_{\text{friction}} \leqslant 0. \tag{124}$$

The space-discretised incremental energy balance is thus either conservative or dissipative, that is to say that no spurious energy is added to the system. We now show that the equivalent incremental energy balance is satisfied by the space-and-time-discretised scheme. Following the method in Acary (2016), the variation of the sum of the kinetic and elastic energy over the time-step is given by

$$\begin{aligned}\Delta \mathsf{K}_{k,k+1} + \Delta \mathsf{U}_{k,k+1} = \left(\frac{1}{2} - \theta\right)\left(\|v_{k+1} - v_k\|_M^2 + \|u_{k+1} - u_k\|_K^2\right)\\ + h v_{k+\theta}^{\top} F_{k+\theta} + v_{\text{N},k+\theta} p_{\text{N},k,k+1} - h v_{\text{N},k+\theta}^{\top}\sigma_c S\beta_{k+\theta}\\ + h v_{\text{T},k+\theta}^{\top} S r_{\text{T},k+\theta}^{\mathsf{r}} + v_{\text{T},k+\theta} p_{\text{T},k,k+1},\end{aligned} \tag{125}$$

where $\|\cdot\|_M^2$ and $\|\cdot\|_K^2$ are the 2-norm and 2-seminorm induced by the matrices M and K respectively.Now, let us define the discrete approximations of the increment of fracture energy, the increment of external work, the increment of contact work and the increment of frictional work:

$$\Delta \mathsf{G}_{k,k+1} = h\left(v_{\text{N},k+\theta}^{\top}\sigma_c S\beta_{k+\theta} + v_{\text{T},k+\theta}^{\top} r_{\text{T},k+\theta}^{\mathsf{r}}\right) \approx \int \sigma_c S\beta v_{\text{N}} + v_{\text{T}} r_{\text{T}}^{\mathsf{r}}\,\mathrm{d}t, \tag{126}$$

$$\Delta \mathsf{W}_{\text{ext},k,k+1} = h v_{k+\theta}^{\top} F_{k+\theta} \approx \int_{t_k}^{t_{k+1}} v^{\top} F\,\mathrm{d}t, \tag{127}$$

$$\Delta \mathsf{W}_{\text{impact},k,k+1} = v_{\text{N},k+\theta}^{\top} p_{\text{N},k,k+1}, \tag{128}$$

$$\Delta \mathsf{W}_{\text{friction},k,k+1} = v_{\text{T},k+\theta}^{\top} p_{\text{T},k,k+1}, \tag{129}$$

where we have used the approximations given in (63) and (64). Now, provided $\frac{1}{2} < \theta \leqslant 1$, we have an estimate for the variation of the energy given by

$$\Delta \mathsf{K}_{k,k+1} + \Delta \mathsf{U}_{k,k+1} + \Delta \mathsf{G}_{k,k+1} - \Delta \mathsf{W}_{\text{ext},k,k+1} < \Delta \mathsf{W}_{\text{impact},k,k+1} + \Delta \mathsf{W}_{\text{friction},k,k+1}. \tag{130}$$

It has been shown (Acary, 2016) that our chosen discretisation of the impact law leads to

$$\mathsf{W}_{\text{impact},k,k+1} \leqslant 0 \text{ if } \theta \leqslant \frac{1}{1+e}. \tag{131}$$

Considering the time-discretised friction law, we have

$$\begin{aligned} v_{\text{T},k+\theta}^{\top} p_{\text{T},k,k+1} &= (1-\theta) v_{\text{T},k} p_{\text{T},k,k+1} + \theta v_{\text{T},k+1} p_{\text{T},k,k+1},\\ &= -(1-\theta) v_{\text{T},k}\mu(p_{\text{N},k,k+1} + S\beta_{k+\theta}\sigma_c)\,\mathrm{sgn}(v_{\text{T},k+1}) - \theta v_{\text{T},k+1}\mu(p_{\text{N},k,k+1} + S\beta_{k+\theta}\sigma_c)\,\mathrm{sgn}(v_{\text{T},k+1}) \end{aligned} \tag{132}$$

Again following Acary (2016), if no contact exists $p_{\text{T},k,k+1} = 0$, while if there is contact $p_{\text{N},k,k+1} \geqslant 0$, and β_k and β_{k+1} always remain $\geqslant 0$, and thus so does $\beta_{k+\theta}$. Thus the term $\mu(p_{\text{N},k,k+1} + S\beta_{k+\theta}\sigma_c) \geqslant 0$. The product of $v_{\text{T},k+1}$ and $\mathrm{sgn}(v_{\text{T},k+1})$ is also always non-negative. In specifying (57), we made the assumption that the sign of the velocity does not change over a time-step, and so the product of $v_{\text{T},k}$ and $\mathrm{sgn}(v_{\text{T},k+1})$ is also always non-negative. Thus, we can conclude that the expression in (132) must be non-positive for any values of θ, $v_{\text{T},k+1}$ and $p_{\text{T},k,k+1}$, and thus $\Delta \mathsf{W}_{\text{friction},k,k+1} \leqslant 0$.

We are thus able to obtain the result

$$\Delta \mathsf{K}_{k,k+1} + \Delta \mathsf{U}_{k,k+1} + \Delta \mathsf{G}_{k,k+1} - \Delta \mathsf{W}_{\text{ext},k,k+1} \leqslant \Delta \mathsf{W}_{\text{impact},k,k+1} + \Delta \mathsf{W}_{\text{friction},k,k+1} \leqslant 0. \tag{133}$$

For $\theta = \frac{1}{2}$, we can sharpen this to

$$\Delta \mathsf{K}_{k,k+1} + \Delta \mathsf{U}_{k,k+1} + \Delta \mathsf{G}_{k,k+1} - \Delta \mathsf{W}_{\text{ext},k,k+1} = \Delta \mathsf{W}_{\text{impact},k,k+1} + \Delta \mathsf{W}_{\text{friction},k,k+1} \leqslant 0. \tag{134}$$

We can compare this with the continuous-in-space-and-time discrete energy balance in (43), and see that the discretised scheme does not spuriously add energy into the system, and is in fact dissipative. In the special case of no friction and contact, the integration scheme is symplectic.

5 Numerical simulations

We implement our discrete system in Python, and resolve the LCP using Siconos (Acary et al., 2019). The LCP (100) can be solved reliably by Lemke's algorithm (Lemke and Howson, Jr., 1964). Specifically, Lemke's algorithm provides a guarantee that if solutions of the LCP exist (as we have proved above), then the algorithm will find one. As in Collins-Craft et al. (2022), in implementation we remove the entries corresponding to the cohesive zone when β is less than a certain threshold, namely $1 \times 10^{-}3$, compared to $\times 10^{-12}$ in Collins-Craft et al. (2022). This larger threshold is chosen for numerical efficiency, as the tangential constraints are two-sided *i.e.* $\hat{r}^{\mathsf{r}}_{\mathrm{T},k+1} \geqslant 0$ and $\mathbb{1}^{\top}\hat{r}^{\mathsf{r}}_{\mathrm{T},k+1} \leqslant \sigma_c\gamma S\beta_{k+1}$, which becomes difficult for the solver to satisfy at small values of β without the use of very small time-steps. While in principle this can be addressed by the use of an enumerative solver, this becomes unworkable for systems of even moderate size, as the scaling properties of enumerative solvers are extremely unfavourable. Hence, we favour the less elegant, but simpler, solution of simply removing these lines from the problem when their resolution becomes overly onerous. We similarly remove those entries corresponding to the contact problem when $u_{\mathrm{N},k} + \dfrac{h}{2}v_{\mathrm{N},k} \geqslant 1 \times 10^{-8}$. The effect of both of these removal procedures is to make the LCP smaller, and thus increase the speed of solution.

5.1 Quasi-static scalar case with elastic spring

In the interests of demonstrating the benefits of working with the dynamic formulation in (100), we demonstrate a pathology that can arise in quasi-static systems. We consider the case of an elastic spring bound to a rigid substrate at one end, but otherwise free to move, in the spirit of Acary and Monerie (2006) and Chaboche et al. (2001).

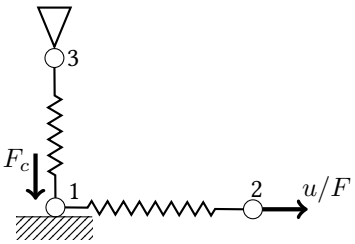

Figure 3: We model the elastic spring as two nodes connected by a linear elastic material. Node 1 is bound to the rigid substrate and has a normal confining force applied to it while node 2 has a controlled displacement or force applied to it. We add a spring in the vertical direction and forbid any displacements at the far end.

We are obliged to add a vertical spring to the system, as in the quasi-static case an absence of stiffness in the normal direction causes the system to be insensitive to the applied confining force and changes in the elasticity of the spring.

We apply a fully implicit discretisation of the system (*i.e.* $\theta = 1$), and work with the contact and friction forces, rather than percussions. D and $\mathbb{1}$ retain their meaning as before. We will make no distinction between the contact and cohesion nodes, so we set $H = \bar{H}$. Consequently there is no distinction between the Delassus matrices $U, V, W, X = HK^{-1}H$ (other than those due to the selection of tangential and normal degrees of freedom), so we will denote all of them as U. Our global elastic-cohesive-frictional-contact problem is thus

$$
\begin{cases}
Ku_{k+1} = F_{k+1} - \sigma_c H_{\mathrm{N}}^{\top} S\beta_{k+1} + H_{\mathrm{N}}^{\top} Sr_{\mathrm{N},k+1} + H_{\mathrm{T}}^{\top} D\hat{r}^{\mathsf{ir}}_{\mathrm{T},k+1} + H_{\mathrm{T}}^{\top} D\hat{r}^{\mathsf{r}}_{\mathrm{T},k+1}, \\
Sr^{\mathsf{r}}_{\mathrm{T},k+1} = D\hat{r}^{\mathsf{r}}_{\mathrm{T},k+1}, \\
Sr^{\mathsf{ir}}_{\mathrm{T},k+1} = D\hat{r}^{\mathsf{ir}}_{\mathrm{T},k+1}, \\
u_{k+1} = u_k + hv_{k+1}, \\
u_{\mathrm{N},k+1} = H_{\mathrm{N}}u_{k+1} + b_{\mathrm{N},k+1}, \quad u_{\mathrm{T},k+1} = H_{\mathrm{T}}u_{k+1} + b_{\mathrm{T},k+1}, \quad v_{\mathrm{T},k+1} = H_{\mathrm{T}}v_{k+1}, \\
\beta_{k+1} = \beta_k - h\lambda_{k+1}, \\
\sigma_c\delta_{c,\mathrm{N}}(\beta_{k+1} - 1) + \sigma_c u_{\mathrm{N},k+1} + \sigma_c\gamma|u_{\mathrm{T},k+1}| + A^{\mathsf{r}}{}_{k+1} = \xi_{k+1}, \\
\nu_{k+1} = r_{\mathrm{N},k+1} + \sigma_c\beta_{k+1}, \\
0 \leqslant SA^{\mathsf{r}}{}_{k+1} \perp \lambda_{k+1} \geqslant 0, \\
0 \leqslant S\beta_{k+1} \perp \xi_{k+1} \geqslant 0, \\
0 \leqslant S\nu_{k+1} \perp u_{\mathrm{N},k+1} \geqslant 0, \\
0 \leqslant \hat{r}_{\mathrm{T},k,k+1} \perp \mathbb{1}\zeta_{k+1} + D^{\top}v_{\mathrm{T},k+1} \geqslant 0, \\
0 \leqslant \zeta_{k+1} \perp \mu\nu_{k+1} - \mathbb{1}^{\top}\hat{r}^{\mathsf{ir}}_{\mathrm{T},k+1} \geqslant 0, \\
0 \leqslant \hat{r}^{\mathsf{r}}_{\mathrm{T},k+1} \perp \mathbb{1}\chi_{k+1} + D^{\top}u_{\mathrm{T},k+1} \geqslant 0, \\
0 \leqslant \chi_{k+1} \perp S\beta_{k+1}\sigma_c\gamma - \mathbb{1}^{\top}\hat{r}^{\mathsf{r}}_{\mathrm{T},k+1} \geqslant 0.
\end{cases}
\tag{135}
$$

Establishing our complementarity vectors w and z as

$$w = \begin{bmatrix} h\lambda_{k+1} \\ \xi_{k+1} \\ u_{\mathrm{N},k+1} \\ \mathbb{1}h\zeta_{k+1} + D^\top h v_{\mathrm{T},k+1} \\ \mu S\nu - \mathbb{1}^\top \hat{r}^{\mathsf{ir}}_{\mathrm{T},k+1} \\ \mathbb{1}\chi_{k+1} + D^\top u_{\mathrm{T},k+1} \\ \sigma_c \gamma S\beta_{k+1} - \mathbb{1}^\top \hat{r}^{\mathsf{r}}_{\mathrm{T},k+1} \end{bmatrix}, \quad z = \begin{bmatrix} SA^{\mathsf{r}}{}_{k+1} \\ S\beta_{k+1} \\ S\nu_{k+1} \\ \hat{r}^{\mathsf{ir}}_{\mathrm{T},k+1} \\ h\zeta_{k+1} \\ \hat{r}^{\mathsf{r}}_{\mathrm{T},k+1} \\ \chi_{k+1} \end{bmatrix}, \tag{136}$$

where we consider hv_{T} and $h\zeta_{k+1}$ to avoid an ill-conditioned matrix as $h \to 0$. We can begin re-arranging our equations to form the LCP proper. Once again, we obtain w_1 trivially as $w_1 = h\lambda_{k+1} = -S^{-1}z_2 + \beta_k$, w_5 as $w_5 = \mu z_3 - \mathbb{1}^\top z_4$ and w_7 as $w_7 = \sigma_c \gamma z_2 - \mathbb{1}^\top z_6$.

Then, assuming a modification of K and F to take into account the boundary conditions, we have

$$\begin{aligned} Ku_{k+1} &= F_{k+1} - \sigma_c H_{\mathrm{N}}^\top S\beta_{k+1} + H_{\mathrm{N}}^\top S\nu_{k+1} + H_{\mathrm{T}}^\top D\hat{r}^{\mathsf{ir}}_{\mathrm{T},k+1} + H_{\mathrm{T}}^\top D\hat{r}^{\mathsf{r}}_{\mathrm{T},k+1}, \\ K\left(u_k + hv_{k+1}\right) &= F_{k+1} - \sigma_c H_{\mathrm{N}}^\top S\beta_{k+1} + H_{\mathrm{N}}^\top S\nu_{k+1} + H_{\mathrm{T}}^\top D\hat{r}^{\mathsf{ir}}_{\mathrm{T},k+1} + H_{\mathrm{T}}^\top D\hat{r}^{\mathsf{r}}_{\mathrm{T},k+1}, \\ hv_{k+1} &= K^{-1}\left(-\sigma_c H_{\mathrm{N}}^\top S\beta_{k+1} + H_{\mathrm{N}}^\top S\nu_{k+1} + H_{\mathrm{T}}^\top D\hat{r}^{\mathsf{ir}}_{\mathrm{T},k+1} + H_{\mathrm{T}}^\top D\hat{r}^{\mathsf{r}}_{\mathrm{T},k+1} + F_{k+1} - Ku_k\right). \end{aligned} \tag{137}$$

Applying the tangential selection matrix H_{T} we obtain

$$\begin{aligned} hv_{\mathrm{T},k+1} &= -\sigma_c U_{\mathrm{TN}} S\beta_{k+1} + U_{\mathrm{TN}} S\nu_{k+1} + U_{\mathrm{TT}} D\hat{r}^{\mathsf{ir}}_{\mathrm{T},k+1} + U_{\mathrm{TT}} D\hat{r}^{\mathsf{r}}_{\mathrm{T},k+1} + H_{\mathrm{T}} K^{-1} F_{k+1} - H_{\mathrm{T}} u_k, \\ hv_{\mathrm{T},k+1} &= -\sigma_c U_{\mathrm{TN}} z_2 + U_{\mathrm{TN}} z_3 + U_{\mathrm{TT}} D z_4 + U_{\mathrm{TT}} D z_6 + H_{\mathrm{T}} K^{-1} F_{k+1} - H_{\mathrm{T}} u_k, \end{aligned} \tag{138}$$

from which we can obtain very directly w_4:

$$w_4 = -\sigma_c D^\top U_{\mathrm{TN}} z_2 + D^\top U_{\mathrm{TN}} z_3 + D^\top U_{\mathrm{TT}} D z_4 + \mathbb{1} z_5 + D^\top U_{\mathrm{TT}} D z_6 + D^\top H_{\mathrm{T}} K^{-1} F_{k+1} - D^\top H_{\mathrm{T}} u_k. \tag{139}$$

Now, we determine the normal displacement:

$$\begin{aligned} u_{\mathrm{N},k+1} &= H_{\mathrm{N}} u_{k+1} + b_{\mathrm{N},k+1}, \\ &= H_{\mathrm{N}} h v_{k+1} + H_{\mathrm{N}} u_k + b_{\mathrm{N},k+1}, \\ &= H_{\mathrm{N}} K^{-1}\left(-\sigma_c H_{\mathrm{N}}^\top S\beta_{k+1} + H_{\mathrm{N}}^\top S\nu_{k+1} + H_{\mathrm{T}}^\top D\hat{r}^{\mathsf{ir}}_{\mathrm{T},k+1} + H_{\mathrm{T}}^\top D\hat{r}^{\mathsf{r}}_{\mathrm{T},k+1} + F_{k+1} - Ku_k\right) + H_{\mathrm{N}} u_k + b_{\mathrm{N},k+1}, \\ &= -\sigma_c U_{\mathrm{NN}} S\beta_{k+1} + U_{\mathrm{NN}} S\nu_{k+1} + U_{\mathrm{NT}} D\hat{r}^{\mathsf{ir}}_{\mathrm{T},k+1} + U_{\mathrm{NT}} D\hat{r}^{\mathsf{r}}_{\mathrm{T},k+1} + H_{\mathrm{N}} K^{-1} F_{k+1} + b_{\mathrm{N},k+1}, \\ &= -\sigma_c U_{\mathrm{NN}} z_2 + U_{\mathrm{NN}} z_3 + U_{\mathrm{NT}} D z_4 + U_{\mathrm{NT}} D z_6 + H_{\mathrm{N}} K^{-1} F_{k+1} + b_{\mathrm{N},k+1}, \end{aligned} \tag{140}$$

which gives w_3 directly. Similarly, we obtain the tangential displacement by

$$\begin{aligned} u_{\mathrm{T},k+1} &= H_{\mathrm{T}} u_{k+1} + b_{\mathrm{T},k+1}, \\ &= H_{\mathrm{T}} h v_{k+1} + H_{\mathrm{T}} u_k + b_{\mathrm{T},k+1}, \\ &= H_{\mathrm{T}} K^{-1}\left(-\sigma_c H_{\mathrm{N}}^\top S\beta_{k+1} + H_{\mathrm{N}}^\top S\nu_{k+1} + H_{\mathrm{T}}^\top D\hat{r}^{\mathsf{ir}}_{\mathrm{T},k+1} + H_{\mathrm{T}}^\top D\hat{r}^{\mathsf{r}}_{\mathrm{T},k+1} + F_{k+1} - Ku_k\right) + H_{\mathrm{T}} u_k + b_{\mathrm{T},k+1}, \\ &= -\sigma_c U_{\mathrm{TN}} S\beta_{k+1} + U_{\mathrm{TN}} S\nu_{k+1} + U_{\mathrm{TT}} D\hat{r}^{\mathsf{ir}}_{\mathrm{T},k+1} + U_{\mathrm{TT}} D\hat{r}^{\mathsf{r}}_{\mathrm{T},k+1} + H_{\mathrm{T}} K^{-1} F_{k+1} + b_{\mathrm{T},k+1}, \\ &= -\sigma_c U_{\mathrm{TN}} z_2 + U_{\mathrm{TN}} z_3 + U_{\mathrm{TT}} D z_4 + U_{\mathrm{TT}} D z_6 + H_{\mathrm{T}} K^{-1} F_{k+1} + b_{\mathrm{T},k+1}, \end{aligned} \tag{141}$$

which allows us to obtain w_6 in a straightforward fashion:

$$w_6 = -\sigma_c D^\top U_{\mathrm{TN}} z_2 + D^\top U_{\mathrm{TN}} z_3 + D^\top U_{\mathrm{TT}} D z_4 + D^\top U_{\mathrm{TT}} D z_6 + \mathbb{1}^\top z_7 + D^\top H_{\mathrm{T}} K^{-1} F_{k+1} + D^\top b_{\mathrm{T},k+1}. \tag{142}$$

Finally, we once again apply the substitution of χ_{k+1} for $|u_{\mathrm{T},k+1}|$ in the equation for ξ_{k+1}:

$$\begin{aligned} \xi_{k+1} =& A^{\mathsf{r}}{}_{k+1} + \sigma_c u_{\mathrm{N},k+1} + \sigma_c \gamma |u_{\mathrm{T},k+1}| + \sigma_c \delta_{c,\mathrm{N}} \left(\beta_{k+1} - \mathbf{1}\right), \\ =& A^{\mathsf{r}}{}_{k+1} - \sigma_c{}^2 U_{\mathrm{NN}} S\beta_{k+1} + \sigma_c U_{\mathrm{NN}} S\nu_{k+1} + \sigma_c U_{\mathrm{NT}} D\hat{r}^{\mathsf{ir}}_{\mathrm{T},k+1} + \sigma_c U_{\mathrm{NT}} D\hat{r}^{\mathsf{r}}_{\mathrm{T},k+1} \\ & + \sigma_c H_{\mathrm{N}} K^{-1} F_{k+1} + \sigma_c b_{\mathrm{N},k+1} + \sigma_c \gamma \chi_{k+1} + \sigma_c \delta_{c,\mathrm{N}} \left(\beta_{k+1} - \mathbf{1}\right), \\ =& S^{-1} z_1 + \sigma_c \left(\delta_{c,\mathrm{N}} S^{-1} - \sigma_c U_{\mathrm{NN}}\right) z_2 + \sigma_c U_{\mathrm{NN}} z_3 + \sigma_c U_{\mathrm{NT}} D z_4 + \sigma_c U_{\mathrm{NT}} D z_6 + \sigma_c \gamma z_7 \\ & + \sigma_c \left(H_{\mathrm{N}} K^{-1} F_{k+1} + b_{\mathrm{N},k+1} - \delta_{c,\mathrm{N}} \mathbf{1}\right), \end{aligned} \tag{143}$$

which gives w_2 directly.

Thus, the quasi-static LCP is given by

$$w = \begin{bmatrix} h\lambda_{k+1} \\ \xi_{k+1} \\ u_{\mathrm{N},k+1} \\ \mathbb{1}h\zeta_{k+1} + D^\top h v_{\mathrm{T},k+1} \\ \mu S\nu - \mathbb{1}^\top \hat{r}^{\mathsf{ir}}_{\mathrm{T},k+1} \\ \mathbb{1}\chi_{k+1} + D^\top u_{\mathrm{T},k+1} \\ \sigma_c \gamma S\beta_{k+1} - \mathbb{1}^\top \hat{r}^{\mathsf{r}}_{\mathrm{T},k+1} \end{bmatrix}, \quad z = \begin{bmatrix} SA^{\mathsf{r}}{}_{k+1} \\ S\beta_{k+1} \\ S\nu_{k+1} \\ \hat{r}^{\mathsf{ir}}_{\mathrm{T},k+1} \\ h\zeta_{k+1} \\ \hat{r}^{\mathsf{r}}_{\mathrm{T},k+1} \\ \chi_{k+1} \end{bmatrix},$$

$$L = \begin{bmatrix} \mathbf{0}^{n\times n} & -S^{-1} & \mathbf{0}^{n\times n} & \mathbf{0}^{n\times 2n} & \mathbf{0}^{n\times n} & \mathbf{0}^{n\times 2n} & \mathbf{0}^{n\times n} \\ S^{-1} & \sigma_c\left(\delta_{c,\mathrm{N}} S^{-1} - \sigma_c U_{\mathrm{NN}}\right) & \sigma_c U_{\mathrm{NN}} & \sigma_c U_{\mathrm{NT}} D & \mathbf{0}^{n\times n} & \sigma_c U_{\mathrm{NT}} D & \sigma_c \gamma I \\ \mathbf{0}^{n\times n} & -\sigma_c U_{\mathrm{NN}} & U_{\mathrm{NN}} & U_{\mathrm{NT}} D & \mathbf{0}^{n\times n} & U_{\mathrm{NT}} D & \mathbf{0}^{n\times n} \\ \mathbf{0}^{2n\times n} & -\sigma_c D^\top U_{\mathrm{TN}} & D^\top U_{\mathrm{TN}} & D^\top U_{\mathrm{TT}} D & \mathbb{1} & D^\top U_{\mathrm{TT}} D & \mathbf{0}^{2n\times n} \\ \mathbf{0}^{n\times n} & \mathbf{0}^{n\times n} & \mu I & -\mathbb{1}^\top & \mathbf{0}^{n\times n} & \mathbf{0}^{n\times 2n} & \mathbf{0}^{n\times n} \\ \mathbf{0}^{2n\times n} & -\sigma_c D^\top U_{\mathrm{TN}} & D^\top U_{\mathrm{TN}} & D^\top U_{\mathrm{TT}} D & \mathbf{0}^{2n\times n} & D^\top U_{\mathrm{TT}} D & \mathbb{1} \\ \mathbf{0}^{n\times n} & \sigma_c \gamma I & \mathbf{0}^{n\times n} & \mathbf{0}^{n\times 2n} & \mathbf{0}^{n\times n} & -\mathbb{1}^\top & \mathbf{0}^{n\times n} \end{bmatrix},$$

$$q = \begin{bmatrix} \beta_k \\ \sigma_c\left(H_{\mathrm{N}} K^{-1} F_{k+1} + b_{\mathrm{N},k+1} - \delta_{c,\mathrm{N}} \mathbf{1}\right) \\ H_{\mathrm{N}} K^{-1} F_{k+1} + b_{\mathrm{N},k+1} \\ D^\top H_{\mathrm{T}} K^{-1} F_{k+1} - D^\top H_{\mathrm{T}} u_k \\ \mathbf{0}^n \\ D^\top H_{\mathrm{T}} K^{-1} F_{k+1} + D^\top b_{\mathrm{T},k+1} \\ \mathbf{0}^n \end{bmatrix} \tag{144}$$

We give the system the material parameters $G_c = 0.25$ N/mm, $\sigma_c = 0.5$ MPa, $\gamma = 1$, $\mu = 0.5$, a surface area $S = 1$ mm^2 and a spring length of 1 mm. We apply a driving displacement of $u = 0.5t$ to the far end of the horizontal spring, apply a confining force of $F = -5$ N in the vertical direction at the cohesive zone node, and then vary the stiffness of the bars in the system. First, setting the bar stiffness to $E = 0.45$ MPa:

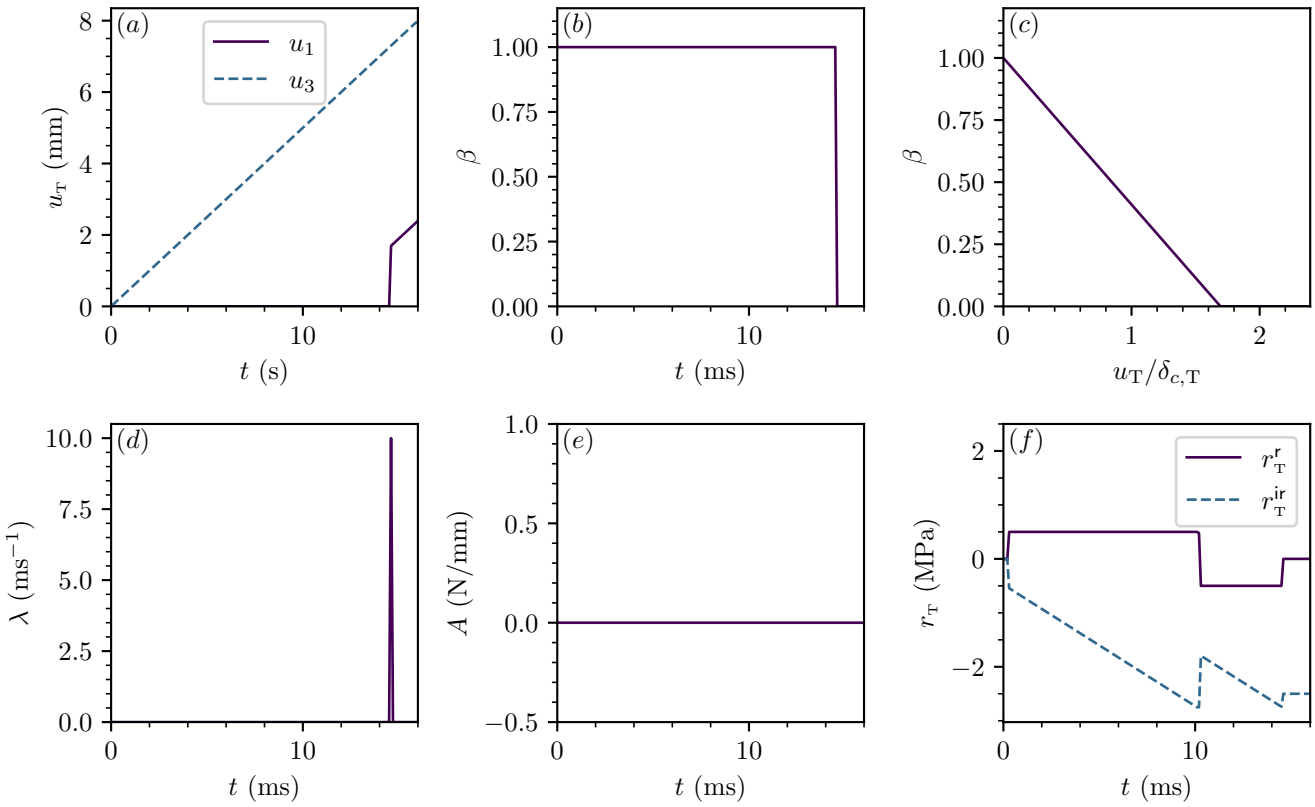

Figure 4: The system with $E = 0.45$ MPa. (a) The nodal displacements u_1 and u_3 as a function of time t. (b) The cohesion β as a function of time t. (c) The cohesion β as a function of crack sliding displacement u_{T}, normalised by the critical sliding distance $\delta_{c,\mathrm{T}}$. (d) The rate of decohesion λ as a function of time t. (e) The driving force A^{r} as a function of time t. (f) The reversible part of the tangential force $r^{\mathrm{r}}_{\mathrm{T}}$ and the frictional force $r^{\mathrm{ir}}_{\mathrm{T}}$ as a function of time t.

We observe behaviour from our system consistent with it being ill-posed. Of particular note, the system decoheres entirely in one time-step, and the graph of the cohesion against the normalised crack sliding displacement demonstrates dramatic "overshoot". As a consequence, an amount of energy greater than G_c will be released by the decohesion process, and thus the numerical results are no longer coherent with the analytical model.

By contrast, if we instead set the bar stiffness to $E = 4.5$ MPa and simulate the system again, we observe:

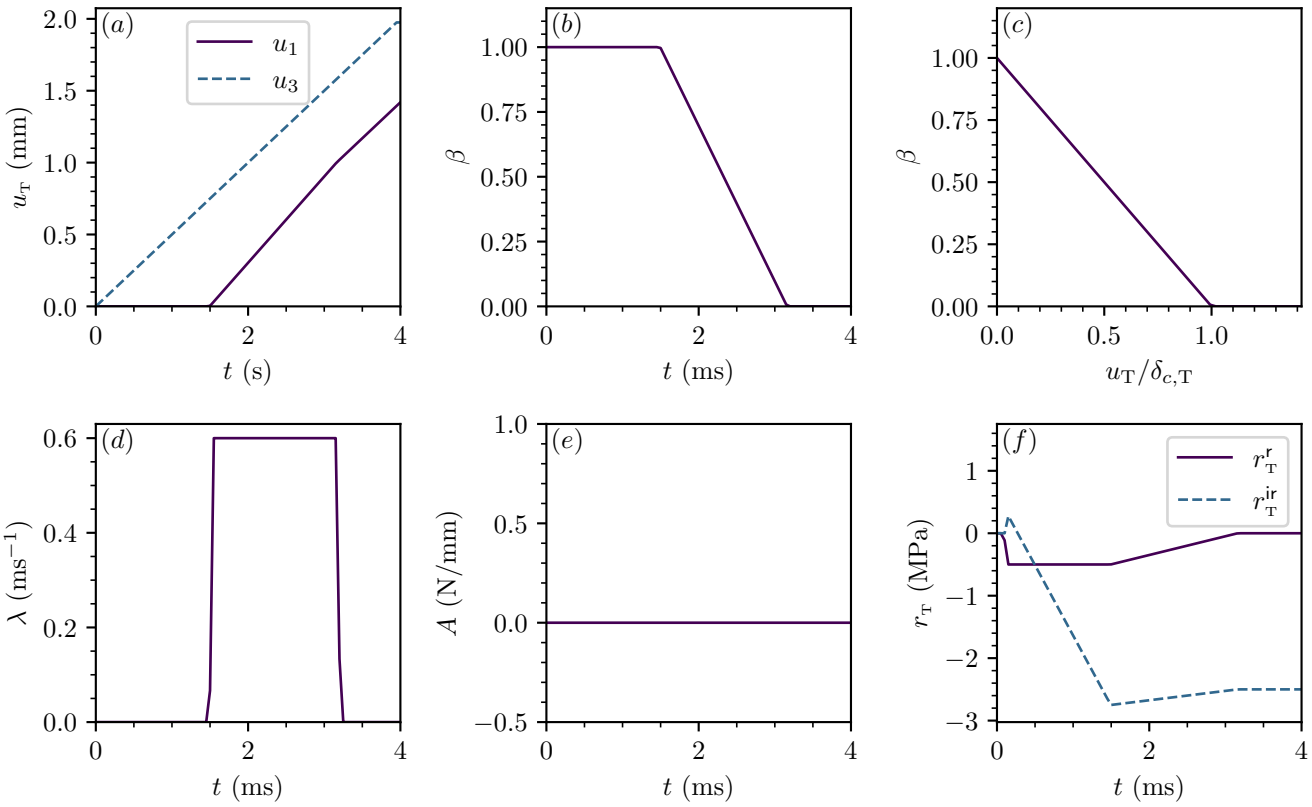

Figure 5: The system with $E = 4.5$ MPa. (a) The nodal displacements u_1 and u_3 as a function of time t. (b) The cohesion β as a function of time t. (c) The cohesion β as a function of crack sliding displacement u_{T}, normalised by the critical sliding distance $\delta_{c,\mathrm{T}}$. (d) The rate of decohesion λ as a function of time t. (e) The driving force A^{r} as a function of time t. (f) The reversible part of the tangential force $r_{\mathrm{T}}^{\mathsf{r}}$ and the frictional force $r_{\mathrm{T}}^{\mathsf{ir}}$ as a function of time t.

In this case, we observe behaviour from our system indicating it is well-posed. All of the variables evolve in a continuous manner, and no "overshoot" is observed with respect to the amount of energy released by the model. So long as we ensure that $\delta_{c,\mathrm{N}} S^{-1} - \sigma_c U_{\mathrm{NN}}$ is positive definite, the matrix L remains copositive, and the system appears to have only a single solution.

5.2 Dynamic scalar case with elastic spring

Now, we illustrate the benefits of working in dynamics by resolving the same system as described in Figure 3 with the spring stiffness set to 0.45 MPa, which lead to manifestly ill-posed behaviour, illustrated in Figure 4. Assigning a mass of 0.25 g to each node, keeping the numerical parameter $\theta = 1$, and now resolving the LCP given in (100), we observe:

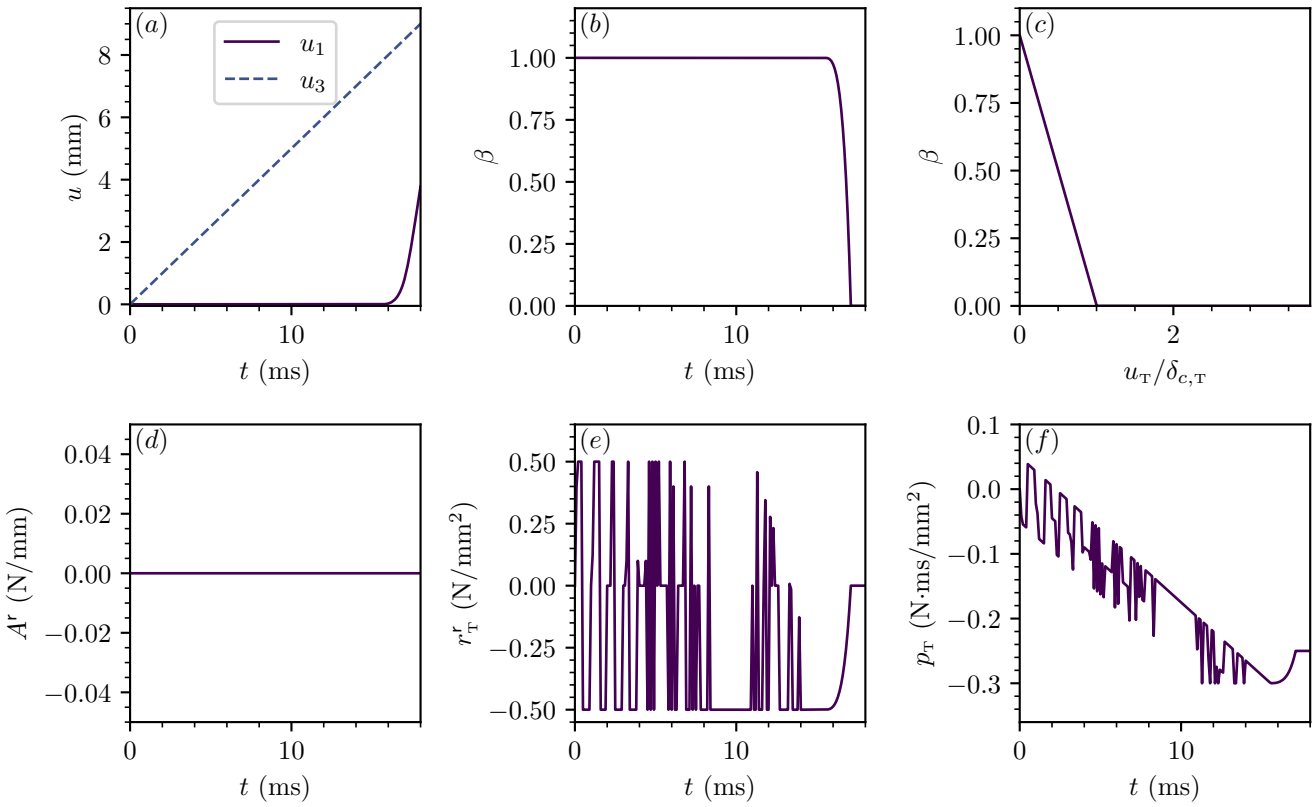

Figure 6: The system with $E = 0.45$ MPa. (a) The nodal displacements u_1 and u_3 as a function of time t. (b) The cohesion β as a function of time t. (c) The cohesion β as a function of crack sliding displacement u_T, normalised by the critical sliding distance $\delta_{c,\mathrm{T}}$. (d) The driving force A^r as a function of time t. (e) The reversible part of the tangential force r_T^r as a function of time t. (f) The frictional percussion p_T as a function of time t.

In this case, despite using material parameters that lead to ill-posed behaviours in quasi-statics, the addition of mass to the system and a change to dynamics was sufficient to achieve seemingly well-posed behaviour (using a time-step $h = 0.1$ ms, although the system remains well-behaved for larger time-steps). Visible in subplots (e) and (f) of Figure 6 are spurious oscillations of the tangential cohesive force and frictional percussion. This behaviour is a legacy of the set-valued nature of these quantities when u_T and v_T are equal to zero, respectively. When both u_T and v_T are simultaneously zero, the only constraint is that the sum of the two quantities (after r_T^r has been multiplied by h) must balance the equilibrium equation, and so the individual quantities can take any admissible value provided the sum respects the constraint. We emphasise that there are no negative consequences to this behaviour, as it only occurs when both the thermodynamic conjugates (u_T and v_T) are equal to zero, hence there is no spurious dissipation or energy storage. As soon as either the displacement or velocity are non-zero, the corresponding force or percussion takes a singular value, which in turn causes the other to be restricted to a particular value. Finally, we note that the particular value of p_T will depend on the size of the time-step h, with bigger time-steps leading to bigger values of p_T, but the dynamic equilibrium equation will always be respected.

Now, we simulate the stiffer system with $E = 4.5$ MPa, but this time provide a driving force $F = 0.375 \exp(0.25t) \sin(\pi t)$ N to the far end of the horizontal spring, and use $h = 0.0125$ ms to ensure correct resolution of the elasto-dynamics, we observe:

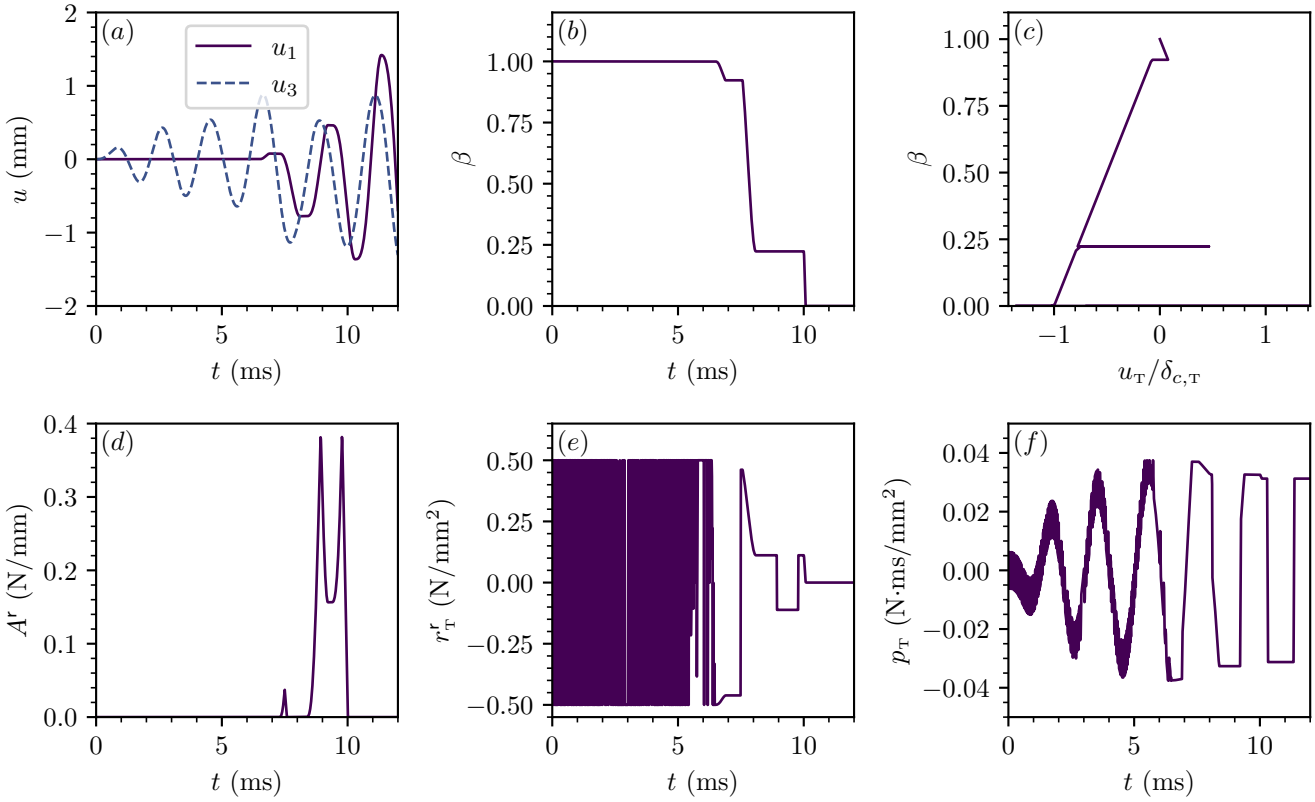

Figure 7: The system with $E = 4.5$ MPa. (a) The nodal displacements u_1 and u_3 as a function of time t. (b) The cohesion β as a function of time t. (c) The cohesion β as a function of crack sliding displacement u_T, normalised by the critical sliding distance $\delta_{c,\mathrm{T}}$. (d) The driving force A^r as a function of time t. (e) The reversible part of the tangential force r^r_T as a function of time t. (f) The frictional percussion p_T as a function of time t.

Once again the spurious oscillations are observable in the tangential cohesive force and frictional percussion, and once again do not have any negative consequences. We may also observe that the system decoheres for both positive and negative values of u_T, with the characteristic horizontal unload–reload behaviour of non-smooth cohesive zone models. Finally, due to the unloading and reloading, we observe that the reversible part of the crack driving force is occasionally non-zero.

5.3 Sliding block

We simulate a sliding block geometry inspired by that found in Berman et al. (2020) (specifically, the geometry of their upper block), shown in Figure 8. In this paper, the authors study (experimentally) the progression of frictional ruptures, which have been analogised to pure mode II cracks and studied using LEFM techniques. Given the convenient geometry that forces the "crack" to remain on the interface, this is an ideal test to enforce pure mode II behaviour in the system, which is otherwise non-trivial for true fractures.

The material is polymethal methacrylate (PMMA), which has a density of 1.17×10^{-3} g/mm^3 and a Young's modulus of 5.75×10^3 MPa, and the measured Rayleigh, shear and longitudinal wave speeds are $c_\mathrm{R} = 1255$ mm/ms, $c_s = 1345$ mm/ms and $c_l = 2680$ mm/ms respectively. The cohesive zone parameters are taken to be those used for PMMA in Collins-Craft et al. (2022), *i.e.* the critical traction $\sigma_c = 45$ MPa, the critical fracture energy G_c=0.14 N/mm, and the critical opening distance $\delta_{c,\mathrm{N}} = 0.0062$ mm. The critical traction ratio $\gamma = 1$, that is to say that we take the mode II properties to be identical to the mode I properties. The coefficient of restitution $e = 0$, and the coefficient of friction $\mu = 0.3$.

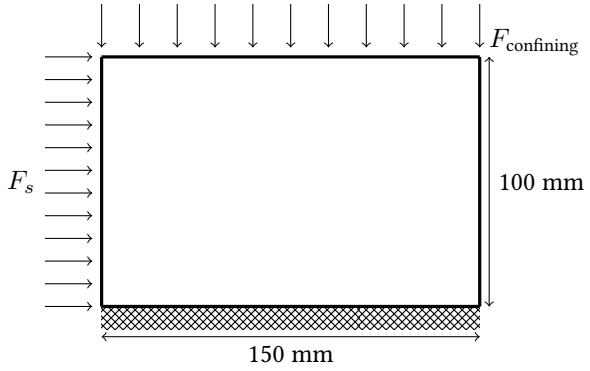

Figure 8: Geometry of the sliding block problem. A cohesive zone attached to a rigid substrate is applied to the bottom boundary (cross hatching), while a uniform pressure of 6.061 MPa is applied to the top boundary (corresponding to a total normal force of 5000 N). F_s is set to a fraction of the total static sliding resistance that the cohesive zone layer can supply and applied quasi-statically, before being set to a value much greater than the sliding resistance for dynamic simulation. The sample has a thickness of 5.5 mm.

The geometry is meshed using Gmsh 4.8.1 (Geuzaine and Remacle, 2009), specifically the Blossom-quad algorithm for generating linear quadrilateral (Q4) elements (Remacle et al., 2012). The plane stress assumption is used, and a consistent mass matrix is chosen. The size of the cohesive zone is given by

$$\ell = \frac{\pi}{8} \frac{E}{1-\nu^2} \frac{G_c}{{\sigma_{\text{ave}}}^2} \tag{145}$$

where we follow Camacho and Ortiz (1996), in turn following Rice (1968), but insert our value of σ_c into the formula, rather than taking the average cohesive stress. This leads to a smaller estimate of the cohesive zone size, and thus requires a finer mesh to resolve it, which is to say we err on the side of greater mesh refinement than we truly need. Inserting our system values, we obtain $\ell = 0.164$ mm. We thus set the characteristic length of the mesh at 0.04 mm for a small region of the contact boundary [72.5 mm, 77.5 mm] where we will fully resolve the cohesive zone (having at least three elements in the cohesive zone is typically regarded as necessary to fully resolve it), and set the characteristic length at the outer corners of the contact boundary as 20 mm, and the characteristic length for the confining load boundary as 10 mm. The algorithm ensures that all of the elements are at least this refined (in practice, typically substantially more so), and the size of elements along the contact boundary progressively decreases towards the finely meshed zone. Finally, the mesh is read into Python 3 via Meshio 5.3.0 (Schlömer, 2022).

The numerical parameter $\theta = 0.5$, and we set the maximum time-step size $h_{\max} = 1 \times 10^{-5}$ ms, but allow adaptive time-stepping. In the case that the LCP fails to resolve, the time-step is divided in half, while in the case where $h < h_{\max}$ and ten time-steps in succession have successfully completed, we multiply the time-step by 2.5, unless this value would exceed $h_{\max}$, in which case we set the time-step to $h_{\max}$. It should be noted that in spite of the mathematical guarantee offered by Lemke's algorithm (Lemke and Howson, Jr., 1964), namely that if a solution exists the algorithm will find it, in practice the finite precision of floating point numbers renders this sometimes untrue, and the combination of solver failure and adaptive time-stepping can cause the system to cascade downwards to arbitrarily small time-steps. In the case that $h < 1 \times 10^{-12}$ *i.e.* approximate machine precision, we simply reset h to $h_{\max}$ in the hope of "boosting out" of the negative spiral. In the case where this fails, and the solver immediately cascades the time-step back below machine precision, we set the simulation to terminate. However in practice, the boosting mechanism works well and allows the simulation to continue at a feasible time-step size.

We set our simulation so that the quasi-static initial loading F_s is at 0.99 of the tangential force limit that can be supported by the contact zone, and then in starting our dynamic simulation set F_s to 100 times this limit to induce very rapid loading (in Berman et al. (2020), they initiate frictional rupture by applying an out-of-plane mode III perturbation, but our plane stress assumption does not allow us to operate in the third dimension). The results of the simulation are shown in Figure 9:

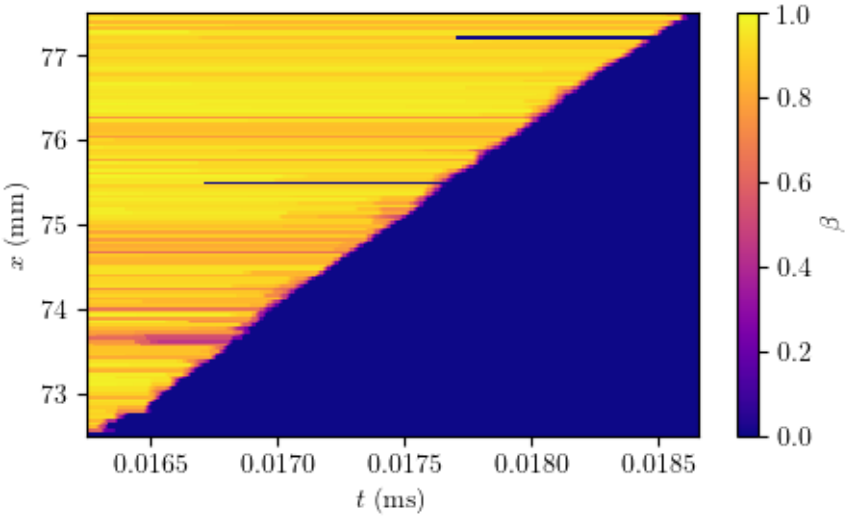

Figure 9: A "phase space" plot of the refined mesh region as the crack passes through the region, showing the values of the cohesion β.

Visible on the plot is a degree of numerical noise that causes some elements to fracture sooner than they otherwise should (which is resolvable with smaller time-steps, at the cost of greater numerical expense), but the global behaviour of the system is well-resolved. The slope of the line in phase-space gives the velocity of the crack front, 2103 mm/ms, which is less than the longitudinal wave velocity (that is to say, physically admissible), but greater than the shear wave velocity. This "supershear" behaviour has been theoretically predicted (Burridge, 1973; Burridge et al., 1979) and experimentally observed (Kammer et al., 2018; Rosakis, 2002; Xia et al., 2004), so the ability of our model to replicate this behaviour in a numerically efficient manner is an indication of the suitability of the method for very fast dynamics.

We may also empirically study the energetic properties of our dissipation algorithm, shown in Figure 10:

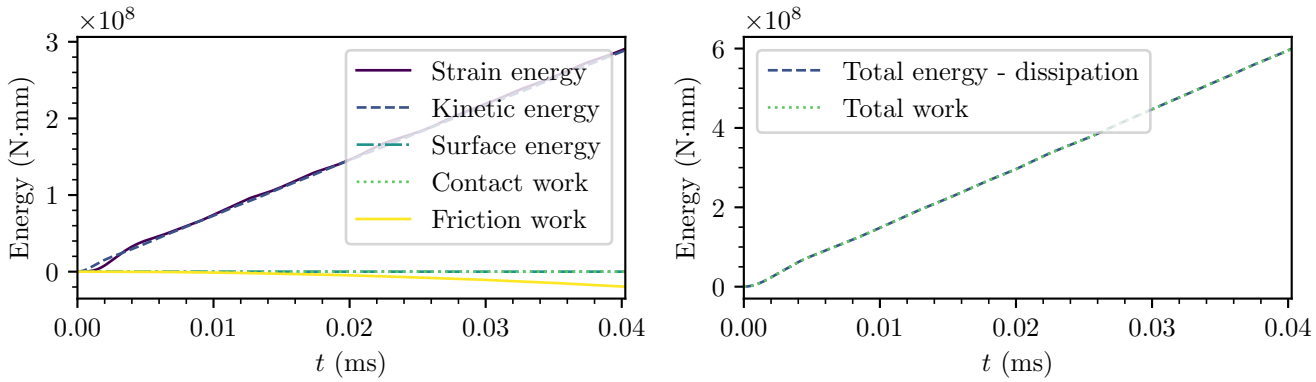

Figure 10: (a) The individual components of the energy and dissipation in the system, and (b) the sum of the internal energy less the dissipation, in comparison with the total work input to the system.

We observe that the strain energy and kinetic energy of our system account for the vast majority of the energy present in the system, the surface energy and contact work are negligible, and the friction work becomes noticeable only towards the end of the simulation. In comparing the difference of the total energy and the dissipative work of friction with the total work input into the system, we observe a very good match. This is to be expected, as the integration method should be energy-preserving for the main energetic components, while the fully implicit frictional contact is dissipative, but the overall contribution of friction to the energetic budget is small enough that the overall dissipative character of the integration algorithm is not significant at the global level of the simulation.

6 Conclusions

In this paper, we used the principal of virtual power to establish the equilibrium and boundary conditions for a body featuring a cohesive zone. We then postulated a free energy potential for the surface that allowed us to obtain non-smooth state laws

for the system. These state laws describe a family of extrinsic cohesive zone models that do not feature the unload–reload elasticity characteristic of those models that have the shifted intrinsic model structure. This mathematical feature guarantees appropriate physical behaviour under complex, non-monotonic loading conditions, where traditional extrinsic cohesive zone models exhibit the same spurious behaviours as intrinsic models. We then specified a non-smooth dissipative pseudo-potential that allowed us to obtain a complete generalised family of constitutive models for the cohesive zone system for both normal and tangential crack opening, and showed that in the case of frictional contact the model is dissipative (otherwise, it is irreversible but non-dissipative).By specifying a particular energetic potential, we obtained a model that gives a linear evolution of the cohesion variable with increasing displacement jump across the crack faces.

We then spatially discretised our system and re-framed certain parts using differential measures. This allowed us to include the non-smooth contact dynamics formulation within our model. By using a θ-method to discretise the system in time, in combination with a fully implicit discretisation of the sliding velocities, we obtained a time-stepping scheme that we were able to write as a linear complementarity problem. We then showed that given a sufficiently small time-step, the solution of the problem is guaranteed to exist. The time-stepping scheme was then shown to be dissipative in the case of contact and friction, and symplectic in their absence.

We then implemented the model numerically by solving the linear complementarity problem at each time-step, followed by a global updating of the degrees of freedom not involved in the monolithic complementarity problem. By using the finite element method, we were able to simulate a system of interest drawn from the literature, and show that our numerical method is able to replicate the "supershear" behaviour that is observed in analytical and experimental studies of frictional rupture. The method empirically demonstrates very good energetic conservation properties, and is able to complete using time-steps that are large enough to be useful for practical simulations.

This work has demonstrated that the applications of convex analysis lead to physically correct and numerically efficient models that can encompass fracture, contact and friction. In formulating this work, we decided to remain in the quasi-two-dimensional and small displacement framework so that we could continue to benefit from the linear complementarity formulation. The natural extension of the work is to pass to a fully three-dimensional model, however this will require formulating the problem as a second-order cone complementarity problem, and is a substantial leap in complexity. Other possible directions of research would be to explore other (nonlinear) forms of the cohesion law, extend the model to model interface phenomena such as "rate-and-state" friction, or combine crack propagation with other physical phenomena such as phase change.

A Reformulation of a bi-dimensional Coulomb-like inclusion into a complementarity problem

From Stewart and Trinkle (1996), we extend the results concerning the reformulation of Coulomb-like friction problem into complementarity relations.

Lemma 2. *Let a be a positive scalar. The solution y_N, y_T, x_N, x_T of the following inclusion*

$$\left\{\begin{array}{lcl} -y_N & \in & N_{\mathbb{R}^+}(x_N) \\ -y_T & \in & (y_N + a)\,\mathrm{sgn}(x_T) = y_N \partial |x_T|, \end{array}\right. \tag{146}$$

is given by solving the following complementarity system

$$\left\{\begin{array}{lcl} 0 \leqslant y_N & \perp & x_N \geqslant 0 \\ 0 \leqslant \hat{y}_T & \perp & \mathbb{1}\lambda + D^\top x_T \geqslant 0 \\ 0 \leqslant \lambda & \perp & y_N + a - \mathbb{1}^\top \hat{y}_T \geqslant 0, \end{array}\right. \tag{147}$$

with $y_T = D\hat{y}_T$ and $D = \Big[1, -1\Big]$. Furthermore, we have $|x_T| = \lambda$.

Proof The following equivalence is a standard result of Convex Analysis

$$-y_N \in N_{\mathbb{R}^+}(x_N) \Longleftrightarrow 0 \leqslant y_N \perp x_N \geqslant 0. \tag{148}$$

Let us consider the cases associated with

$$\begin{array}{lcl} 0 \leqslant \hat{y}_T & \perp & \mathbb{1}\lambda + D^\top x_T \geqslant 0 \\ 0 \leqslant \lambda & \perp & y_N - \mathbb{1}^\top \hat{y}_T \geqslant 0 \end{array} \tag{149}$$

1. $\lambda = 0$. In that case, the complementarity condition implies

$$x_{\mathrm{T}} = 0, \hat{y}_{\mathrm{T},1} + \hat{y}_{\mathrm{T},2} \leqslant y_{\mathrm{N}} + a \tag{150}$$

and then $\lambda = |x_{\mathrm{T}}|$. Since $\hat{y}_{\mathrm{T},1} \geqslant 0, \hat{y}_{\mathrm{T},2} \geqslant 0$, we also have

$$\begin{aligned} y_{\mathrm{T}} &= \hat{y}_{\mathrm{T},1} - \hat{y}_{\mathrm{T},2} = \hat{y}_{\mathrm{T},1} + \hat{y}_{\mathrm{T},2} - 2\hat{y}_{\mathrm{T},2} \leqslant \hat{y}_{\mathrm{T},1} + \hat{y}_{\mathrm{T},2} \leqslant y_{\mathrm{N}} + a \\ - \quad y_{\mathrm{T}} &= \hat{y}_{\mathrm{T},2} - \hat{y}_{\mathrm{T},1} = \hat{y}_{\mathrm{T},2} + \hat{y}_{\mathrm{T},1} - 2\hat{y}_{\mathrm{T},1} \leqslant \hat{y}_{\mathrm{T},1} + \hat{y}_{\mathrm{T},2} \leqslant y_{\mathrm{N}} + a \end{aligned} \tag{151}$$

and we conclude $|y_{\mathrm{T}}| \leqslant y_{\mathrm{N}} + a$.

2. $\lambda > 0, \hat{y}_{\mathrm{T},1} > 0, \hat{y}_{\mathrm{T},2} = 0$. In that case, the complementarity condition implies

$$\lambda = -x_{\mathrm{T}} > 0, x_{\mathrm{T}} < 0, y_{\mathrm{T},1} = y_{\mathrm{N}} + a, \tag{152}$$

and then $y_{\mathrm{T}} = y_{\mathrm{N}} + a$, $x_{\mathrm{T}} < 0$, $\lambda = |x_{\mathrm{T}}|$.

3. $\lambda > 0, \hat{y}_{\mathrm{T},1} = 0, \hat{y}_{\mathrm{T},2} > 0$. In that case, the complementarity condition implies

$$\lambda = x_{\mathrm{T}} > 0, x_{\mathrm{T}} > 0, y_{\mathrm{T},2} = y_{\mathrm{N}} + a, \tag{153}$$

and then $y_{\mathrm{T}} = -(y_{\mathrm{N}} + a)$, $x_{\mathrm{T}} > 0$, $\lambda = |x_{\mathrm{T}}|$.

4. $\lambda > 0, \hat{y}_{\mathrm{T},1} > 0, \hat{y}_{\mathrm{T},2} > 0$. In that case, the complementarity condition implies

$$\lambda = 0. \tag{154}$$

This case is not possible.

5. $\lambda > 0, \hat{y}_{\mathrm{T},1} = 0, \hat{y}_{\mathrm{T},2} = 0$. In that case, the complementarity condition implies

$$y_{\mathrm{N}} = -a, \lambda \geqslant -x_{\mathrm{T}}, \lambda \geqslant x_{\mathrm{T}}. \tag{155}$$

This case is not possible since $a > 0$.

□

References

Acary, V. (May 2016). "Energy conservation and dissipation properties of time-integration methods for nonsmooth elastodynamics with contact". In: *Journal of Applied Mathematics and Mechanics / Zeitschrift für Angewandte Mathematik und Mechanik* 96.5, pp. 585–603. DOI: 10.1002/zamm.201400231. URL: https://hal.inria.fr/hal-01235240.

Acary, V. and B. Brogliato (2008). *Numerical methods for nonsmooth dynamical systems. Applications in mechanics and electronics.* English. Lecture Notes in Applied and Computational Mechanics 35. Berlin: Springer. xxi, 525 p.

Acary, V. and Y. Monerie (2006). *Nonsmooth fracture dynamics using a cohesive zone approach.* English. Research Report RR-6032. INRIA, p. 56. URL: http://hal.inria.fr/inria-00110560/en/.

Acary, V. et al. (2019). *An introduction to Siconos.* Tech. rep. Grenoble: INRIA.

Auth, K.L., J. Brouzoulis, and M. Ekh (July 1, 2022). "A Fully Coupled Chemo-Mechanical Cohesive Zone Model for Oxygen Embrittlement of Nickel-Based Superalloys". In: *Journal of the Mechanics and Physics of Solids* 164, p. 104880. ISSN: 00225096. DOI: 10.1016/j.jmps.2022.104880. URL: https://linkinghub.elsevier.com/retrieve/pii/S0022509622000898.

Azab, M., G. Parry, and R. Estevez (Mar. 2020). "An analytical model for DCB/wedge tests based on Timoshenko beam kinematics for accurate determination of cohesive zone lengths". In: *International Journal of Fracture* 222.1-2, pp. 137–153. ISSN: 15732673. DOI: 10.1007/s10704-020-00438-2. URL: https://doi.org/10.1007/s10704-020-00438-2.

Barenblatt, G.I. (Jan. 1, 1962). "The Mathematical Theory of Equilibrium Cracks in Brittle Fracture". In: *Advances in Applied Mechanics*. Ed. by H. L. Dryden et al. Vol. 7. Elsevier, pp. 55–129. DOI: 10.1016/S0065-2156(08)70121-2. URL: https://www.sciencedirect.com/science/article/pii/S0065215608701212.

Bergfeld, B. et al. (Dec. 2021). "Crack propagation speeds in weak snowpack layers". In: *Journal of Glaciology*, pp. 1–14. ISSN: 0022-1430. DOI: 10.1017/JOG.2021.118. URL: https://www.cambridge.org/core/journals/journal-of-glaciology/article/crack-propagation-speeds-in-weak-snowpack-layers/C28905FA3198DF87B0A18AB135FC4766.

Berman, N., G. Cohen, and J. Fineberg (2020). "Dynamics and properties of the cohesive zone in rapid fracture and friction". In: *Physical Review Letters* 125.12, p. 125503. ISSN: 10797114. DOI: 10.1103/PhysRevLett.125.125503. URL: https://doi.org/10.1103/PhysRevLett.125.125503.

Burridge, R. (Dec. 1, 1973). "Admissible Speeds for Plane-Strain Self-Similar Shear Cracks with Friction but Lacking Cohesion". In: *Geophysical Journal International* 35.4, pp. 439–455. ISSN: 0956-540X. DOI: 10.1111/j.1365-246X.1973.tb00608.x. URL: https://doi.org/10.1111/j.1365-246X.1973.tb00608.x.

Burridge, R., G. Conn, and L.B. Freund (1979). "The Stability of a Rapid Mode II Shear Crack with Finite Cohesive Traction". In: *Journal of Geophysical Research* 84.B5, p. 2210. ISSN: 0148-0227. DOI: 10.1029/JB084iB05p02210. URL: http://doi.wiley.com/10.1029/JB084iB05p02210.

Bybordiani, M. and D. Dias-da-Costa (Apr. 2021). "A consistent finite element approach for dynamic crack propagation with explicit time integration". In: *Computer Methods in Applied Mechanics and Engineering* 376, p. 113652. ISSN: 00457825. DOI: 10.1016/j.cma.2020.113652. URL: https://doi.org/10.1016/j.cma.2020.113652%20https://linkinghub.elsevier.com/retrieve/pii/S0045782520308379.

Camacho, G.T. and M. Ortiz (1996). "Computational modelling of impact damage in brittle materials". In: *International Journal of Solids and Structures* 33.20, pp. 2899–2938. ISSN: 0020-7683. DOI: 10.1016/0020-7683(95)00255-3. URL: http://www.sciencedirect.com/science/article/pii/0020768395002553.

Camanho, P.P., C.G. Davila, and M.F. De Moura (2003). "Numerical Simulation of Mixed-Mode Progressive Delamination in Composite Materials". In: *Journal of Composite Materials* 37.16, pp. 1415–1438. DOI: 10.1177/0021998303034505. URL: https://www.researchgate.net/publication/37650396.

Cazes, F., M. Coret, and A. Combescure (2013). "A two-field modified lagrangian formulation for robust simulations of extrinsic cohesive zone models". In: *Computational Mechanics* 51, pp. 865–884. URL: https://hal.archives-ouvertes.fr/hal-00938515.

Célarié, F. et al. (2003). "Glass Breaks like Metal, but at the Nanometer Scale". In: *Physical Review Letters* 90.7, pp. 075504-1–075504-4. ISSN: 10797114. DOI: 10.1103/PhysRevLett.90.075504.

Chaboche, J.L., F. Feyel, and Y. Monerie (2001). "Interface debonding models: A viscous regularization with a limited rate dependency". In: *International Journal of Solids and Structures* 38.18, pp. 3127–3160. ISSN: 00207683. DOI: 10.1016/S0020-7683(00)00053-6.

Collins-Craft, N.A., F. Bourrier, and V. Acary (Oct. 1, 2022). "On the Formulation and Implementation of Extrinsic Cohesive Zone Models with Contact". In: *Computer Methods in Applied Mechanics and Engineering* 400, p. 115545. ISSN: 0045-7825. DOI: 10.1016/j.cma.2022.115545. URL: https://www.sciencedirect.com/science/article/pii/S0045782522005369.

Cottle, R.W., J.-S. Pang, and R.E. Stone (2009). *The Linear Complementarity Problem*. Ed. by R.E. O'Malley. Second. Philadelphia: Society for Industrial and Applied Mathematics, p. 781. ISBN: 978-0-89871-686-3. DOI: 10.1137/1.9780898719000. URL: http://epubs.siam.org/doi/book/10.1137/1.9780898719000.

Dugdale, D.S. (May 1960). "Yielding of Steel Sheets Containing Slits". In: *Journal of the Mechanics and Physics of Solids* 8.2, pp. 100–104. ISSN: 00225096. DOI: 10.1016/0022-5096(60)90013-2. URL: https://linkinghub.elsevier.com/retrieve/pii/0022509660900132.

Falk, M.L., A. Needleman, and J.R. Rice (2001). "A critical evaluation of dynamic fracture simulations using cohesive surfaces". In: *Jounal de Physique IV*. Vol. 11, Pr5-43–Pr5-50. DOI: 10.1051/jp4:2001506.

Foulk, J.W. (Jan. 2010). "An examination of stability in cohesive zone modeling". In: *Computer Methods in Applied Mechanics and Engineering* 199.9-12, pp. 465–470. ISSN: 0045-7825. DOI: 10.1016/J.CMA.2009.08.025.

Frémond, M. (1988). "Contact with Adhesion". In: *Nonsmooth Mechanics and Applications*. Vienna: Springer Vienna, pp. 177–221. DOI: 10.1007/978-3-7091-2624-03. URL: http://link.springer.com/10.1007/978-3-7091-2624-03.

— (2002). *Non-Smooth Thermomechanics*. Berlin, Heidelberg: Springer Berlin Heidelberg. ISBN: 978-3-642-08578-9. DOI: 10.1007/978-3-662-04800-9. URL: http://link.springer.com/10.1007/978-3-662-04800-9.

— (2012a). "Contact with Adhesion". In: *Phase Change in Mechanics*. Vol. 13. Lecture Notes of the Unione Matematica Italiana 4. Berlin, Heidelberg: Springer Berlin Heidelberg, pp. 151–156. ISBN: 978-3-642-24608-1. DOI: 10.1007/978-3-642-24609-8. URL: http://link.springer.com/10.1007/978-3-642-24609-8.

— (2012b). "Damage of Solids Glued on One Another: Coupling of Volume and Surface Damages". In: *Phase Change in Mechanics*. Lecture Notes of the Unione Matematica Italiana. Berlin, Heidelberg: Springer Berlin Heidelberg, pp. 115–130. ISBN: 978-3-642-24608-1. DOI: 10.1007/978-3-642-24609-8. URL: http://link.springer.com/10.1007/978-3-642-24609-8.

Geuzaine, C. and J.-F. Remacle (Sept. 2009). "Gmsh: A 3-D finite element mesh generator with built-in pre- and post-processing facilities". In: *International Journal for Numerical Methods in Engineering* 79.11, pp. 1309–1331. ISSN: 00295981. DOI: 10.1002/nme.2579. URL: http://doi.wiley.com/10.1002/nme.2579.

Griffith, A.A. (Jan. 1921). "The phenomena of rupture and flow in solids". In: *Philosophical Transactions of the Royal Society of London. Series A: Mathematical, Physical and Engineering Sciences* 221.582-593, pp. 163–198. ISSN: 0264-3952. DOI: 10.1098/rsta.1921.0006. URL: https://royalsocietypublishing.org/doi/10.1098/rsta.1921.0006.

Gvirtzman, S. and J. Fineberg (Aug. 2, 2021). "Nucleation Fronts Ignite the Interface Rupture That Initiates Frictional Motion". In: *Nature Physics 2021*, pp. 1–6. ISSN: 1745-2481. DOI: 10.1038/s41567-021-01299-9. URL: https://www.nature.com/articles/s41567-021-01299-9.

Halphen, B. and Q.S. Nguyen (Jan. 1, 1975). "Sur les Matériaux Standard Généralisés". In: *Journal de Mécanique* 14, pp. 39–63.

Houlsby, G.T. (2019). "Frictional Plasticity in a Convex Analytical Setting". In: *Open Geomechanics* 1.3, pp. 1–10. DOI: 10.5802/ogeo.2. URL: https://opengeomechanics.centre-mersenne.org/item/OGEO20191A30.

Jean, M. (July 1999). "The non-smooth contact dynamics method". In: *Computer Methods in Applied Mechanics and Engineering* 177.3-4, pp. 235–257. ISSN: 00457825. DOI: 10.1016/S0045-7825(98)00383-1. URL: https://linkinghub.elsevier.com/retrieve/pii/S0045782598003831.

Jean, M., V. Acary, and Y. Monerie (2001). "Non Smooth Contact dynamics approach of cohesive materials". In: *Philisophical Transactions : Mathematical, Physical & Engineering Sciences, The Royal Society, London A* A359.1789, pp. 2497–2518.

Jean, M. and J.J. Moreau (1992). "Unilaterality and dry friction in the dynamics of rigid body collections". In: *1st Contact Mechanics International Symposium*. Ed. by A. Curnier. Lausanne, pp. 31–48. URL: https://hal.archives-ouvertes.fr/hal-01863710.

Jiang, S. et al. (Sept. 2021). "Characterisation of fracture evolution of a single cemented brittle grain using in-situ X-ray computed tomography". In: *International Journal of Rock Mechanics and Mining Sciences* 145, p. 104835. ISSN: 1365-1609. DOI: 10.1016/J.IJRMMS.2021.104835.

Kammer, D.S. et al. (July 18, 2018). "The Equation of Motion for Supershear Frictional Rupture Fronts". In: *Science Advances* 4.7, eaat5622. DOI: 10.1126/sciadv.aat5622. URL: https://www.science.org/doi/full/10.1126/sciadv.aat5622.

Kubair, D.V. and P.H. Geubelle (2003). "Comparative analysis of extrinsic and intrinsic cohesive models of dynamic fracture". In: *International Journal of Solids and Structures* 40.15, pp. 3853–3868. ISSN: 0020-7683. DOI: https://doi.org/10.1016/S0020-7683(03)00171-9. URL: http://www.sciencedirect.com/science/article/pii/S0020768303001719.

Lemke, C.E. and J.T. Howson, Jr. (June 1964). "Equilibrium Points of Bimatrix Games". In: *Journal of the Society for Industrial and Applied Mathematics* 12.2, pp. 413–423. ISSN: 0368-4245. DOI: 10.1137/0112033. URL: http://epubs.siam.org/doi/10.1137/0112033.

Lorentz, E. (2008). "A mixed interface finite element for cohesive zone models". In: *Computer Methods in Applied Mechanics and Engineering* 198.2, pp. 302–317. ISSN: 0045-7825. DOI: https://doi.org/10.1016/j.cma.2008.08.006. URL: https://www.sciencedirect.com/science/article/pii/S0045782508002880.

Marigo, J.J. (1981). "Formulation d'une loi d'endommagement d'un materiau élastique". In: *Comptes rendus de l'Académie des sciences. Série 2, Mécanique, Physique, Chimie, Sciences de l'univers, Sciences de la Terre* 292.May, pp. 1309–1312.

Moës, N. and T. Belytschko (2002). "Extended Finite Element Method for Cohesive Crack Growth". In: *Engineering Fracture Mechanics* 69.7, pp. 813–833. ISSN: 00137944. DOI: 10.1016/S0013-7944(01)00128-X.

Monerie, Y. and V. Acary (2001). "Formulation dynamique d'un modèle de zone cohésive tridimensionnel couplant endommagement et frottement". In: *Revue Européenne des Éléments Finis* 10.2-4, pp. 489–503. DOI: 10.1080/12506559.2001.11869264. eprint: https://doi.org/10.1080/12506559.2001.11869264. URL: https://doi.org/10.1080/12506559.2001.11869264.

Moreau, J.J. (1970). "Sur les lois de frottement, de plasticité et de viscosité". In: *Comptes rendus de l'Académie des sciences. Série A - Sciences mathématiques* 271, pp. 608–611.

— (1974). "On Unilateral Constraints, Friction and Plasticity". In: *New Variational Techniques in Mathematical Physics*. Springer Berlin Heidelberg, pp. 171–322. DOI: 10.1007/978-3-642-10960-77. URL: https://link.springer.com/chapter/10.1007/978-3-642-10960-77.

— (1986). "Une formulation du contact à frottement sec; application au calcul numérique". In: *Comptes rendus de l'Académie des sciences. Série 2, Mécanique, Physique, Chimie, Sciences de l'univers, Sciences de la Terre* 302.13, pp. 799–801. ISSN: 0764-4450.

— (July 1999). "Numerical aspects of the sweeping process". In: *Computer Methods in Applied Mechanics and Engineering* 177.3-4, pp. 329–349. ISSN: 0045-7825. DOI: 10.1016/S0045-7825(98)00387-9.

Nguyen, V.P. (2014). "Discontinuous Galerkin/extrinsic cohesive zone modeling: Implementation caveats and applications in computational fracture mechanics". In: *Engineering Fracture Mechanics* 128, pp. 37–68. ISSN: 0013-7944. DOI: 10.1016/j.engfracmech.2014.07.003. URL: http://www.sciencedirect.com/science/article/pii/S0013794414002136.

Nkoumbou Kaptchouang, N.B. et al. (2021). "Cohesive GTN model for ductile fracture simulation". In: *Engineering Fracture Mechanics* 242, p. 107437. ISSN: 0013-7944. DOI: 10.1016/j.engfracmech.2020.107437. URL: https://www.sciencedirect.com/science/article/pii/S0013794420310080.

Okubo, K. et al. (Nov. 2019). "Dynamics, Radiation, and Overall Energy Budget of Earthquake Rupture With Coseismic Off-Fault Damage". In: *Journal of Geophysical Research: Solid Earth* 124.11, pp. 11771–11801. ISSN: 2169-9313. DOI: 10.1029/2019JB017304. eprint: 1901.01771. URL: https://onlinelibrary.wiley.com/doi/10.1029/2019JB017304.

Papoulia, K.D., C.-H. Sam, and S.A. Vavasis (Oct. 2003). "Time continuity in cohesive finite element modeling". In: *International Journal for Numerical Methods in Engineering* 58.5, pp. 679–701. ISSN: 0029-5981. DOI: 10.1002/nme.778. URL: http://doi.wiley.com/10.1002/nme.778.

Parrinello, F. (Sept. 2020). "Hybrid equilibrium element with interelement interface for the analysis of delamination and crack propagation problems". In: *International Journal for Numerical Methods in Engineering* August. ISSN: 0029-5981. DOI: 10.1002/nme.6531. URL: https://onlinelibrary.wiley.com/doi/10.1002/nme.6531.

Parrinello, F. and G. Borino (2020). "Cohesive-frictional interface in an equilibrium based finite element formulation". In: *Proceedings of XXIV AIMETA Conference 2019*. Ed. by A. Carcaterra, A. Paolone, and G. Graziani. Lecture Notes in Mechanical

Engineering September. Cham: Springer International Publishing, pp. 419–426. ISBN: 978-3-030-41056-8. DOI: 10.1007/978-3-030-41057-5. URL: http://link.springer.com/10.1007/978-3-030-41057-5.

Perales, F. et al. (2010). "A NonSmooth Contact Dynamics-based multi-domain solver". In: *European Journal of Computational Mechanics* 19.4, pp. 389–417. DOI: 10.3166/ejcm.19.389-417. eprint: https://doi.org/10.3166/ejcm.19.389-417. URL: https://doi.org/10.3166/ejcm.19.389-417.

Raous, M., L. Cangémi, and M. Cocou (1999). "A consistent model coupling adhesion, friction, and unilateral contact". In: *Computer Methods in Applied Mechanics and Engineering*. DOI: 10.1016/S0045-7825(98)00389-2. URL: https://hal.archives-ouvertes.fr/hal-03178187.

Remacle, J.-F. et al. (2012). "Blossom-Quad: A Non-Uniform Quadrilateral Mesh Generator Using a Minimum-Cost Perfect-Matching Algorithm". In: *International Journal for Numerical Methods in Engineering* 89.9, pp. 1102–1119. ISSN: 1097-0207. DOI: 10.1002/nme.3279. URL: https://onlinelibrary.wiley.com/doi/abs/10.1002/nme.3279.

Réthoré, J. and R. Estevez (2013). "Identification of a cohesive zone model from digital images at the micron-scale". In: *Journal of the Mechanics and Physics of Solids* 61.6, pp. 1407–1420. ISSN: 00225096. DOI: 10.1016/j.jmps.2013.01.011.

Rice, J.R. (1968). "Mathematical Analysis in the Mechanics of Fracture". In: *Fracture: An Advanced Treatise*. Ed. by H. Liebowitz. Vol. 2. New York: Academic Press, pp. 191–311.

Rosakis, A.J. (June 2002). "Intersonic Shear Cracks and Fault Ruptures". In: *Advances in Physics* 51.4, pp. 1189–1257. ISSN: 0001-8732, 1460-6976. DOI: 10.1080/00018730210122328. URL: http://www.tandfonline.com/doi/abs/10.1080/00018730210122328.

Sam, C.-H., K.D. Papoulia, and S.A. Vavasis (Sept. 2005). "Obtaining initially rigid cohesive finite element models that are temporally convergent". In: *Engineering Fracture Mechanics* 72.14, pp. 2247–2267. ISSN: 00137944. DOI: 10.1016/j.engfracmech.2004.12.008. URL: https://linkinghub.elsevier.com/retrieve/pii/S0013794405000895.

Samimi, M., J.A.W. van Dommelen, and M.G.D. Geers (Dec. 2011). "A three-dimensional self-adaptive cohesive zone model for interfacial delamination". In: *Computer Methods in Applied Mechanics and Engineering* 200.49-52, pp. 3540–3553. ISSN: 0045-7825. DOI: 10.1016/J.CMA.2011.08.021.

Schlömer, N. (2022). *meshio: Tools for mesh files*. DOI: 10.5281/zenodo.1173115. URL: https://github.com/nschloe/meshio.

Seagraves, A. and R. Radovitzky (2009). "Advances in Cohesive Zone Modeling of Dynamic Fracture". In: *Dynamic Failure of Materials and Structures*. Boston, MA: Springer US, pp. 349–405. ISBN: 978-1-4419-0445-4. DOI: 10.1007/978-1-4419-0446-112. URL: https://link.springer.com/chapter/10.1007/978-1-4419-0446-112.

Stewart, D.E. and J.C. Trinkle (Aug. 15, 1996). "An Implicit Time-Stepping Scheme for Rigid Body Dynamics with Inelastic Collisions and Coulomb Friction". In: *International Journal for Numerical Methods in Engineering* 39.15, pp. 2673–2691. ISSN: 0029-5981. DOI: 10.1002/(SICI)1097-0207(19960815)39:15¡2673::AID-NME972¿3.0.CO;2-I. URL: https://onlinelibrary.wiley.com/doi/10.1002/(SICI)1097-0207(19960815)39:15%3C2673::AID-NME972%3E3.0.CO;2-I.

Talon, C. and A. Curnier (2003). "A model of adhesion coupled to contact and friction". In: *European Journal of Mechanics - A/Solids* 22.4, pp. 545–565. ISSN: 0997-7538. DOI: https://doi.org/10.1016/S0997-7538(03)00046-9. URL: https://www.sciencedirect.com/science/article/pii/S0997753803000469.

"The direct observation of the core region of a propagating fracture crack in glass" (1996). In: *Europhysics Letters (EPL)* 34.7, pp. 549–554. ISSN: 0295-5075. DOI: 10.1209/epl/i1996-00493-3.

Vargas, R. et al. (Dec. 2020). "On the identification of cohesive zone model for curved crack in mortar". In: *Strain* 56.6. ISSN: 0039-2103. DOI: 10.1111/str.12364. URL: https://doi.org/10.1111/str.12364%20https://onlinelibrary.wiley.com/doi/10.1111/str.12364.

Venzal, V. et al. (Aug. 2020). "Frictional cohesive zone model for quasi-brittle fracture: Mixed-mode and coupling between cohesive and frictional behaviors". In: *International Journal of Solids and Structures* 198, pp. 17–30. ISSN: 00207683. DOI: 10.1016/j.ijsolstr.2020.04.023. URL: https://linkinghub.elsevier.com/retrieve/pii/S0020768320301402.

Versino, D. et al. (2015). "A thermodynamically consistent discontinuous Galerkin formulation for interface separation". In: *Composite Structures* 133, pp. 595–606. ISSN: 0263-8223. DOI: 10.1016/j.compstruct.2015.07.080. URL: http://www.sciencedirect.com/science/article/pii/S0263822315006261.

Xia, K., A.J. Rosakis, and H. Kanamori (Mar. 19, 2004). "Laboratory Earthquakes: The Sub-Rayleigh-to-Supershear Rupture Transition". In: *Science* 303.5665, pp. 1859–1861. ISSN: 0036-8075, 1095-9203. DOI: 10.1126/science.1094022. URL: https://www.science.org/doi/10.1126/science.1094022.

Zhou, F. and J.-F. Molinari (Jan. 2004). "Dynamic crack propagation with cohesive elements: a methodology to address mesh dependency". In: *International Journal for Numerical Methods in Engineering* 59.1, pp. 1–24. ISSN: 0029-5981. DOI: 10.1002/nme.857. URL: http://doi.wiley.com/10.1002/nme.857.